ISSN 2413-9432

BIOMEDICAL PHOTONICS

Volume 14, # 2, 2025

In the issue:

BMP

Российская Фотодинамическая Ассоциация

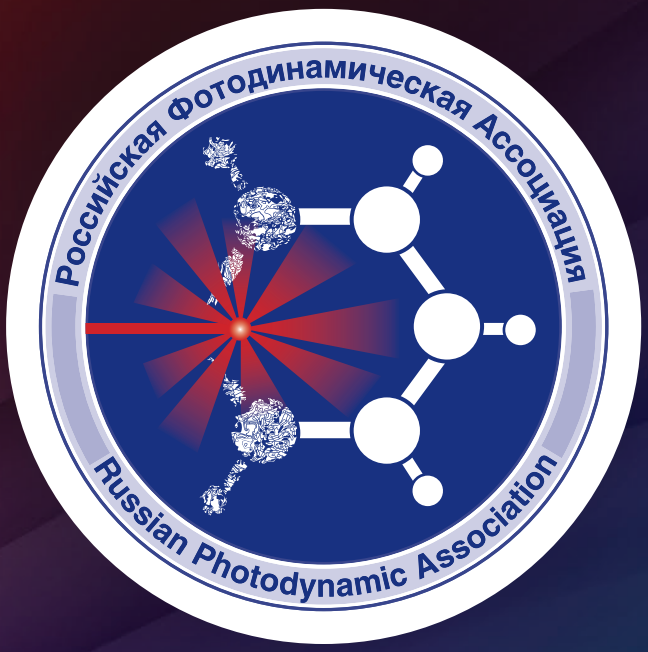

www.pdt-association.com

BIOMEDICAL PHOTONICS

BIOMEDICAL PHOTONICS –
research and practice, peer-reviewed, multidisciplinary journal.
The journal is issued 4 times per year.
The circulation – 1000 copies., on a quarterly basis.

The journal is included into the List of peer-reviewed science press of the State Commission for Academic Degrees and Titles of Russian Federation
The journal is indexed in the international abstract and citation database – Scopus.

The publisher «Agentstvo MORE».
Moscow, Khokhlovskiy lane, 9

Editorial staff:

Chief of the editorial staff	Ivanova-Radkevich V.I.
Science editor professor	Mamontov A.S.
Literary editor	Moiseeva R.N.
Translators	Kalyagina N.A.
Computer design	Kreneva E.I.
Desktop publishing	Shalimova N.M.

The Address of Editorial Office:
Russia, Moscow, 2nd Botkinskiy proezd, 3
Tel. 8 (495) 945–86–60
www: PDT-journal.com
E-mail: PDT-journal@mail.ru

Corresponding to:
125284, Moscow, p/o box 13

Registration certificate ПИ № ФС 77–51995, issued on 29.11.2012 by the Federal Service for Supervision of Communications, Information Technology, and Mass Media of Russia

The subscription index of «Rospechat» agency – 70249

BIOMEDICAL PHOTONICS

BIOMEDICAL PHOTONICS –
научно-практический, рецензируемый,
мультидисциплинарный журнал.
Выходит 4 раза в год.
Тираж – 1000 экз., ежеквартально.

Входит в Перечень ведущих рецензируемых научных журналов ВАК РФ.
Индексируется в международной реферативной базе данных Scopus.

Издательство «Агентство МОРЕ».
Москва, Хохловский пер., д. 9

Редакция:

Зав. редакцией	Иванова-Радкевич В.И.
Научный редактор	проф. Мамонтов А.С.
Литературный редактор	Моисеева Р.Н.
Переводчики	Калягина Н.А.
Компьютерный дизайн	Кренева Е.И.
Компьютерная верстка	Шалимова Н.М.

Адрес редакции:
Россия, Москва, 2-й Боткинский пр., д. 3
Тел. 8 (495) 945–86–60
www: PDT-journal.com
E-mail: PDT-journal@mail.ru

Адрес для корреспонденции:
125284, Москва, а/я 13

Свидетельство о регистрации ПИ
№ ФС 77–51995, выдано 29.11.2012 г.
Федеральной службой по надзору в сфере связи, информационных технологий и массовых коммуникаций (Роскомнадзор)

Индекс по каталогу агентства «Роспечать» – 70249

ORIGINAL ARTICLES

ОРИГИНАЛЬНЫЕ СТАТЬИ

REVIEWS OF LITERATURE

ОБЗОРЫ ЛИТЕРАТУРЫ

ORIGINAL ARTICLES

STUDY OF ACCUMULATION OF WATER-SOLUBLE ASYMMETRIC CATIONIC PORPHYRINS IN GRAM-POSITIVE WOUND INFECTION PATHOGENS DURING PHOTODYNAMIC INACTIVATION

Kvashnina D.V.[1], Shirokova I.Yu.[1], Belyanina N.A.[1], Syrbu S.A.[2], Lebedeva N.Sh.[2], Boeva Zh.V.[1], Burashnikova A.A.[1], Gorshkova E.N.[3], Razzorenova E.A.[3], Kovalishena O.V.[1], LazarevD.K.[1]
[1]Privolzhsky Research Medical University, Nizhny Novgorod, Russia
[2]G.A. Krestov Institute of Solution Chemistry of the Russian Academy of Sciences, Ivanovo, Russia
[3]National Research Lobachevsky State University of Nizhny Novgorod, Nizhny Novgorod, Russia

Abstract

The paper presents the results of a study on the accumulation of three different compounds of water-soluble asymmetric cationic porphyrins by the bacteria *S. aureus*, *S. epidermidis, S. haemolyticus* and *E. faecalis* using flow cytofluorimetry and fluorescence microscopy. The studied microorganisms were a sample (n=4) of isolates from biomaterial (wound discharge) from patients with wound infections (burn wound, trophic ulcer, infection of the surgical area, etc.). The tested strains showed resistance to 1-7 antibiotics, two strains were carriers of the *mecA* gene. Porphyrins containing heterocyclic fragments (benzoxazole, N-methyl benzimidazole, and benzothiazole residues) on the periphery of the porphyrin cycle can accumulate in bacterial cells to varying degrees: porphyrin with N-methyl benzimidazole penetrates bacteria to a greater extent, and the fluorescence signal is most intense for S. aureus and E. faecalis after incubation with this species. connections. There is some heterogeneity in the bacterial cell population with respect to the ability to accumulate porphyrins, and the presence of bacterial lysis has been proven. S aureus after incubation with S-porphyrin and subsequent photodynamic inactivation under the influence of light. The data obtained determine the prospects for further study of compounds and determination of their bactericidal potential.

Keywords: antimicrobial photodynamic inactivation, photochemistry, porphyrin, antibiotic resistance, wound infection, accumulation.

Contacts: Kvashnina D.V., e-mail: daria_tsariova@mail.ru

For citations: Kvashnina D.V., Shirokova I.Yu., Belyanina N.A., Syrbu S.A., Lebedeva N.Sh., Boeva Zh.V., Burashnikova A.A., Gorshkova E.N., Razzorenova E.A., Kovalishena O.V., Lazarev D.K. Study of accumulation of water-soluble asymmetric cationic porphyrins in gram-positive wound infection pathogens during photodynamic inactivation, *Biomedical Photonics*, 2025, vol. 14, no. 2, pp. 4–11. doi: 10.24931/2413–9432–2025–14–2–4–11

ИЗУЧЕНИЕ НАКОПЛЕНИЯ ВОДОРАСТВОРИМЫХ НЕСИММЕТРИЧНЫХ КАТИОННЫХ ПОРФИРИНОВ В ГРАМПОЛОЖИТЕЛЬНЫХ ВОЗБУДИТЕЛЯХ РАНЕВЫХ ИНФЕКЦИЙ ПРИ ФОТОДИНАМИЧЕСКОЙ ИНАКТИВАЦИИ

Д.В. Квашнина[1], И.Ю. Широкова[1], Н.А. Белянина[1], С.А. Сырбу[2], Н.Ш. Лебедева[2], Ж.В. Боева[1], А.А. Бурашникова[1], Е.Н. Горшкова[3], Е.А. Раззоренова[3], О.В. Ковалишена[1], Д.К. Лазарев[1]
[1]Федеральное государственное бюджетное образовательное учреждение высшего образования «Приволжский исследовательский медицинский университет» Министерства здравоохранения Российской Федерации, Нижний Новгород, Россия
[2]Федеральное государственное бюджетное учреждение науки Институт химии растворов им. Г.А. Крестова Российской академии наук, Иваново, Россия
[3]Федеральное государственное автономное образовательное учреждение высшего образования «Национальный исследовательский Нижегородский государственный университет им. Н.И. Лобачевского», Нижний Новгород, Россия

Резюме

В работе представлены результаты исследования по изучению накоплении трёх разных соединений водорастворимых несимметричных катионных порфиринов бактериями *S. aureus*, *S. epidermidis*, *S. haemolyticus* и *E. faecalis* с помощью проточной цитофлуориметрии и флуоресцентной микроскопии. Исследуемые микроорганизмы – выборка (n=4) изолятов из биоматериала (раневое отделяемое) от пациентов с раневыми инфекциями (ожоговая рана, трофическая язва, инфекция области хирургического вмешательства и др.). Тестируемые штаммы проявляли устойчивость к 1-7 антибиотикам, два штамма были носителями гена *mecA*. Порфирины, содержащие на периферии порфиринового цикла гетероциклические фрагменты (остатки бензоксазола, N-метил бензимидазола и бензотиазола), в разной степени способны накапливаться в бактериальных клетках: порфирин с N-метил бензимидазолом в большей степени проникает в клетки бактерий, и сигнал флуоресценции наибольшей интенсивности наблюдается для *S. aureus* и *E. faecalis* после инкубации с данным видом соединения. Наблюдается некоторая гетерогенность популяции бактериальных клеток в отношении способности накапливать порфирины, доказано наличие лизиса бактерий *S. aureus* после инкубации с фотосенсибилизатором и последующей фотодинамической инактивацией под действием света. Полученные данные определяют перспективы для дальнейшего изучения соединений и определения их бактерицидного потенциала.

Ключевые слова: антимикробная фотодинамическая инактивация, фотохимия, порфирин, антибиотикорезистентность, раневая инфекция, накопление.

Контакты: Квашнина Д.В., e-mail: daria_tsariova@mail.ru

Для цитирования: Квашнина Д.В., Широкова И.Ю., Белянина Н.А., Сырбу С.А., Лебедева Н.Ш., Боева Ж.В., Бурашникова А.А., Горшкова Е.Н., Раззоренова Е.А., Ковалишена О.В., Лазарев Д.К. Изучение накопления водорастворимых несимметричных катионных порфиринов в грамположительных возбудителях раневых инфекций при фотодинамической инактивации // Biomedical Photonics. – 2025. – Т. 14, № 2. – С. 4–11. doi: 10.24931/2413–9432–2025–14–2–4–11

Introduction

With the increasing resistance of microorganisms to antibiotics [1,2], there is a growing interest worldwide in alternative methods and biocides capable of overcoming the polyresistance of leading infectious agents. One promising area is antimicrobial photodynamic inactivation (PDI), based on photochemical reactions in which the main role is played by reactive oxygen species produced by molecules of a non-toxic dye or photosensitizer in the presence of low-intensity visible light to destroy microbial cells [3,4].

Antimicrobial photodynamic therapy, being a particular option of photodynamic therapy (PDT), has found its place in the fight against infectious diseases in various areas of clinical medicine: dentistry [5,6], dermatology [7-9], gynecology [10,11], urology [12], otolaryngology [13,14], etc.

In addition, in recent years, clinical interest has increased and serious scientific prerequisites for the use of PDI for the treatment of infected wounds of the skin and soft tissues have emerged. From a therapeutic point of view, this is determined by a number of advantages for the patient like high precision and selectivity of local action, low invasiveness, atraumatic nature, and additional effects in the form of stimulation of regeneration processes with acceleration of healing. From a microbiological point of view, it is important that this type of therapy can be used repeatedly with the same photosensitizer without any apparent risk of developing resistance, since at the moment there are no unambiguous reports that microorganisms exhibit resistance, in a certain sense of the word, to PDI. Moreover, although authors from different research teams [15-17] observed the effect of decreasing the susceptibility of the population of archival and clinical strains to sublethal doses of irradiation after several cycles of photoinactivation [15-17], this cannot be interpreted as the development of resistance to PDI, since when using more stringent experimental conditions (increasing the concentration of the photosensitizer and/or increasing the number of light doses), bacteria were destroyed [18].

Limitations in the active use of the antimicrobial PDI method in medical practice are associated with a shortage of non-toxic drugs with high bactericidal efficacy against planktonic and biofilm forms of microorganisms.

Studying the properties of experimental photosensitizers to find compounds with optimal antimicrobial activity that participate in the fight against resistant pathogens is a priority task in clinical, microbiological and epidemiological terms.

It is known that anionic, neutral and cationic photosensitizers are active against gram-positive bacteria, while only cationic ones have an effect on gram-negative bacteria [19]. Thus, to expand the spectrum of bactericidal action, it is more appropriate to use cationic photoinactivators.

The potential of water-soluble asymmetric cationic porphyrins is determined by the efficient production of singlet oxygen and the advantage of the possibility of chemical modification of peripheral substituents for selective binding to biotargets of microbial cells [19-21]. However, to understand the bactericidal potential of these compounds in an *in vitro* experiment, additional studies are needed, including studies of the

accumulation of the photosensitizer in microbial cells of clinical strains of microorganisms.

Studying the features of photochemical reactions in a population of antibiotic-resistant clinical strains of pathogens brings our experience closer to conducting preclinical studies *in vivo* and clinical trials.

It is extremely important to note that the scientific and practical task is not only to search for new compounds or modify existing molecules to maximize the quantum yield of singlet oxygen in *in vitro* tests, but also to study the molecular bonds inside microbial cells and the factors influencing differences in the susceptibility of microbes to photoinactivation [22]. The search for mechanisms, phenotypic and genotypic features underlying various microbial responses to photodynamic inactivation is an important problem of antimicrobial PDI, since even a population of one bacterial agent existing in one infection site is heterogeneous in its properties. Moreover subpopulations of the pathogen can exhibit different susceptibility to antimicrobial factors, including PDI, which can be determined by a number of factors: persistent cells are less susceptible to antimicrobial PDI than fast-growing ones, have a higher potential for producing antioxidant enzymes, etc. One of the main conditions determining the antimicrobial effect of PDI is the ability of cells to accumulate a photosensitizer.

The aim of the study is to study the features of porphyrin accumulation in cells of gram-positive antibiotic-resistant bacteria during PDI *in vitro*.

Materials and methods

This study is planned as an exploratory, comprehensive and multi-stage one. In the first stages of the work, a group of researchers from the G. A. Krestov Institute of Solution Chemistry of the Russian Academy of Sciences (Ivanovo) synthesized asymmetric water-soluble porphyrins containing heterocyclic fragments (benzoxazole, N-methyl benzimidazole and benzothiazole residues) [23] on the periphery of the porphyrin cycle using the C—H activation method. The experiments conducted on direct and reverse spectrophotometric titration of the interaction (binding) of albumin with monoheteryl-substituted porphyrins [23] allowed us to assume that porphyrins, when interacting with a bacterial cell, target surface proteins and the genetic material of microorganisms. These data served as the basis for further work.

This study presents the following research results: data on the accumulation of porphyrins *in vitro* in gram-positive bacteria using flow cytofluorometry and fluorescence microscopy.

Experimental studies were carried out at three bases:

1. synthesis of chemical compounds: Federal State Budgetary Scientific Institution G.A. Krestov Institute of Solution Chemistry of the Russian Academy of Sciences, Ivanovo;
2. microbiological studies on the isolation, identification and study of antibiotic resistance of microorganisms: bacteriological laboratory of the University Clinic of the Federal State Budgetary Educational Institution of Higher Education "Priority Medical University" of the Ministry of Health of the Russian Federation, Nizhny Novgorod;
3. studies on the accumulation of a photosensitizer in bacterial cells: Research Center of Molecular Biology and Biomedicine of the Federal State Autonomous Educational Institution of Higher Education "National Research Nizhny Novgorod State University named after N.I. Lobachevsky", Nizhny Novgorod.

In a series of laboratory experiments, the main objects of study were three different compounds of monoheteryl-substituted porphyrins and strains of gram-positive bacteria.

The porphyrins studied were:

1) 5-[4′-(1′′,3′′-benzothiazol-2′′-yl) phenyl]-10,15,20-tris(N-methylpyridin-3′-yl) porphyrin triiodide (S-por). PBS (phosphate buffered saline) (7.4) M=1176.73 C=1*10-5 mol/l;
2) 5-[4′-(1′′,3′′-benzoxazol-2′′-yl) phenyl]-10,15,20-tris(N-methylpyridin-3′-yl) porphyrin triiodide (O-por). PBS (7.4) M=1160.67 C=1*10-5 mol/l;
3) 5-[4-(N-methyl-1′′,3′′-benzimidazole-2′′-yl) phenyl]-10,15,20-tris(N-methyl-pyridin-3′-yl)-porphyrin triiodide (N-por). PBS (7.4) M=1173.74 C=1*10-5 mol/l.

The studied microorganisms are a sample (n=85) of microorganism isolates from biomaterial (wound discharge) of patients with wound infections. The experiment included clinical material from patients of the Burn Center and the Institute of Traumatology and Orthopedics of the University Clinic of the Federal State Budgetary Educational Institution of Higher Education "Privolzhsky Research Medical University (PRMU)" of the Ministry of Health of the Russian Federation with various purulent-septic infections of the skin and soft tissues (burn wound, trophic ulcer, surgical site infection, etc.). Species composition of the collection:

To study the features of porphyrin accumulation in bacterial cells, one strain of *S. aureus, S. epidermidis, S. haemolyticus,* and *E. faecalis.* were selected from the general population.

Species identification of microorganisms was carried out by MALDI-TOF mass spectrometry on the appropriate equipment (MALDI-TOF MS (Germany) and MALDI-TOF AUTOF MS1000 (Autobio, China)). The study of susceptibility to antibacterial drugs was carried out on a Vitek 2 bacteriological analyzer (France), with subsequent interpretation according to the adopted

rules of EUCAST (European Committee on Antimicrobial Susceptibility Testing) [24]. The prevalence of resistance genes was determined using the AmpliSens MDR MBL-FL and Litekh reagent kits (Russia) for the isolation of resistance genes by PCR with hybridization-fluorescence detection of amplification products in real time. The *mecA* gene was detected in staphylococci. The properties of the isolated strains (antibiotic resistance) were described using the version 2023 of the WHONET program.

To obtain data on the accumulation of porphyrins in bacterial cells, the following steps were performed:

1.1 Preparation of bacterial cell culture. An overnight culture of *S. aureus, S. epidermidis, S.haemolyticus* and *E. faecalis* was grown in sterile liquid LB medium (10 g of tryptone, 10 g of NaCl, 5 g of yeast extract (all from Sigma-Aldrich, USA)) for 16-18 h at 37 °C. The resulting suspension was centrifuged (10 min, 4000g) and diluted to a concentration of $1.5x10^8$ cells/ml in sterile 0.9% NaCl solution.

1.2 Incubation of bacterial cells with porphyrins. S-, O- and N-porphyrins were dissolved in sterile PBS (pH 7.4) (10 μM) and added to the bacterial suspension ($1.5x10^7$ cells/ml). For photoinactivation, the bacterial suspension was irradiated with LED lamps (20 W power) for 15 min at room temperature.

1.3 Evaluation of absorption and accumulation of porphyrins by bacteria. To assess the absorption of the studied porphyrins by bacteria after incubation, the bacteria were washed twice with sterile PBS (10 min, 4000 g, 4 °C) and the resulting suspension was analyzed using a Cytoflex S flow cytometer (Beckman Coulter, USA) and CytExpert 1.2.10.0 software (Beckman Coulter, USA).

The accumulation of porphyrins was estimated based on the average values of the fluorescence signal (mean fluorescence intensity, MFI), measured in relative units and recorded for *S. aureus, S. epidermidis, S. haemolyticus* and *E. faecalis bacteria* after treatment with S-, O- and N-porphyrins after 15 minutes of light irradiation. For fluorescence analysis using microscopy, a bacterial suspension ($1.5x10^7$ cells/ml) after incubation with 10 μM solutions of S-, O-, and N-porphyrins was centrifuged (5 min, 4000 g, 4 °C). The pellet was resuspended in sterile PBS (pH 7.4) and applied to glass slides.

A drop containing the bacterial suspension was dried in air, fixed in a burner flame, then placed in Faramount Mounting Medium (Agilent, USA) and covered with a coverslip. The study was carried out on an LSM 800 setup (Carl Zeiss, Germany) using ZEISS Axio Vert.A1 software (Carl Zeiss, Germany). The accumulation of porphyrins was assessed by the presence of fluorescence (excited using a 488 nm laser, the fluorescent signal was detected in the wavelength range of 640-740 nm using appropriate optical filters).

Statistical data processing was performed in the R environment (Rstudio 1.1.463), and GraphPad Prism 8.4.3 software (GraphPad Software, USA) was used for data visualization. Two-way analysis of variance was used to compare mean fluorescent signal (MFI) values. The level of statistical significance of differences in hypothesis testing was chosen at $p \leq 0.05$.

Results and discussion

The tested strains (n=4) showed resistance to 1-7 antibiotics. The resistance profiles of the selected cultures are presented in Table 1. Two strains (*S.haemolyticus* 525, *S.epidermidis* 7) were resistant to cefoxitin, which is an alarming microbiological and clinical sign, since, according to the EUCAST guidelines, resistance to this antibiotic is a sign of resistance to the entire group of penicillins. At the same time, these strains were carriers of the *mecA* gene.

In an *in vitro* experiment to study the accumulation of porphyrins by bacterial cells of clinical strains of *S. aureus*, *E. faecalis*, *S. epidermidis* and *S. haemolyticus* using

Таблица 1
Профили антибиотикорезистентности клинических штаммов

Table 1
Profiles of antibiotic resistance of clinical strains

Микроорганизм и идентификационный номер по лабораторному журналу / результаты ПЦР The microorganism and the identification number according to the laboratory journal / PCR results	Профиль резистентности Resistance profile
S.aureus 229 / бета-лактамазы +	B_--__PL_-___H__
S.epidermidis 7 / *mecA*+	-_--XGPLN-_Z_H_-
S.haemolyticus 525 / *mecA*+	----X----------
E. faecalis 2025	--_- G-_NM_-_---

В столбце «Профиль резистентности» использована знаковая система: «буква» – резистентность или промежуточная чувствительность к определенному антибиотику; «_» – чувствительность; «-» – чувствительность не определялась. Расшифровка буквенных кодов в профилях резистентности: B – бензилпенициллин; R – рифампицин; C – цефтриаксон; F – цефотаксим; X – цефокситин; G – гентамицин; P – ципрофлоксацин; L – левофлоксацин; N – клиндамицин; M – линкомицин; E – эритромицин; Z – линезолид; V – ванкомицин; H – хлорамфеникол; T – тетрациклин; Y – тигециклин. «mecA+» – у штамма обнаружен соответствующий ген.

The column "resistance profile" uses a sign system: "letter" – resistance or intermediate sensitivity to a particular antibiotic; "_" – sensitivity; "-" – sensitivity to a particular antibiotic. Interpretation of letter codes in resistance profiles: B – benzylpenicillin; R – rifampicin; c – ceftriaxone; F – cefotaxime; X – cefoxitin; G – gentamicin; P – vrofloxacin; L – levofloxacin; N – clindamycin; M – lincomycin; e – erythromycin; Z – linezolid; V – vancomycin; H – chloramphenicol; T – tetracycline; Y – tigrecycline. XR – resistance to cefoxitin. "mecA+" – the corresponding gene was found in the strain.

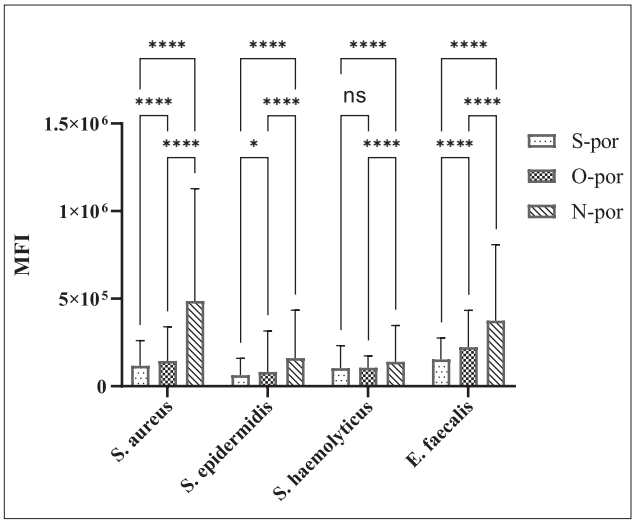

cytofluorimetric analysis, it was found that N-porphyrin accumulates in bacterial cells to a greater extent than S- and O-porphyrins, as evidenced by the increasing mean fluorescence intensity (MFI) in the series S-porphyrin > O-porphyrin > N-porphyrin (Fig. 1).

Рис. 1. Значения среднего флуоресцентного сигнала (MFI), регистрируемого для бактерий *S. aureus, S. epidermidis, S. haemolyticus* и *E. faecalis* после обработки S-, O- и N-порфиринами через 15 минут облучения светом (статистика: двухфакторный дисперсионный анализ, *– p<0,05; ****– p<0,0001, данные отображают среднее и стандартное отклонение).

Fig. 1. The values of the average fluorescent signal (MFI) recorded for *S. aureus, S. epidermidis, S. haemolyticus* and *E. faecalis* bacteria after treatment with S-, O-, and N-porphyrins after 15 minutes of light exposure (statistics: two–factor analysis of variance, *– p<0.05; ****– p<0.0001, the data shows the mean and standard deviation).

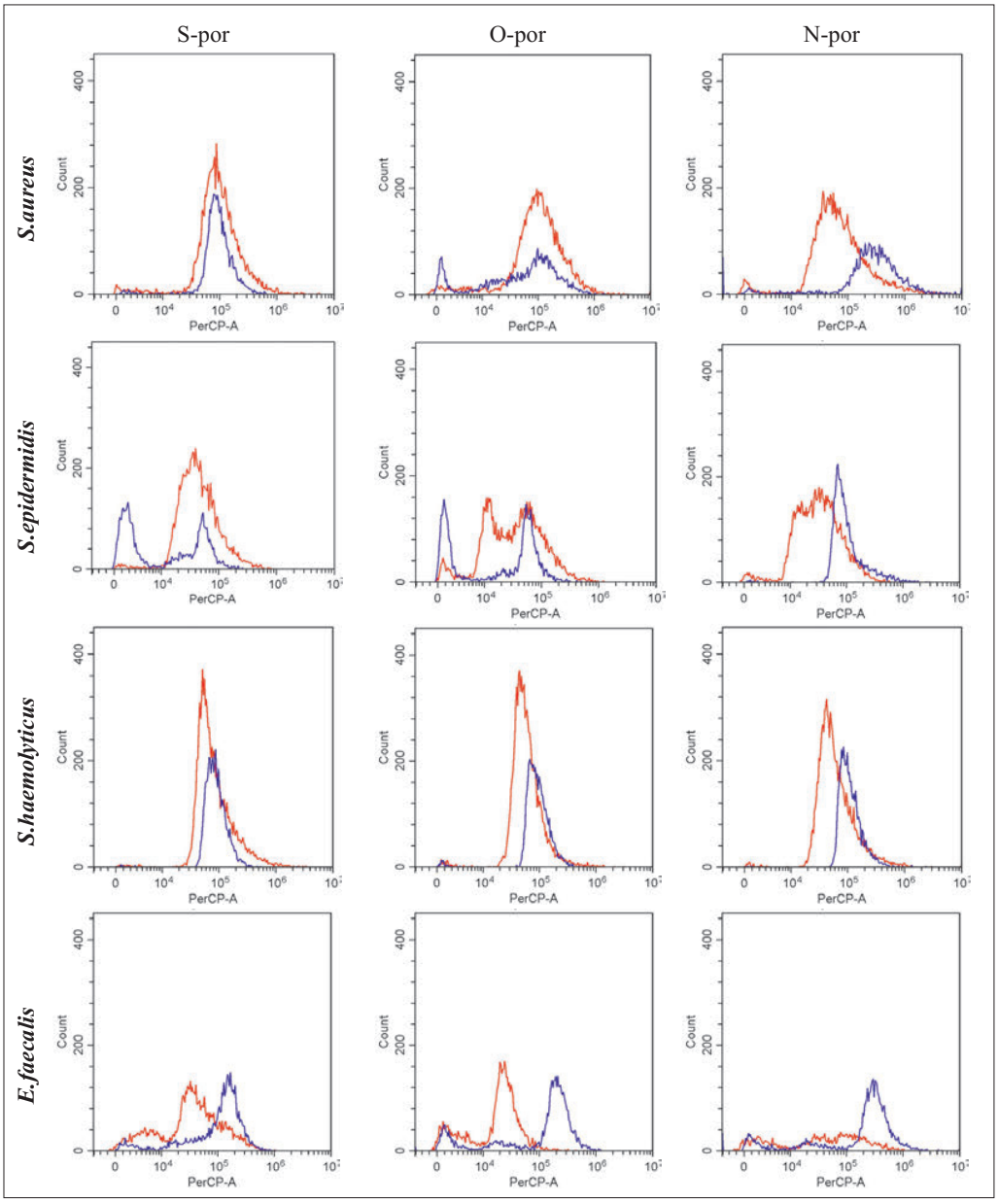

Рис. 2. Репрезентативные гистограммы флуоресценции бактерий *S. aureus, S. epidermidis, S. haemolyticus* и *E. faecalis* после обработки S-, O- и N-порфиринами: ■ – до обработки светом, ■ – после обработки светом 15 мин.

Fig. 2. Representative histograms of fluorescence of *S. aureus, S. epidermidis, S. haemolyticus* and *E. faecalis* bacteria after treatment with S-, O- and N-porphyrins: ■ –before light treatment, ■ – after light treatment for 15 min.

Moreover, for *S. aureus* and *E. faecalis*, the mean fluorescence intensities were higher than for *S. epidermidis* and *S. haemolyticus*. Also, for *S. epidermidis* and *S. haemolyticus*, the difference between S- and O-porphyrin accumulation was not as significant (5% difference in significance for *S. epidermidis* and no difference for *S. haemolyticus*) than *for S. aureus* and *E. faecalis*.

Representative graphs obtained during cytofluorometric analysis are shown in Fig. 2. The graphs demonstrate that the fluorescence peak is shifted along the PerCP-A axis to the right for N-porphyrin to a greater extent than for S- and O-porphyrin. Moreover, in accordance with Fig. 1, in Fig. 2 it is observed that this shift is more pronounced for *S. aureus* and *E. faecalis*, which is probably due to the greater accumulation of N-porphyrin by these cells.

For *S. aureus, S. epidermidis* and *S. haemolyticus*, the graphs demonstrate a decrease in the peak height and/or the appearance of an additional peak, which probably characterizes the presence of cells that do not accumulate S- and O-porphyrins or accumulate them to a lesser extent.

Using fluorescence microscopy, data were obtained confirming the fact of accumulation of the porphyrins used in the work by *S. aureus*, *S. epidermidis, S. haemolyticus* and *E. faecalis* (Fig. 3).

We also observed that some cells accumulate porphyrins to a lesser extent than the main population (Fig. 4a), which confirms the data obtained using flow cytofluorimetry on the presence of cells with lower fluorescence intensity or its absence in the population. In addition, it was shown that coincubation with porphyrins followed by photoinactivation leads to cell lysis (Fig. 4b), which determines the bactericidal potential of the studied compounds.

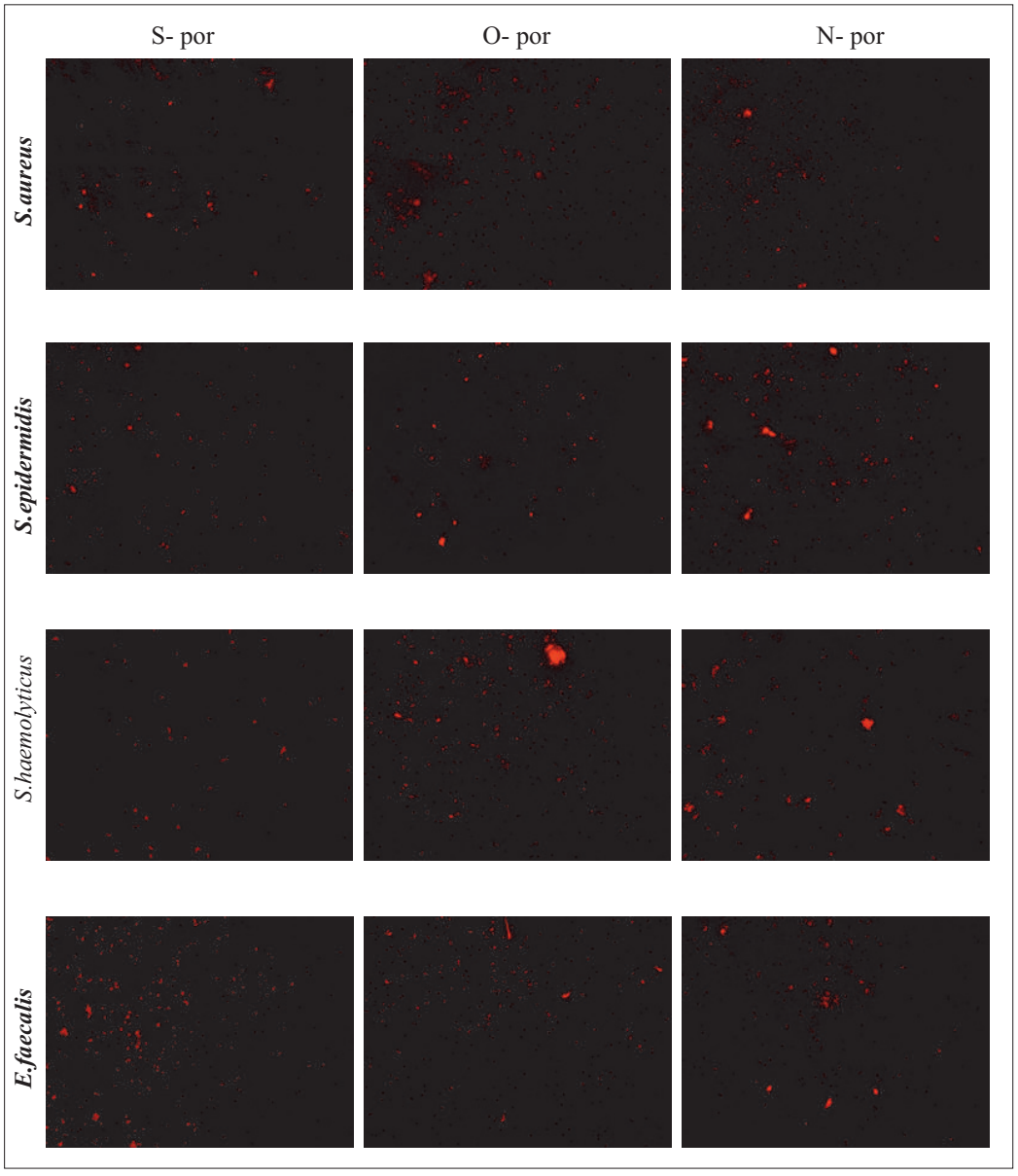

Рис. 3. Репрезентативные микрофотографии флуоресценции бактерий *S. aureus, S. epidermidis, S. haemolyticus* и *E. faecalis* после обработки S-, O- и N-порфиринами (данные получены с помощью микроскопа ZEISS Axio Vert.A1 (Carl Zeiss, Германия), увеличение 40x).

Fig. 3. Representative micrographs of the fluorescence of *S. aureus, S. epidermidis, S. haemolyticus* and *E. faecalis* bacteria after treatment with S-, O- and N-porphyrins (data obtained using a ZEISS Axio Vert. A1 microscope (Carl Zeiss, Germany), magnification 40x).

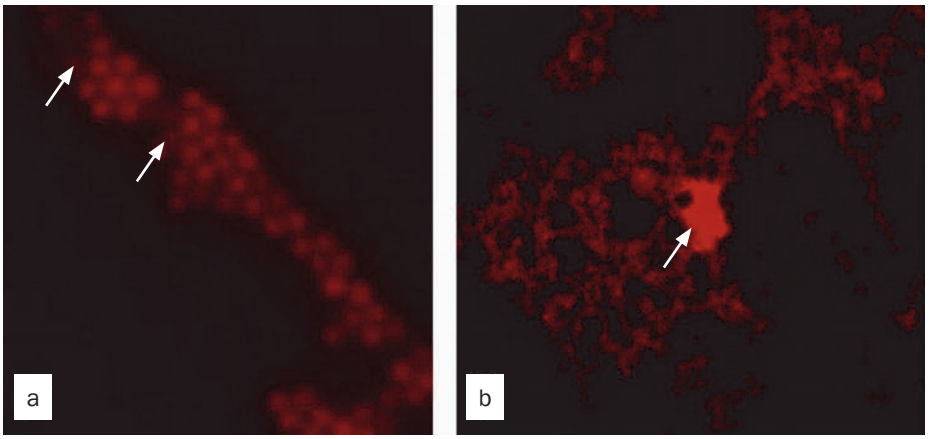

Рис. 4. Репрезентативные микрофотографии флуоресценции бактерий *S. aureus* после обработки S-порфирином, демонстрирующие (а) различия в интенсивности флуоресценции для отдельных бактерий (увеличение 100х), (б) наличие лизиса бактерий (увеличение 40х).
Fig. 4. Representative micrographs of *S. aureus* fluorescence after S-porphyrin treatment, showing (a) differences in fluorescence intensity for individual bacteria (magnification of 100x), (b) the presence of bacterial lysis (magnification of 40x).

In experimental conditions, evidence was obtained that the population of antibiotic-resistant microorganisms – causative agents of wound infections, is heterogeneous in its ability to accumulate porphyrin, which means that the bactericidal effect can also vary. This is important for further research and determining the basic parameters of antimicrobial PDI using porphyrins in patients with infection. Namely, it is necessary to more carefully approach the development of exposure conditions (volume and concentration of the photosensitizer, irradiation time), since it is possible for some part (subpopulation) of microorganisms to survive after irradiation.

Conclusion

Based on the results of the *in vitro* experiment, it was determined that asymmetrical water-soluble porphyrins containing heterocyclic fragments (benzoxazole, N-methyl benzimidazole and benzothiazole residues) on the periphery of the porphyrin cycle are able to accumulate in bacterial cells to varying degrees. The study assessed the accumulation of S-, O-, and N-porphyrins by *S. aureus, S. epidermidis, S. haemolyticus,* and *E. faecalis bacteria* using flow cytometry and fluorescence microscopy. It was confirmed that the porphyrins used were able to accumulate in bacterial cells, and a comparison of their accumulation efficiency in different types of gram-positive bacteria was performed.

It was shown that N-porphyrin penetrates bacteria to a greater extent, and the fluorescence signal of the highest intensity is observed for *S. aureus* and *E. faecalis* after incubation with this type of porphyrin. The data obtained were confirmed by fluorescence microscopy. It was also found that there is some heterogeneity in the bacterial cell population with respect to the ability to accumulate water-soluble asymmetric cationic porphyrins, and the presence of lysis of *S. aureus* bacteria after incubation with S-porphyrin and subsequent photodynamic inactivation under the light was demonstrated.

The study was supported by the Russian Science Foundation grant No. 23-75-01087, https://rscf.ru/project/23-75-01087/.

REFERENCES

1. World health statistics 2024: monitoring health for the SDGs, Sustainable Development Goals // Geneva: World Health Organization. – 2024. Licence: CC BY-NC-SA 3.0 IGO.
2. European Centre for Disease Prevention and Control. *Antimicrobial resistance in the EU/EEA (EARS-Net) – Annual Epidemiological Report*, 2023. *Stockholm: ECDC*, 2024.
3. Kharkwal G.B., Sharma S.K., Huang Y.Y., et al. Photodynamic therapy for infections: clinical applications. *Lasers Surg Med*, 2011, Vol. 43(7), pp. 755-67. https://doi.org/10.1002/lsm.21080.
4. Semyonov D.Yu., Vasil'ev Yu.L., Dydykin S.S. et al. Antimicrobial and antimycotic photodynamic therapy (review of literature). *Biomedical,* 2021, Vol. 10(1), pp. 25-31. https://doi.org/10.24931/2413-9432-2021-10-1-25-31
5. Mishutina O.L., Volchenkova G.V., Kovaleva N.S., et al. Photodynamic therapy in dentistry (literature review). *Smolensk Medical Almanac*, 2019, Vol. 3, pp. 102-111. (In Russian) – EDN PMCRWJ.
6. Risovannaya O.N., Andreasyan T.Sh. Photodynamic therapy – modern views and innwovations in dentistry. *Medical alphabet*, 2024, Vol. (18), pp. 78-84. (In Russian) https://doi.org/10.33667/2078-5631-2024-18-78-84
7. Morgado L.F., Travolo A.R.F., Muehlmann L.A., et al. Photodynamic Therapy treatment of onychomycosis with Aluminium-Phthalo-

ЛИТЕРАТУРА

1. World health statistics 2024: monitoring health for the SDGs, Sustainable Development Goals // Geneva: World Health Organization. – 2024. Licence: CC BY-NC-SA 3.0 IGO.
2. European Centre for Disease Prevention and Control // Antimicrobial resistance in the EU/EEA (EARS-Net) – Annual Epidemiological Report 2023. Stockholm: ECDC. – 2024.
3. Kharkwal G.B., Sharma S.K., Huang Y.Y., et al. Photodynamic therapy for infections: clinical applications // Lasers Surg Med. – 2011. – Vol. 43(7). – P. 755-67. https://doi.org/10.1002/lsm.21080.
4. Semyonov D.Yu., Vasil'ev Yu.L., Dydykin S.S. et al. Antimicrobial and antimycotic photodynamic therapy (review of literature) // Biomedical Photonics. – 2021. – Vol. 10(1). – P. 25-31. https://doi.org/10.24931/2413-9432-2021-10-1-25-31
5. Мишутина О. Л., Волченкова Г.В., Ковалева Н.С. и др. Фотодинамическая терапия в стоматологии (обзор литературы) // Смоленский медицинский альманах. – 2019. – №3. – С.102-111. – EDN: PMCRWJ.
6. Рисованная, О. Н. Фотодинамическая терапия – современные взгляды и новшества в стоматологии / О. Н. Рисованная, Т. Ш. Андреасян // Медицинский алфавит. – 2024. – № 18. – С. 78-84. https://doi.org/10.33667/2078-5631-2024-18-78-84
7. Morgado L.F., Travolo A.R.F., Muehlmann L.A., et al. Photodynamic Therapy treatment of onychomycosis with Aluminium-Phthalocyanine

cyanine Chloride nanoemulsions: A proof of concept clinical trial. *J Photochem Photobiol B.*, 2017, Vol. 173, pp. 266-270. https://doi.org/10.1016/j.jphotobiol.2017.06.010.
8. La Selva A., Negreiros R.M, Bezerra D.T., et al. Treatment of herpes labialis by photodynamic therapy: Study protocol clinical trial (SPIRIT compliant). *Medicine (Baltimore)*, 2020, Vol. 99 (12), pp. e19500. https://doi.org/10.1097/MD.0000000000019500.
9. Galinari C.B., Conrado P.C.V., Arita G.S., et al. Nanoencapsulated hypericin in P-123 associated with photodynamic therapy for the treatment of dermatophytosis. *J Photochem Photobiol B.*, 2021, Vol. 215, pp. 112103. https://doi.org/10.1016/j.jphotobiol.2020.112103.
10. Maldonado A.E., Osorio Peralta M.O., Moreno V.A., et al. Effectiveness of Photodynamic Therapy in Elimination of HPV-16 and HPV-18 Associated with CIN I in Mexican Women. *Photochem Photobiol*, 2017, Vol. 93(5), pp.1269-1275. https://doi.org/10.1111/php.12769.
11. Shanazarov N.A., Zinchenko S.V., Kisikova S.D., et al. Photodynamic therapy in the treatment of HPV-associated cervical cancer: mechanisms, challenges and future prospects. *Biomedical Photonics*, 2024, Vol. 13(1), pp. 47-55. https://doi.org/10.24931/2413-9432-2023-13-1-47-55
12. Streltsova O.S., Antonian A.E., Sedova E.S., et al. Method of treating patients with chronic recurrent bacterial cystitis. Patent RU2820135 C1. 29.05.2024. EDN ITHDET.
13. Logunova E.V., Egorov V.I., Nasedkin A.N., et al. The use of the enzymes for the enhancement of the effectiveness of antimicrobial photodynamic treatment of the patients presenting with chronic tonsillitis. *Russian Bulletin of Otorhinolaryngology*, 2016, Vol. 81(2), pp. 44-48. (In Russian) https://doi.org/10.17116/otorino201681244-48
14. Plavskii V.Y., Plavskaya L.G., Dudinova O.N., et al. Endogenous Photoacceptors Sensitizing Photobiological Reactions in Somatic Cells. *Zhurnal Prikladnoii Spektroskopii*, 2023, Vol. 90(2), pp. 239-252. (In Russian) https://doi.org/10.47612/0514-7506-2023-90-2-239-252
15. Guffey J.S, Payne W., Jones T., et al. Evidence of resistance development by Staphylococcus aureus to an in vitro, multiple stage application of 405 nm light from a supraluminous diode array. *Photomed Laser Surg*, 2013, Vol. 31, pp. 179-82. https://doi.org/10.1089/pho.2012.3450
16. Amin R.M., Bhayana B., Hamblin M.R., et al. Antimicrobial blue light inactivation of Pseudomonas aeruginosa by photo-excitation of endogenous porphyrins: In vitro and in vivo studies. *Lasers Surg Med*, 2016, Vol. 48, pp. 562-568. https://doi.org/10.1002/lsm.22474
17. Pieranski M., Sitkiewicz I., Grinholc M. Increased photoinactivation stress tolerance of Streptococcus agalactiae upon consecutive sublethal phototreatments. *Free Radic Biol Med*, 2020, Vol. 160, pp. 657-69. https://doi.org/10.1016/j.freeradbiomed.2020.09.003
18. Rapacka-Zdonczyk A., Wozniak A., Pieranski M., et al. Development of Staphylococcus aureus tolerance to antimicrobial photodynamic inactivation and antimicrobial blue light upon sub-lethal treatment. *Sci Rep*, 2019, Vol. 9, pp.1-18. https://doi.org/10.1038/s41598-019-45962-x
19. Tiganova I.G., Makarova E.A., Meerovich G.A., et al. Photodynamic inactivation of pathogenic bacteria in biofilms using new synthetic bacteriochlorin derivatives. *Biomedical Photonics*, 2017, Vol. 6(4), pp. 27-36. (In Russian) https://doi.org/10.24931/2413-9432-2017-6-4-27-36
20. Lebedeva N.S., Gubarev Y.A., Koifman M.O., et al. The Application of Porphyrins and Their Analogues for Inactivation of Viruses. *Molecules*, 2020, Vol. 2325(19), pp. 4368. https://doi.org/10.3390/molecules25194368.
21. Lebedeva N. Sh., Koifman O. I. Supramolecular Systems Based on Macrocyclic Compounds with Proteins. Application Prospects. *J. Bioorg. Chem*. 2022, Vol. 48(1), pp. 3-31. (In Russian) https://doi.org/10.1134/S1068162022010071
22. Rapacka-Zdończyk A., Woźniak A., Michalska K., et al. Factors Determining the Susceptibility of Bacteria to Antibacterial Photodynamic Inactivation. *Front Med (Lausanne)*, 2021, Vol. 8, pp. 642609. https://doi.org/10.3389/fmed.2021.642609
23. Kiselev A.N., Lebedev M.A., Syrbu S.A., et al. Synthesis and study of water-soluble asymmetric cationic porhyrins as potential photoinactivators of pathogens. *Russian Chemical Bulletin*. 2022, Vol. 12, pp. 2691-2700. (In Russian)
24. The European Committee on Antimicrobial Susceptibility Testing. Breakpoint tables for interpretation of MICs and zone diameters. Version 13.0, 2023. http://www.eucast.org.

Chloride nanoemulsions: A proof of concept clinical trial // J Photochem Photobiol B. – 2017. – Vol. 173. – P. 266-270. https://doi.org/10.1016/j.jphotobiol.2017.06.010.
8. La Selva A., Negreiros R.M, Bezerra D.T., et al. Treatment of herpes labialis by photodynamic therapy: Study protocol clinical trial (SPIRIT compliant) // Medicine (Baltimore). – 2020. – P. 99 (12): e19500. https://doi.org/10.1097/MD.0000000000019500.
9. Galinari C.B., Conrado P.C.V., Arita G.S., et al. Nanoencapsulated hypericin in P-123 associated with photodynamic therapy for the treatment of dermatophytosis. J Photochem Photobiol B. – 2021. – Vol. 215. – P. 112103. https://doi.org/10.1016/j. jphotobiol.2020.112103.
10. Maldonado A.E., Osorio Peralta M.O., Moreno V.A., et al. Effectiveness of Photodynamic Therapy in Elimination of HPV-16 and HPV-18 Associated with CIN I in Mexican Women // Photochem Photobiol. – 2017. – Vol. 93(5). – P. 1269-1275. https://doi.org/10.1111/php.12769.
11. Shanazarov N.A., Zinchenko S.V., Kisikova S.D., et al. Photodynamic therapy in the treatment of HPV-associated cervical cancer: mechanisms, challenges and future prospects // Biomedical Photonics. – 2024. – Vol. 13(1). – P. 47-55. https://doi.org/10.24931/2413-9432-2023-13-1-47-55
12. Патент № 2820135 C1 Российская Федерация, МПК A61N 5/067, A61K 33/14, A61M 25/10. Способ лечения больных хроническим рецидивирующим бактериальным циститом: № 2023122177: заявл. 25.08.2023: опубл. 29.05.2024 / Стрельцова О.С., Антонян А.Э., Седова Е.С. [и др.]; заявитель федеральное государственное бюджетное образовательное учреждение высшего образования «Приволжский исследовательский медицинский университет» Министерства здравоохранения Российской Федерации.
13. Логунова Е.В., Егоров В.И., Наседкин А.Н и др. Использование ферментов с целью повышения эффективности антимикробной фотодинамической терапии больных хроническим тонзиллитом // Вестник оториноларингологии. – 2016. – № 81(2). – С.44-48. https://doi.org/10.17116/otorino201681244-48
14. Плавский В.Ю., Плавская Л.Г., Дудинова О.Н. и др. Эндогенные фотоакцепторы, сенсибилизирующие фотобиологические реакции в соматических клетках // Журнал прикладной спектроскопии. – 2023. – № 90(2). – С. 239-252. https://doi.org/10.47612/0514-7506-2023-90-2-239-252
15. Guffey J.S, Payne W., Jones T., et al. Evidence of resistance development by Staphylococcus aureus to an in vitro, multiple stage application of 405 nm light from a supraluminous diode array // Photomed Laser Surg. – 2013. – Vol. 31. – P. 179-82. https://doi.org/10.1089/pho.2012.3450
16. Amin R.M., Bhayana B., Hamblin M.R., et al. Antimicrobial blue light inactivation of Pseudomonas aeruginosa by photo-excitation of endogenous porphyrins: In vitro and in vivo studies // Lasers Surg Med. – 2016. – Vol. 48. – P. 562-568. https://doi.org/10.1002/lsm.22474
17. Pieranski M., Sitkiewicz I., Grinholc M. Increased photoinactivation stress tolerance of Streptococcus agalactiae upon consecutive sublethal phototreatments // Free Radic Biol Med. – 2020. – Vol. 160. – P. 657-69. https://doi.org/10.1016/j.freeradbiomed.2020.09.003
18. Rapacka-Zdonczyk A., Wozniak A., Pieranski M., et al. Development of Staphylococcus aureus tolerance to antimicrobial photodynamic inactivation and antimicrobial blue light upon sub-lethal treatment // Sci Rep. – 2019. – Vol. 9. – P.1-18. https://doi.org/10.1038/s41598-019-45962-x
19. Тиганова И.Г., Макарова Е.А., Меерович Г.А. и др. Фотодинамическая инактивация патогенных бактерий в биопленках с использованием новых синтетических производных бактериохлорина // Biomedical Photonics. – 2017. – Т. 6, № 4. – С. 27-36.
20. Lebedeva N.S., Gubarev Y.A., Koifman M.O., et al. The Application of Porphyrins and Their Analogues for Inactivation of Viruses // Molecules. – 2020. – vol. 23. – no.25(19). – P. 4368. https://doi.org/10.3390/molecules25194368.
21. Лебедева Н.Ш., Койфман О.И. Супрамолекулярные системы на основе макроциклических соединений с протеинами. Перспективы применения. // Биоорганическая химия. – 2022. – Vol. 48(1). – P. 3-31. https://doi.org/10.31857/S0132342322010079.
22. Rapacka-Zdończyk A., Woźniak A., Michalska K., et al. Factors Determining the Susceptibility of Bacteria to Antibacterial Photodynamic Inactivation // Front Med (Lausanne). – 2021. – Vol. 8. – P. 642609. https://doi.org/10.3389/fmed.2021.642609.
23. Киселев А.Н., Лебедев М.А., Сырбу С.А. и др. Синтез и исследование водорастворимых несимметричных катионных порфиринов как потенциальных фотоинактиваторов патогенов // Известия Академии наук. Серия химическая. – 2022. – № 12. – С. 2691-2700.
24. Европейский комитет по определению чувствительности к антимикробным препаратам. Таблицы пограничных значений для интерпретации значений МПК и диаметров зон подавления роста. Версия 13.0, 2023. – URL: https://www.antibiotic.ru/library/eucast-eucast-clinical-breakpoints-bacteria-13-0-rus/ (дата обращения: 18.02.2024)

ORIGINAL ARTICLES

LOCAL SCATTERING ANISOTROPY OF THE SKIN AS A POSSIBLE FACTOR OF FLUORESCENCE BORDERS DISTORTION OF NEOPLASMS

Kiryushchenkova N.P.[1], **Novikov I.A.**[1,2]
[1]M.M. Krasnov Research Institute of Eye Diseases, Moscow, Russia
[2]Prokhorov General Physics Institute of Russian Academy of Sciences, Moscow, Russia

Abstract

The use of protoporphyrin IX fluorescence imaging in skin tumors is limited by the complexity of light propagation in tissues. A non-invasive scattering anisotropy test (comparison of the fluorescence pattern of a tumor with that of a point source applied to the same spot) would be useful in distinguishing between cases of subsurface tumor growth and local fluorescence pattern distortions. However, the knowledge is missing of whether the distribution from an external light source would be representative. The experiment described here addressed the correlation between patterns in which light is dispersed from an external and an internal source within the same area of the skin. A pig's head was chosen as the model. Four zones of interest were identified, all different in optical properties. The wavelength of the light source was selected as to simulate the PpIX fluorescence. The correspondence of light distribution patterns was quantified using the correlation method. The results have clearly demonstrated the strong relationship between the fluorescence distribution pattern of a tumor and the condition/topography of the surrounding tissues and proved the possibility of using an external light source to assess the local scattering anisotropy of the skin *in vivo*.

Keywords: scattering anisotropy, skin neoplasm, fluorescence, tumor border, protoporphyrin IX.

Contacts: Nataliya Kiryushchenkova, e-mail: nkir@niigb.ru

For citations: Kiryushchenkova N.P., Novikov I.A. Local scattering anisotropy of the skin as a possible factor of fluorescence borders distortion of neoplasms, *Biomedical Photonics*, 2025, vol. 14, no. 2, pp. 12–20. doi: 10.24931/2413–9432–2025–14–2–12–20

ЛОКАЛЬНАЯ АНИЗОТРОПИЯ РАССЕЯНИЯ КОЖИ КАК ВОЗМОЖНЫЙ ФАКТОР ИСКАЖЕНИЯ ФЛУОРЕСЦЕНТНЫХ ГРАНИЦ ОПУХОЛИ

Н.П. Кирющенкова[1], **И.А. Новиков**[1,2]
[1]Научно-исследовательский институт глазных болезней им. М.М. Краснова, Москва, Россия
[2]Институт общей физики им. А.М. Прохорова Российской академии наук, Москва, Россия

Резюме

Широкое применение диагностики новообразований кожи на основе анализа флуоресценции протопорфирина IX ограничено сложностью распространения, в частности рассеяния, света в тканях. Для оценки влияния локальной анизотропии рассеяния кожи на картину флуоресценции опухоли предлагается производить сравнение последней с флуоресцентной картиной распространения света от точечного источника, приложенного к поверхности кожи в проекции опухоли. Такой тест был бы полезен для выявления случаев скрытого роста новообразования, однако, репрезентативность его неизвестна. В описанном здесь эксперименте изучалась корреляция между паттернами рассеяния света от внешнего и внутреннего источника в пределах одного и того же участка кожи. Моделью служила голова свиньи. Четыре зоны интереса с различными оптическими свойствами были подобраны с учетом строения средней трети лица человека. Длина волны источника света была выбрана так, чтобы имитировать флуоресценцию протопорфирина IX. Соответствие моделей распределения света было определено количественно корреляционным методом. Полученные результаты наглядно продемонстрировали сильную взаимосвязь между характером распределения флуоресценции опухоли и состоянием/топографией окружающих тканей и доказали возможность использования внешнего источника света для оценки локальной анизотропии рассеяния кожи *in vivo*.

Ключевые слова: анизотропия рассеяния, новообразование кожи, флуоресценция, граница опухоли, протопорфирин IX.

Контакты: Кирющенкова Н.П., nkir@niigb.ru

Для цитирования: Кирющенкова Н.П., Новиков И.А. Локальная анизотропия рассеяния кожи как возможный фактор искажения флуоресцентных границ опухоли // Biomedical Photonics. – 2025. – Т. 14, № 2. – С. 12–20. doi: 10.24931/2413–9432–2025–14–2–12–20

Introduction

Malignant skin neoplasms, well-known for their high incidence worldwide, mainly include basal cell carcinoma (BCC) and other tumors of epithelial origin [1,2]. Close attention is paid to accurately defining tumor borders and optimal surgical margins due to the frequent head and neck localization of BCC and associated complicacy of its removal [3,4].

Biomedical fluorescence imaging, or fluorescence diagnostics, is a compact area of research aimed at assessing tissue concentrations of pathology markers by exciting their characteristic emission. In oncology, one such marker is protoporphyrin IX (PpIX), a precursor of heme, which is known to accumulate in rapidly dividing cells [5-12]. PpIX fluorescence imaging allows detection of increased proliferative activity of the tissue and potentially can help identify areas of subsurface tumor growth [13-15]. Most of the existing techniques of endogenous PpIX fluorescence analysis involve the use of fluorescence induction [13,14], but some authors prefer to work with non-induced endogenous signals [15]. Regardless, the final result of fluorescence imaging greatly depends on skin properties such as the preferential orientation of collagen fibres in the dermis [16-23]. The complexity of light propagation in the skin constrains the development of fluorescence imaging as a diagnostic modality.

We believe that the impact of scattering anisotropy of the skin could be addressed by comparing the actual fluorescence distribution pattern of a tumor with that of a point source emitting at same wavelengths within the same location. In an abstract isotropic model, radiation from a point source would be evenly distributed in all directions and brightness isolines would have the shape of a circle in any section. In reality, however, skin projection of a point light source would not match its original geometry due to scattering anisotropy of the medium. All the distortions thus determined, could then be used to interpret the fluorescence diagnostics results.

Given the absolute impossibility of introducing a point light source directly into a tumor in vivo, we propose that the source may be externally applied to the skin surface. We assume that the light propagation from an internal and an external source will have a high degree of agreement in our case, and thus, the surface source will serve as an acceptable model of intradermal neoplasm fluorescence.

The aim of this study was to prove our assumption and to determine experimentally the correlation between patterns in which light is dispersed from an external and an internal source within the same area of the skin.

Material and methods

A pig's head (collected at a meat processing plant 12 hours after death) was chosen as the model. The head was divided in two parts along the sagittal suture, the brain was removed.

Optical scheme

Light source: we used a 560-660 nm incoherent light source with adjustable intensity built on the basis of the BioSpecLSH-4 (Russia) compact halogen source with a dichroic filter for the simulation of PpIX fluorescence. The source was connected to a 400 μm single-mode optical fiber equipped with a custom made matte hemisphere (diffuser) at its distal end. To deliver the fiber across bones and soft tissues, a Tro-Venocath 16-gauge intravenous cannula (Vogt Medical, Germany) was used.

To study the intensity distribution of light scattered by the diffuser relative to the longitudinal axis of the fiber, we performed the following.

The cannula with the fiber inside was mounted on a bracket able to rotate in the horizontal plane. The axis of rotation was perpendicular to the cannula and passed through the center of the diffuser. A Lesa-01-BioSpec spectrometer (Russia) was installed in the plane of rotation of the cannula. The distance between the aperture of the spectrometer and the diffuser was 10 centimeters. The position of the cannula's axis that coincided with the direction of the spectrometer was taken as 0 degrees.

Light intensity was then evaluated through the *area under curve* (AUC) values of the emission spectrum at various positions of the cannula with respect to the spectrometer. The maximum intensity was obtained at 30 degrees and taken as 1. Other intensities were calculated relatively to this position (Table 1).

Таблица 1
Относительные значения площади под кривой (AUC) спектра излучения при различных положениях источника света относительно спектрометра

Table 1
Relative AUC values of the emission spectrum at various positions of the light source with respect to the spectrometer

Направление, ° Direction, °	0	30	60	90	-90
Относительная интенсивность излучения Relative light intensity	0.79	1.00	0.92	0.94	0.88

Registration system

Digital camera: Canon EOS 2000D (Japan).

Shooting mode: aperture priority, f/8 aperture, 0.6 sec shutter speed, ISO-400, neutral white balance.

Lens distortions were preliminarily evaluated while using a rectangular mesh target.

The camera was mounted on a tripod and fixed in front of the experimental tissue block.

To navigate across the surface of the skin, a LED backlight with a built-in ZS11 filter (480-570 nm) (OLTECH Photonics, Russia) was used.

The wavelength of the backlight was chosen so that it would not interfere with the main signal in the RGB color model. The intensity of the backlight, as well as that of the test source, was within the dynamic range of the camera.

The course of the experiment:

We have planned to study four skin zones with potentially different optical features:

1) a relatively smooth area of skin within one face region,
2) a relatively smooth area of skin at the border between two regions,
3) an area of skin with a pronounced microrelief,
4) an area of skin in the projection of ligaments and/or tendons.

As a result, in step 1, four areas were selected (Fig. 1), including one within the frontal region (zone of interest 1), two in the periorbital region – close to the medial and latheral canthi (zones of interest 2 and 4), and one within the region that corresponds to the nasolacrimal sulcus in humans (zone of interest 3).

Within each of the zones, a 1.8-mm drill was used to create an access to the subcutaneous space from the cranial cavity (Fig. 2A). A skin-mountable strain sensor (GML624A, Galoce, China) was used for depth monitoring (Fig. 2B). During the formation of the bone tunnel, the readings on the sensor fluctuated within the range of +/-0.1 gram-force (gf), which we considered to be mechanical noise. At the value of 0.2 gf, the drilling was stopped. The position of the tip of the drill was then detected using a conical magnetic pendulum and marked on the preliminary photo (Fig. 2C). After this, the drill was removed (Fig. 2D).

In step 2, the light distribution pattern from an internally (intradermally) located light source was recorded (Test 1). For that, an intravenous cannula with the fiber inside was inserted from the cranial cavity into each of the four access tunnels such that the end of the fiber was gently pressed against the dermis (Fig. 2E,F).

In step 3, the light distribution pattern from an externally located light source was recorded (Test 2). For that, the optic fiber was applied to the four spots on the skin surface earlier determined with the pendulum (see step 1) (Fig. 2G,H).

Рис. 1. Расположение зон интереса на модели. Масштаб прямоугольников 1-4 соответствует полученным кадрам.
Fig. 1. Location of the four zones of interest. The scale of the yellow rectangles corresponds to the resultant images.

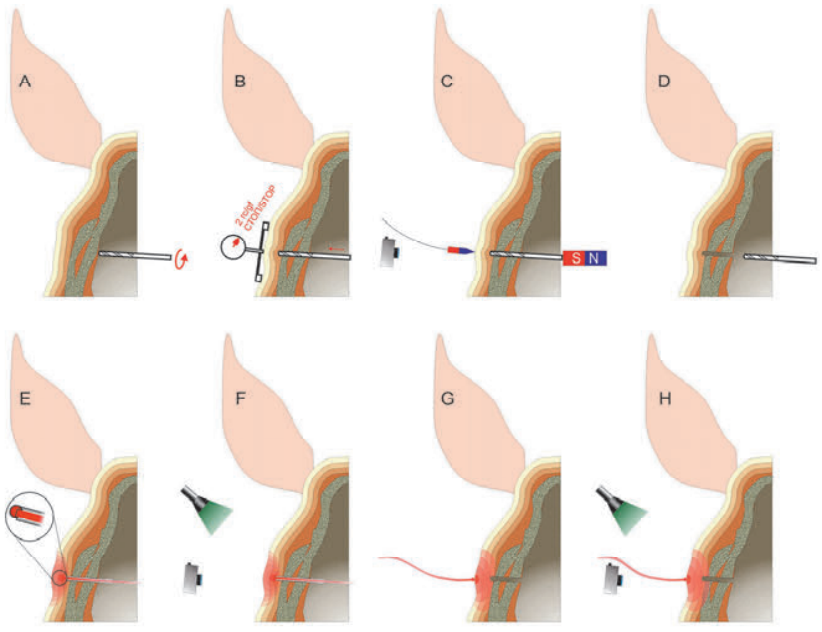

Рис. 2. Последовательность проведения эксперимента. A – сверление доступа со стороны полости черепа; B – остановка сверления; C – определение проекции сверла на поверхность кожи; D – извлечение сверла из сформированного доступа; E – введение интравенозной канюли с помещенным внутрь волноводом; матовая полусфера на конце волокна (врезка); F – фотофиксация картины распределения сигнала от внутрикожного источника (тест 1); G – аппликация волновода на поверхность кожи; H – фотофиксация картины распределения сигнала от наружного источника (тест 2).
Fig. 2. Course of the experiment. A – access drilling from the cranial cavity; B – drilling stop; C – the detection of the tip of the drill projection to the skin; D – drill removal from the created access tunnel; E – introduction of an intravenous cannula with the optical fiber; close view of the fiber end equipped with a matted hemisphere (inset); F – taking photo of the light distribution pattern from an intradermally located light source (Test 1); G – optical fiber application to the skin surface; H – taking photo of the light distribution pattern from a superficially located light source (Test 2).

Image preprocessing

Image preprocessing was done with the ImageJ 1.50d free software (Wayne Rasband National Institutes of Health, USA). Each of the obtained images (Fig. 3A,B) was split into RGB channels. The red channel was then smoothed with a 20-pixel Gaussian window (which exceeds the size of most microstructural elements of the skin, such as hair follicle openings) and posterized (Fig. 3C,D), which made it possible to create isolines of the red channel brightness gradient. After that, the red channel images with traced isolines were combined in pairs in accordance with the four zones of interest such that the first image in each pair was the one obtained at Test 1 (internal light source), and the second – the one obtained at Test 2 (external light source).

Quantitative assessment of the correspondence between skin projections of light distribution at different positions of the source

The skin projection of the tip of the drill determined using a magnetic pendulum (step 1, Fig. 2C) was taken as the origin (0,0). Then, in each pair of images (i.e. Test 1 and Test 2 images of the same zone of interest), brightness isolines were identified being similarly distant from the origin. After that, the distance from the origin to the selected isolines was measured in 24 directions at 15-degree intervals (Fig. 3E). In all cases, the value obtained from the Test 1 isoline was taken as the X-coordinate, while that from the Test 2 isoline – as the Y-coordinate of the same point on the scatter plot. Thus, for each pair of isolines a 24-point X,Y cloud was produced. For each cloud, the *k* coefficient of the linear trend of approximation was calculated.

Estimation of the parameters of ellipses that approximate the isolines of the brightness gradient

For each isoline that was analyzed at the previous stage, the axis ratio of the approximating ellipse was additionally determined with the ImageJ 1.50d free software (Wayne Rasband National Institutes of Health, USA).

Results

The pairs of Test 1 and Test 2 photos (Fig. 4) show the similarity in the overall pattern of light propagation in the skin, regardless of whether the light source was applied externally or located intradermally. Note that the use of the selected smoothing radius resulted in complex-shaped isolines in the second zone of interest, where multiple large pores were present (Fig. 4D-F). Also, in the images taken at the external position of the light source (Fig. 4C,F,I,L), the shape of the isolines was affected to varying degrees by the presence of the fiber in the field of view of the camera.

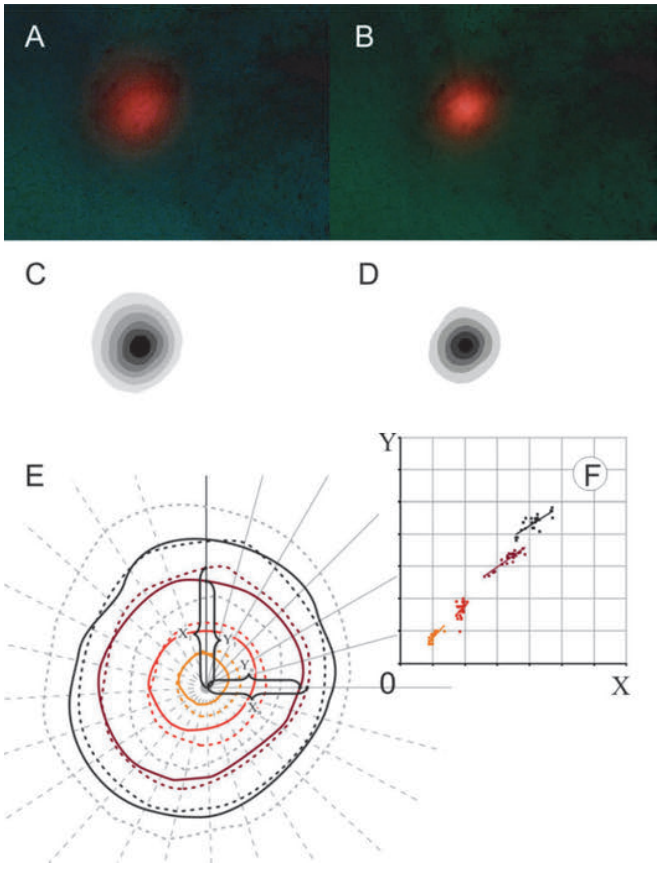

Рис. 3. Порядок обработки изображений (зона интереса 4 в качестве примера). A, B – фотографии одного и того участка кожи, подсвеченных сине-зеленым прожектором, при различном положении источника, имитирующего флуоресценцию протопорфирина IX – внутрикожно (A) или поверхностно (B); C,D – красный канал изображений A,B, соответственно. Применено сглаживание гауссовым окном и постеризация; E – трассированные изолинии градиента яркости красного канала для рисунок C и D, совмещенные по центру координат (пояснение в тексте). Сплошным цветом нанесены изолинии с первого изображения из пары (внутрикожная установка источника, тест 1), пунктиром – со второго (наружная установка источника, тест 2). Показан принцип получения координат X,Y для пары изолиний на сходном удалении от центра. Во всех случаях значение Xn присваивали точке, полученной в тесте 1, Yn – в тесте 2; F – пример диаграммы распределения совокупности точек, полученных для одной зоны интереса.

Fig. 3. Image preprocessing and quantitative assessment example (zone of interest 4). A, B – internal (A) and external (B) position of the PpIX-simulating light source within the same skin area (blue-green backlit). C,D – red channel images derived from A and B photographs, respectively. Gaussian smoothing and posterization are applied. E – traced isolines of the brightness gradient from C and D images, aligned by the origin (explanation in the text). The isolines from the first image of the pair (internal light source) are solid, from the second (external light source) are dotted. The principle of obtaining X- and Y-coordinates from a pair of isolines is shown. In all cases, the Test 1 isoline measurement was taken as the X-coordinate and the Test 2 isoline measurement – as the Y-coordinate of the same point on the scatter plot. F – a scatter plot example, where four X,Y point clouds describe four pairs of isolines chosen for analysis. The measurements were done in 24 directions.

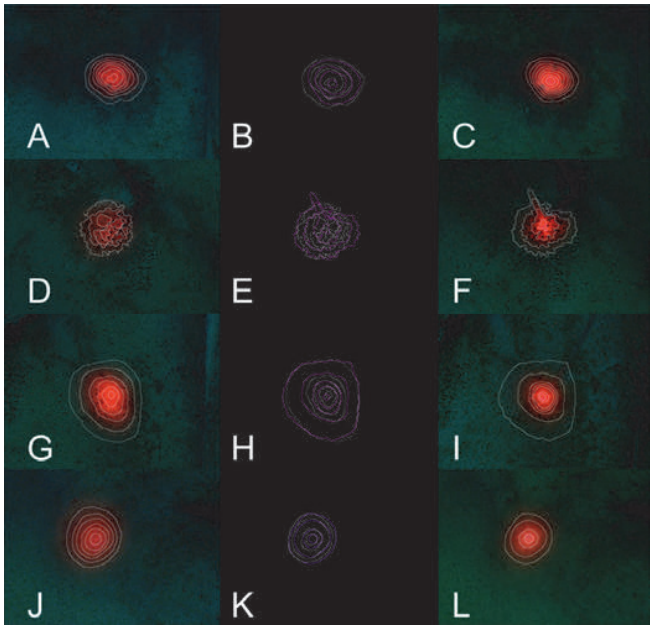

Рис. 4. Оптический результат эксперимента.
Пары фотографий участков кожи (см. зоны интереса на рисунке 1), подсвеченных сине-зеленым прожектором, при различном положении источника, имитирующего флуоресценцию протопорфирина IX – внутрикожно (A, D, G, J) или поверхностно (C, F, I, L). Белым цветом на все фотографии нанесены изолинии градиентов яркости красного канала, которые, кроме того, совмещены по центру координат для каждой пары фотографии и вынесены на отдельное изображение (B, E, H, K). Зоне интереса 1 соответствуют изображения A,B,C; зоне интереса 2 соответствуют изображения D, E, F; зоне интереса 3 – G, H, I; зоне интереса 4 – J, K, L.
Fig. 4. Results of the optical experiment.
Pairs of photographs of the same skin areas (see zones of interest in Fig. 1) at internal (A, D, G, J) and external (C, F, I, L) position of the PpIX-simulating light source (blue-green backlit) with isolines of the red channel brightness gradient applied in white. Additionally, the isolines of the red channel brightness gradient from the corresponding photos are aligned by the origin and presented separately in images B, E, H, K. Images A, B, C correspond to the zone of interest 1; images D, E, F correspond to the zone of interest 2; G, H, I – to the zone of interest 3; J, K, L – to the zone of interest 4.

To assess the correspondence between skin projections of light distribution from an external and an internal source, the scatter diagrams were created for all zones of interest (Fig. 5) such that every X,Y point cloud corresponded to a certain pair of isolines derived from the Test 1 and Test 2 photographs. For quantitative description, the *k* coefficient of the linear trend equation was calculated for each point cloud (Fig. 5, Table 2). As one can see, the correspondence of light distribution increases ($k \to 1$) with distance from the origin in all zones of interest.

The axis ratios of the ellipses approximating the analyzed isolines are also provided in Table 2.

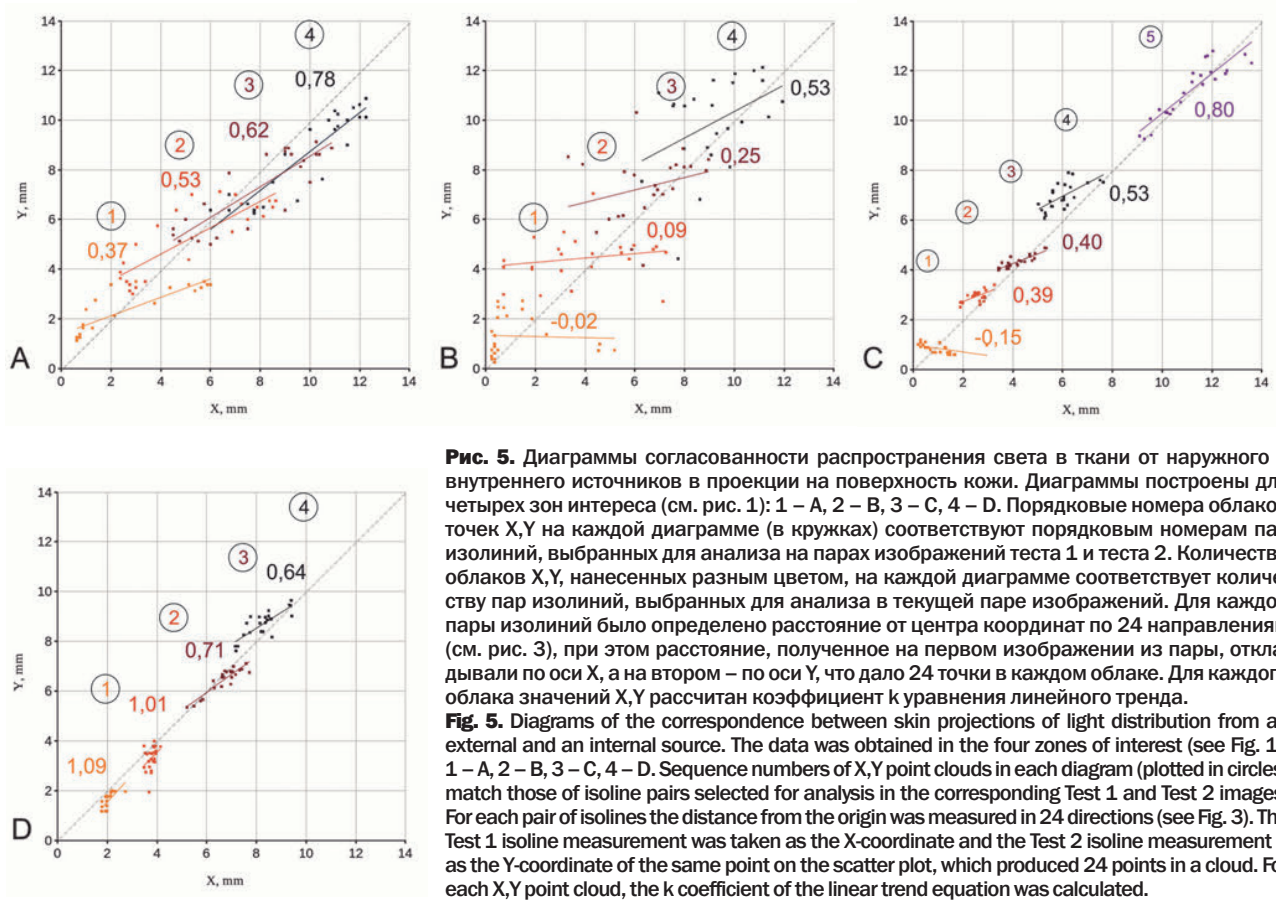

Рис. 5. Диаграммы согласованности распространения света в ткани от наружного и внутреннего источников в проекции на поверхность кожи. Диаграммы построены для четырех зон интереса (см. рис. 1): 1 – A, 2 – B, 3 – C, 4 – D. Порядковые номера облаков точек X,Y на каждой диаграмме (в кружках) соответствуют порядковым номерам пар изолиний, выбранных для анализа на парах изображений теста 1 и теста 2. Количество облаков X,Y, нанесенных разным цветом, на каждой диаграмме соответствует количеству пар изолиний, выбранных для анализа в текущей паре изображений. Для каждой пары изолиний было определено расстояние от центра координат по 24 направлениям (см. рис. 3), при этом расстояние, полученное на первом изображении из пары, откладывали по оси X, а на втором – по оси Y, что дало 24 точки в каждом облаке. Для каждого облака значений X,Y рассчитан коэффициент k уравнения линейного тренда.
Fig. 5. Diagrams of the correspondence between skin projections of light distribution from an external and an internal source. The data was obtained in the four zones of interest (see Fig. 1): 1 – A, 2 – B, 3 – C, 4 – D. Sequence numbers of X,Y point clouds in each diagram (plotted in circles) match those of isoline pairs selected for analysis in the corresponding Test 1 and Test 2 images. For each pair of isolines the distance from the origin was measured in 24 directions (see Fig. 3). The Test 1 isoline measurement was taken as the X-coordinate and the Test 2 isoline measurement – as the Y-coordinate of the same point on the scatter plot, which produced 24 points in a cloud. For each X,Y point cloud, the k coefficient of the linear trend equation was calculated.

Таблица 2
Оценка параметров эллипсов, аппроксимирующих изолинии градиентов яркости*

Table 2
Parameters of ellipses approximating the isolines of the brightness gradient*

	Отношение сторон эллипса (внутренний источник) Axis ratio of the ellipse (internal light source)	Отношение сторон эллипса (наружный источник) Axis ratio of the ellipse (external light source)	Коэффициент уравнения линейного тренда, k Coefficient of the linear trend equation, k
Зона интереса 1 / Zone of interest 1			
Пара изолиний / isoline pair 1	1.37	1.09	0.37
Пара изолиний / isoline pair 2	1.29	1.24	0.53
Пара изолиний / isoline pair 3	1.45	1.30	0.62
Пара изолиний / isoline pair 4	1.48	1.33	0.78
Зона интереса 2 / Zone of interest 2			
Пара изолиний / isoline pair 1	2.73	2.98	-0.02
Пара изолиний / isoline pair 2	1.30	1.11	0.09
Пара изолиний / isoline pair 3	1.01	1.18	0.25
Пара изолиний / isoline pair 4	1.04	1.35	0.53
Зона интереса 3 / Zone of interest 3			
Пара изолиний / isoline pair 1	1.28	1.27	-0.15
Пара изолиний / isoline pair 2	1.84	1.66	0.39
Пара изолиний / isoline pair 3	1.23	1.19	0.40
Пара изолиний / isoline pair 4	1.09	1.10	0.53
Пара изолиний / isoline pair 5	1.27	1.27	0.80
Зона интереса 4 / Zone of interest 4			
Пара изолиний / isoline pair 1	1.04	1.05	1.09
Пара изолиний / isoline pair 2	1.06	1.17	1.01
Пара изолиний / isoline pair 3	1.13	1.13	0.71
Пара изолиний / isoline pair 4	1.20	1.04	0.64

* Пары изолиний пронумерованы от центра координат.
* Pairs of isolines are numerated from the origin.

Discussion

First of all, it should be noted that all designs in this work are practical and do not aim to provide a thorough analysis of quantum light-molecules interactions in the skin.

From an optical point of view, a skin neoplasm can be considered as a complex multicomponent object [16-22]. In the epidermis, a significant portion of the radiation in the range of 350-1200 nm is absorbed by melanin, and in the ultraviolet region (with wavelengths less than 300 nm) the light is absorbed by aromatic amino acids, nucleic acids, urocanoic acid, and other molecules. In the dermis, red blood cell hemoglobin serves as the primary light absorber. Light scattering occurs as well due to the differences in the refractive indices of skin structures. Spatial distribution of scattered light and its intensity depends on the size and shape of these "inhomogeneities" in the medium relative to the wavelength, which, in turn, affects the results of spectral measurements due to the Rayleigh and Mie scattering. Research also shows that these parameters can change over the course of a lifetime due to changes in melanin concentration and collagen density [23].

A significant contribution to the formation of the optical spectrum of the skin is made by endogenous fluorescence (Table 3). The light emitted during the fluorescence process is also absorbed and scattered, and is influenced by fibrous anisotropic structures having the properties of imperfect optical fibers. This effect makes it challenging to analyze the distribution pattern on the skin surface and limits the practical application of fluorescent diagnostics. Empirical assessment of signal distortion from an intradermally located light source has become the main focus of this work.

Theoretically, any fluorophore listed in Table 3 could be the object of our study. However, not all of these are equally informative for oncodiagnostics. According to the published data, changes in the characteristic fluorescence of tryptophan [24], collagen [25], NADH [8] and especially

Таблица 3
Спектральные характеристики основных эндогенных флуорофоров кожи

Table 3
Spectral characteristics of the most common endogenous skin fluorophores

Название Name	Длина волны максимального возбуждения λ_{EX}, нм Maximum excitation wavelength λ_{EX}, nm	Длина волны максимального испускания флуоресценции λ_{FL}, нм Maximum fluorescence emission wavelength λ_{FL}, nm
НАД(Ф)Н / NAD(P)H	365	420-490
Кератин / Keratin	355-405	450
Коллаген/Эластин Collagen/Elastin	300-340	390-430
Липофусцин Lipofuscin	400-500	480-700
Пироксидин Pyroxidine	320	390
Порфирины Porphyrins	405	630-700
Тирозин / Tyrosine	220, 275	305
Триптофан Tryptophan	250-290	320-350
Флавины / Flavins	450	520-535

protoporphyrin IX are of value. PpIX fluorescence analysis is widely used in the examination and treatment of patients with malignant neoplasms, as well as in their postoperative care [10, 26-29]. Therefore, we have focused our basic interest on this particular compound.

We have also chosen to focus on the periorbital region, which is known for its uneven topography and high cosmetic and functional requirements.

The choice of a pig as a model for the experiment was not random. Unlike accepted laboratory animals (dogs, cats, rabbits, and mice), the size of its facial skull is comparable to that of humans. Moreover, similarly to humans, a pig does not have much hair in the periorbital region.

In the course of image preprocessing, isolines of the brightness gradient of the red channel were derived. Their shape was later used to assess the correspondence between patterns in which light is dispersed in tissues from an external and an internal source. Note that the "ovality" of the light distribution in the projection onto the skin surface was generally greater than the diffuser's impact in all directions (see Table 1).

In most studies on optics, the authors prefer to use ellipse parameters to describe the correspondence of light distribution [19, 30-32]. This is partly due to the possibility of multiple convolutions of the data, but also because an ellipse is a cross section of the indicatrix of scattering, which is commonly used to describe anisotropy of optical properties. Nevertheless, we assumed that in the conditions we have modeled, approximation of the brightness gradient with an ellipse might destroy critical details of light propagation in tissues, like, for example, thin optical "apophyses" associated with stacks of unidirectional fibers in narrow skin folds, or with a zone of continued tumor growth. Therefore, we have decided not only to evaluate the parameters of the approximating ellipses, but also to perform a quantitative assessment of the correspondence using the correlation method. For that, the *k* coefficient from the linear regression equation, $Y=k*X+b$, that describes point clouds plotted for each pair of brightness isolines, was chosen as the correspondence criterion. The higher the correlation, the closer the *k* value was to 1. Please note that the proposed correlation method will only be accurate if the isolines are clearly elongated in one or more directions, but not largely distorted by noise from minor surface irregularities, such as skin pores.

To sum up, the correlation between the skin projections of light distribution from an internal and an external source in this experiment should be regarded as high in two cases:

1) **both axis ratios of the ellipses corresponding to one pair of isolines are within the range of 0.95 to 1.05** (deviation of less than 5% was considered as insignificant). This means that both light sources produce roughly *circular* spots on the skin surface, which can happen when the light travels through a relatively homogeneous and isotropic medium in both tests;
2) **the axis ratios of the ellipses corresponding to one pair of isolines fall outside the range 0.95 to 1.05, but *k* is greater than 0.7** (i.e. strong or very strong correlation according to the Chaddock scale). This means that both light spots on the skin surface are *non-circular but still similar*, which can happen when the light spreads unevenly in different directions, but the directivity of light distribution correlates with the average strength of the signal between the tests.

In the studied skin areas, the correlation of light distribution from the two sources generally increased with the distance from the origin (Fig. 5A-C and Table 2), except for the zone of interest 4, where the trend was the opposite. Perhaps, the latter was due to a more accurate alignment between the locus of the maximum light density at Test 1 (internal light source) and the position of the external light source at Test 2. Besides uneven light distribution across the given area, another possible explanation for that could be an error in determining the position of the tip of the drill with a magnetic pendulum. Due to the fact that the pig's head was fixed almost vertically (Fig. 1), it is logical to assume that there could be a displacement of the pendulum under the influence of gravity in the moment when the drill and the pendulum were located in the same horizontal plane. An empirical test of this assumption in the air showed that

such a 'slip' may be up to 0.80+/-0.05 mm. At the distance from the light source, however, this effect diminishes and the correspondence increases (Fig. 5).

Also, attention should be drawn to the results obtained in the zone of interest 2, where the *k* coefficient was low for all pairs of isolines and even took a negative value for the pair 1, which is probably due to the presence of multiple "coarse" skin pores that caused scalloped edges of brightness gradients. Nevertheless, the overall isometricity of the gradients remained high.

And finally, since we have selected truly "similar" isolines (not equalized by their mean X and Y values), each of the point clouds in Figure 4 appears to be slightly shifted relative to the X=Y line. We could, of course, use an iterative or analytical method to obtain perfectly matched pairs of isolines in a quasi-smooth gradient field from the very beginning, but this would not be very useful in illustrating the correlation of light distribution in tissues for the two arrangements of light sources.

Having analyzed the described results, we can conclude that the registration of the light distribution pattern from a source applied to the skin surface allowed us to satisfactorily evaluate light propagation from an intradermal source. Quantitative estimations were positive for the outer regions of all zones of interest, except for the zone 2, as well as the inner regions of the zones 1 and 4. The relative failure of the zone 2 tests, as stated above, can be attributed to significant skin irregularities (larger than the selected filtering window) and an obvious artifact produced by the optical fiber within the field of view of the camera.

We suggest that "correction for anisotropy" could be incorporated into the fluorescence diagnostics routine. However, this would require some kind of a device that projects light of a specific wavelength onto the skin surface and which is a) simple enough to enable rapid examination and b) free from geometric distortions caused by opaque structural elements in the field of view of the camera. Having these requirements met, such a device could be used in practical oncology, including ophthalmology, since it is the periorbital neoplasms that are often located at the junctions of tissues with different optical properties.

Conclusion

This experiment has clearly demonstrated the previously theoretical relationship between the fluorescence distribution pattern of a tumor on the one hand, and the condition and/or topography of the tissues containing this tumor, on the other. It has also proved the possibility of using an external light source to assess the local scattering anisotropy of the skin, particularly in the periorbital region.

REFERENCES

1. Kaprin A.D., Starinsky V.V., Shakhzadova A.O. eds. Malignant neoplasms in Russia in 2020 (morbidity and mortality). M.: P.A. Herzen Moscow Oncology Research Institute. – 2021. (In Russ.)
2. Sung H., Ferlay J., Siegel R.L., Laversanne M., Soerjomataram I., Jemal A., Bray F. Global cancer statistics 2020: GLOBOCAN estimates of incidence and mortality worldwide for 36 cancers in 185 countries. *CA Cancer J Clin*, 2021, Vol. 71, pp. 209-249. https://doi.org/10.3322/caac.21660
3. Peris K., Fargnoli M.C., Garbe C., Kaufmann R., Bastholt L., Seguin N.B., Bataille V., Marmol V. D., Dummer R., Harwood C.A., Hauschild A., Höller C., Haedersdal M., Malvehy J., Middleton M.R., Morton C.A., Nagore E., Stratigos A.J., Szeimies R.M., Tagliaferri L., Trakatelli M., Zalaudek I., Eggermont A., Grob J.J. Diagnosis and treatment of basal cell carcinoma: European consensus-based interdisciplinary guidelines. *Eur J Cancer*, 2019, Vol. 118, pp. 10-34.
4. Vornicescu C., Șenilă S.C., Bejinariu N.I., Vesa Ș.C., Boșca A.B., Chirilă D.N., MelincoviciC.S., Soriță O., Mihu C.M. Predictive factors for the recurrence of surgically excised basal cell carcinomas: A retrospective clinical and immunopathological pilot study. *Experimental and Therapeutic Medicine*, 2021, Vol. 22(5), pp.1336. https://doi.org/10.3892/etm.2021.10771
5. Policard A. Etudes sur les aspects offerts par des tumeurs experimentales ex aminées a la lumière de Wood. *C R Soc Biol*, 1924, Vol. 91, pp. 1423-1428.
6. GalkinaE.M., Utz S.R. Fluorescence diagnosis in dermatology (review). *Saratov Journal of Medical Scientific Research*, 2013, Vol. 9(3), pp. 566-572. (In Russ.)
7. Wizenty J., Schumann T., Theil, D., Stockmann M., Pratschke J., Tacke F., Aigner F., Wuensch T. Recent Advances and the Potential for Clinical Use of Autofluorescence Detection of Extra-Ophthalmic Tissues. *Molecules*, 2020, Vol. 25(9), pp. 2095.
8. Croce A.C., Bottiroli G. Autofluorescence spectroscopy and imaging: A tool for biomedical research and diagnosis. *Eur. J. Histochem*, 2014, Vol. 58. – P. 2461.
9. Vo-Dinh T. Biomedical photonics handbook: biomedical diagnostics. *CRC press. Boca Raton*. – 2014.
10. McNicholas K., MacGregor M.N., Gleadle J.M. In order for the light to shine so brightly, the darkness must be present-why do cancers fluoresce with 5-aminolaevulinic acid? *Br J Cancer,* 2019, Vol. 121(8), pp. 631-639. https://doi.org/10.1038/s41416-019-0516-4.
11. Pavlova NN, Thompson CB. The emerging hallmarks of cancer metabolism. *Cell Metab,* 2016, Vol. 23(1), pp. 27-47. https://doi.org/10.1016/j.cmet.2015.12.006.

ЛИТЕРАТУРА

1. Kaprin A.D., Starinsky V.V., Shakhzadova A.O. eds. Malignant neoplasms in Russia in 2020 (morbidity and mortality). M.: P.A. Herzen Moscow Oncology Research Institute. – 2021. (In Russ.)
2. Sung H., Ferlay J., Siegel R.L., Laversanne M., Soerjomataram I., Jemal A., Bray F. Global cancer statistics 2020: GLOBOCAN estimates of incidence and mortality worldwide for 36 cancers in 185 countries // CA Cancer J Clin. – 2021. – Vol.71. – P. 209-249. https://doi.org/10.3322/caac.21660
3. Peris K., Fargnoli M.C., Garbe C., Kaufmann R., Bastholt L., Seguin N.B., Bataille V., Marmol V. D., Dummer R., Harwood C.A., Hauschild A., Höller C., Haedersdal M., Malvehy J., Middleton M.R., Morton C.A., Nagore E., Stratigos A.J., Szeimies R.M., Tagliaferri L., Trakatelli M., Zalaudek I., Eggermont A., Grob J.J. Diagnosis and treatment of basal cell carcinoma: European consensus-based interdisciplinary guidelines // Eur J Cancer. – 2019. – Vol. 118. – P.10-34.
4. Vornicescu C., Șenilă S.C., Bejinariu N.I., VesaȘ.C., Boșca A.B., Chirilă D.N., MelincoviciC.S., Soriță O., Mihu C.M. Predictive factors for the recurrence of surgically excised basal cell carcinomas: A retrospective clinical and immunopathological pilot study // Experimental and Therapeutic Medicine. – 2021. – Vol. 22(5). – P.1336. https://doi.org/10.3892/etm.2021.10771
5. Policard A. Etudes sur les aspects offerts par des tumeurs experimentales ex aminées a la lumière de Wood // C R Soc Biol. – 1924. – Vol. 91. – P. 1423-1428.
6. GalkinaE.M., Utz S.R. Fluorescence diagnosis in dermatology (review) // Saratov Journal of Medical Scientific Research. – 2013. – Vol. 9(3). – P. 566-572. (In Russ.)
7. Wizenty J., Schumann T., Theil, D., Stockmann M., Pratschke J., Tacke F., Aigner F., Wuensch T. Recent Advances and the Potential for Clinical Use of Autofluorescence Detection of Extra-Ophthalmic Tissues // Molecules. – 2020. – Vol. 25(9). – P. 2095.
8. Croce A.C., Bottiroli G. Autofluorescence spectroscopy and imaging: A tool for biomedical research and diagnosis // Eur. J. Histochem. – 2014. – Vol. 58. – P. 2461.
9. Vo-Dinh T. Biomedical photonics handbook: biomedical diagnostics // CRC press. Boca Raton. – 2014.
10. McNicholas K., MacGregor M.N., Gleadle J.M. In order for the light to shine so brightly, the darkness must be present-why do cancers fluoresce with 5-aminolaevulinic acid? // Br J Cancer. – 2019. – Vol. 121(8). – P. 631-639. https://doi.org/10.1038/s41416-019-0516-4.
11. Pavlova N.N., Thompson C.B. The emerging hallmarks of cancer metabolism // Cell Metab. – 2016. – Vol. 23 (1). – P.27-47. https://doi.org/10.1016/j.cmet.2015.12.006.

12. Potapov A.A., Goriaĭnov S.A., Loshchenov V.B., Savel'eva T.A., Gavrilov A.G., Okhlopkov V.A., Zhukov V.Iu., Zelenkov P.V., Gol'bin D.A., Shurkhaĭ V.A., Shishkina L.V., Grachev P.V., Kholodtsova M.N., Kuz'min S.G., Vorozhtsov G.N., Chumakova A.P. Intraoperative combined spectroscopy (optical biopsy) of cerebral gliomas. *ZhVoprNeirokhirIm N. N. Burdenko*, 2013, Vol. 77(2), pp. 3-10. (In Eng., Russ.)
13. Na R., Stender I.M., Wulf H.C. Can autofluorescence demarcate basal cell carcinoma from normal skin? A comparison with protoporphyrin IX fluorescence. *Acta Derm Venereol*, 2001, Vol. 81, pp. 246-249. https://doi.org/10.1080/00015550152572859
14. Hegyi J., Hegyi V., New developments in fluorescence diagnostics. In: Michael R. Hamblin, Pinar Avci, Gaurav K. Gupta, eds. *Imaging in Dermatology. Academic Press*, 2016, pp. 89-94. https://doi.org/10.1016/B978-0-12-802838-4.00009-1
15. Grusha Ia.O., Kiryushchenkova N.P., Novikov I.A., Fedorov A.A., Ismailova D.S. Histological verification of autofluorescence borders of periorbital skin tumors. *Vestnik Oftalmologii*, 2020, Vol. 136(6), pp. 32-41. (In Russ.) https://doi.org/10.17116/oftalma202013606132
16. Kienle A., Foschum F., Hohmann A. Light propagation in structural anisotropic media in the steady-state and time domains. *Phys. Med. Biol*, 2013, Vol. 58(17), pp. 6205. https://doi.org/10.1088/0031-9155/58/17/6205
17. Jacques S.L. Optical properties of biological tissues: a review. *Phys Med Biol*, 2013, Vol. 58(11), pp. 37-61. https://doi.org/0.1088/0031-9155/58/11/R37.
18. Nickell S. et al. Anisotropy of light propagation in human skin. *Phys. Med. Biol,* 2000, Vol. 45, pp. 2873-2886.
19. Tuchin V.V. Lasers and optical fibers in biomedical studies (2d ed.). *Fizmatlit*, 2010 (In Russ.)
20. Tuchin V.V. Optical biomedical diagnosis. *Izvestiya of Saratov University. Physics*, 2005, Vol. 1(5), pp. 39-53. (In Russ.) https://doi.org/10.18500/1817-3020-2005-5-1-39-53.
21. Anderson RR, Parrish JA. The optics of human skin. *J Invest Dermatol*, 1981, Vol. 77 (1), pp. 13-9. https://doi.org/10.1111/1523-1747.ep12479191.
22. Colas V., Daul C., Khairallah G., Amouroux M., Blondel W. Spatially resolved diffuse reflectance and autofluorescence photon depth distribution in human skin spectroscopy: a modeling study. *Proc. SPIE* 11553, *Optics in Health Care and Biomedical Optics X*, 115531A. https://doi.org/10.1117/12.2575069
23. Brancaleon L., Durkin A.J., Tu J.H., Menaker G., Fallon J.D., Kollias N. In vivo Fluorescence Spectroscopy of Nonmelanoma Skin Cancer. *Photochemistry and Photobiology*, 2001, Vol. 73(2), pp. 178-183. https://doi.org/10.1562/0031-8655(2001)073
24. Masuda Y., Ogura Y., Inagaki Y., Yasui T., Aizu Y. Analysis of the influence of collagen fibres in the dermis on skin optical reflectance by Monte Carlo simulation in a nine-layered skin model. *Skin Res Technol*, 2018, Vol. 24, pp. 248-255. https://doi.org/10.1111/srt.12421
25. Smirnova O.D., Rogatkin D., Litvinova K. Collagen as in vivo quantitative fluorescent biomarkers of abnormal tissue changes. *J. Innov. Opt. Health Sci*, 2012, Vol. 05(2), pp.1250010.
26. Yagi R., Kawabata S., Ikeda N. et al. Intraoperative 5-aminolevulinic acid-induced photodynamic diagnosis of metastatic brain tumors with histopathological analysis. *World J SurgOnc,* 2017, Vol. 15, pp.179. https://doi.org/10.1186/s12957-017-1239-8
27. Redondo P., Marquina M., Pretel M., Aguado L., Iglesias M.E. Methyl-ALA-Induced Fluorescence in Photodynamic Diagnosis of Basal Cell Carcinoma Prior to Mohs Micrographic Surgery. *ArchDermatol*, 2008, Vol. 144(1), pp.115-117. https://doi.org/10.1001/archdermatol.2007.3
28. Kiryushchenkova N.P., Grusha Y., The use of autofluorescence diagnostics in monitoring and evaluating the effectiveness of local chemotherapy for superficial basal cell carcinoma of the skin (clinical case). *Modern technologies in ophthalmology*, 2020, Vol. 4 (35), pp.162-163. (In Russ.) https://doi.org/10.25276/2312-4911-2020-4-162-163
29. Hefti M., von Campe G., Moschopulosa M., Siegnerb A., Looserc H., Landolt H. 5-aminolaevulinic acid-induced protoporphyrin IX fluorescence in high-grade glioma surgery. *SWISS MED WKLY*, 2008, Vol. 138(11-12), pp.180-185.
30. Sapronov M.V., Skornyakova N.M. Computer visualization of Rayleigh scattering indicatrix in dynamic. *Scientific visualization*, 2017, Vol.3(9), pp.42-53. (In Russ.)
31. Kalyagina N., Loschenov V., Wolf D., Daul C., Blondel W., Savelieva T. Experimental and Monte Carlo investigation of visible diffuse-reflectance imaging sensitivity to diffusing particle size changes in an optical model of a bladder wall. *Applied Physics B*, 2011, Vol. 105. (3), pp. 631-639. doi:10.1007/s00340-011-4678-x
32. Colas V., Amouroux M., Daul C., Perrin-Mozet C., Blondel W. Comparative study of optical properties estimation on liquid optical phantoms using spatially-resolved diffuse reflectance spectroscopy and double integrating spheres methods. *Proc. SPIE 12147. – Tissue Optics and Photonics II*, pp. 1214705. https://doi.org/10.1117/12.2621496

12. Potapov A.A., Goriaĭnov S.A., Loshchenov V.B., Savel'eva T.A., Gavrilov A.G., Okhlopkov V.A., Zhukov V.Iu., Zelenkov P.V., Gol'bin D.A., Shurkhaĭ V.A., Shishkina L.V., Grachev P.V., Kholodtsova M.N., Kuz'min S.G., Vorozhtsov G.N., Chumakova A.P. Intraoperative combined spectroscopy (optical biopsy) of cerebral gliomas // ZhVoprNeirokhirIm N. N. Burdenko. – 2013. – Vol. 77(2). – P. 3-10. (In Eng., Russ.)
13. Na R., Stender I.M., Wulf H.C. Can autofluorescence demarcate basal cell carcinoma from normal skin? A comparison with protoporphyrin IX fluorescence // Acta Derm Venereol. – 2001. – Vol. 81. – P. 246-249. https://doi.org/10.1080/00015550152572859
14. Hegyi J., Hegyi V., New developments in fluorescence diagnostics. In: Michael R. Hamblin, Pinar Avci, Gaurav K. Gupta, eds // Imaging in Dermatology. Academic Press. – 2016. – P. 89-94. https://doi.org/10.1016/B978-0-12-802838-4.00009-1
15. Grusha Ia.O., Kiryushchenkova N.P., Novikov I.A., Fedorov A.A., Ismailova D.S. Histological verification of autofluorescence borders of periorbital skin tumors // Vestnik Oftalmologii. – 2020. – Vol. 136(6). – P. 32-41. (In Russ.) https://doi.org/10.17116/oftalma202013606132
16. Kienle A., Foschum F., Hohmann A. Light propagation in structural anisotropic media in the steady-state and time domains // Phys. Med. Biol. – 2013. – Vol. 58(17). – P. 6205. https://doi.org/10.1088/0031-9155/58/17/6205
17. Jacques S.L. Optical properties of biological tissues: a review // Phys Med Biol. – 2013. – Vol. 58(11). – P. 37-61. https://doi.org/0.1088/0031-9155/58/11/R37.
18. Nickell S. et al. Anisotropy of light propagation in human skin // Phys. Med. Biol. – 2000. – Vol. 45. – P. 2873-2886.
19. Tuchin V.V. Lasers and optical fibers in biomedical studies (2d ed.) // Fizmatlit. – 2010 (In Russ.)
20. Tuchin V.V. Optical biomedical diagnosis // Izvestiya of Saratov University. Physics. – 2005. – Vol. 1(5). – P. 39-53. (In Russ.) https://doi.org/10.18500/1817-3020-2005-5-1-39-53.
21. Anderson RR, Parrish JA. The optics of human skin // J Invest Dermatol. – 1981. – Vol.77 (1). – P. 13-9. https://doi.org/10.1111/1523-1747.ep12479191.
22. Colas V., Daul C., Khairallah G., Amouroux M., Blondel W. Spatially resolved diffuse reflectance and autofluorescence photon depth distribution in human skin spectroscopy: a modeling study // Proc. SPIE 11553.- Optics in Health Care and Biomedical Optics X. – 115531A. https://doi.org/10.1117/12.2575069
23. Brancaleon L., Durkin A.J., Tu J.H., Menaker G., Fallon J.D., Kollias N. *In vivo* Fluorescence Spectroscopy of Nonmelanoma Skin Cancer // Photochemistry and Photobiology. –2001. – Vol. 73(2). – P. 178-183. https://doi.org/10.1562/0031-8655(2001)073<0178: IVFSON>2.0.CO;2
24. Masuda Y., Ogura Y., Inagaki Y., Yasui T., Aizu Y. Analysis of the influence of collagen fibres in the dermis on skin optical reflectance by Monte Carlo simulation in a nine-layered skin model // Skin Res Technol. – 2018. – Vol. 24. – P. 248-255. https://doi.org/10.1111/srt.12421
25. Smirnova O.D., Rogatkin D., Litvinova K. Collagen as in vivo quantitative fluorescent biomarkers of abnormal tissue changes // J. Innov. Opt. Health Sci. – 2012. – Vol. 05(2). – P.1250010.
26. Yagi R., Kawabata S., Ikeda N. *et al.* Intraoperative 5-aminolevulinic acid-induced photodynamic diagnosis of metastatic brain tumors with histopathological analysis // World J SurgOnc – 2017. – Vol. 15 – P. 179. https://doi.org/10.1186/s12957-017-1239-8
27. Redondo P., Marquina M., Pretel M., Aguado L., Iglesias M.E. Methyl-ALA-Induced Fluorescence in Photodynamic Diagnosis of Basal Cell Carcinoma Prior to Mohs Micrographic Surgery // ArchDermatol. – 2008. – Vol. 144(1). – P. 115-117. https://doi.org/10.1001/archdermatol.2007.3
28. Kiryushchenkova N.P., Grusha Y., The use of autofluorescence diagnostics in monitoring and evaluating the effectiveness of local chemotherapy for superficial basal cell carcinoma of the skin (clinical case) // Modern technologies in ophthalmology. – 2020. – Vol. 4 (35). – P. 162-163. (In Russ.) https://doi.org/10.25276/2312-4911-2020-4-162-163
29. Hefti M., von Campe G., Moschopulosa M., Siegnerb A., Looserc H., Landolt H. 5-aminolaevulinic acid-induced protoporphyrin IX fluorescence in high-grade glioma surgery // SWISS MED WKLY – 2008. –Vol. 138(11-12). – P. 180-185.
30. Sapronov M.V., Skornyakova N.M. Computer visualization of Rayleigh scattering indicatrix in dynamic // Scientific visualization. – 2017. – Vol. 3(9). – P. 42-53. (In Russ.)
31. Kalyagina N., Loschenov V., Wolf D., Daul C., Blondel W., Savelieva T. Experimental and Monte Carlo investigation of visible diffuse-reflectance imaging sensitivity to diffusing particle size changes in an optical model of a bladder wall // Applied Physics B. – 2011. – Vol. 105(3). – P. 631-639.doi:10.1007/s00340-011-4678-x
32. Colas V., Amouroux M., Daul C., Perrin-Mozet C., Blondel W. Comparative study of optical properties estimation on liquid optical phantoms using spatially-resolved diffuse reflectance spectroscopy and double integrating spheres methods // Proc. SPIE 12147. – Tissue Optics and Photonics II. – P. 1214705. https://doi.org/10.1117/12.2621496

ON THE DEPENDENCE OF FLUORESCENCE INTENSITY ON THE CONCENTRATION OF PHOTOSENSITIZER SOLUTIONS

Meerovich G.A.[1,2], **Romanishkin I.D.**[1,2], **Akhlyustina E.V.**[2], **Loschenov V.B.**[1,2]
[1]Prokhorov General Physics Institute of Russian Academy of Sciences, Moscow, Russia
[2]National Research Nuclear University MEPhI (Moscow Engineering Physics Institute), Moscow, Russia

Abstract

When studying the optical properties of photosensitizers, it is assumed that their fluorescence intensity depends linearly on concentration. However, there are many factors that need to be taken into account. At low photosensitizer concentrations, a part of the excitation radiation energy is lost beyond the volume of the excited solution, and due to local or one-directional registration, a large part of isotropically emitted fluorescence radiation is also not registered. At higher concentrations, the loss of fluorescence light increases due to its partial re-absorption by the photosensitizer molecules and subsequent isotropic re-emission with quantum yield much lower than 1, and further increase of concentration leads to partial aggregation of PS, and to the following decrease of effective fluorescence. At high absorption, fluorescence is excited only in a limited volume close to the excitation radiation source, leading to higher significance of light registration geometry. This should be taken into account in fluorescence diagnostics and navigation using this characteristic.

Keywords: photosensitizer, concentration, fluorescence, mathematical modeling.

Contacts: Romanishkin I.D., e-mail: igor.romanishkin@nsc.gpi.ru

For citations: Meerovich G.A., Romanishkin I.D., Akhlyustina E.V., Loschenov V.B. On the dependence of fluorescence intensity on the concentration of photosensitizer solutions, *Biomedical Photonics*, 2025, vol. 14, no. 2, pp. 21–26. doi: 10.24931/2413–9432–2025–14–2–21–26

О ЗАВИСИМОСТИ ИНТЕНСИВНОСТИ ФЛУОРЕСЦЕНЦИИ ОТ КОНЦЕНТРАЦИИ РАСТВОРОВ ФОТОСЕНСИБИЛИЗАТОРОВ

Г.А. Меерович[1,2], **И.Д. Романишкин**[1,2], **Е.В. Ахлюстина**[2], **В.Б. Лощенов**[1,2]
[1]Институт общей физики им. А. М. Прохорова Российской академии наук, Москва, Россия
[2]Национальный исследовательский ядерный университет «МИФИ», Москва, Россия

Резюме

При исследовании оптических свойств фотосенсибилизаторов принято считать, что интенсивность их флуоресценции линейно зависит от концентрации. Однако, есть много факторов, которые необходимо учитывать. При низких концентрациях фотосенсибилизатора часть энергии возбуждающего излучения, выходящая за пределы объема возбуждаемого раствора, теряется, а из-за локальной или «односторонней» регистрации часть изотропно распространяющегося излучения флуоресценции, также не регистрируется. При более высоких концентрациях потери флуоресцентного света увеличиваются за счет перепоглощения его части молекулами фотосенсибилизатора и последующего изотропного переизлучения с квантовым выходом значительно ниже 1, а дальнейшее увеличение концентрации приводит к частичной агрегации ФС, и к следующему из этого снижению эффективной флуоресценции. При высоком поглощении, флуоресценция возбуждается только в ограниченном объеме вблизи источника возбуждающего излучения, из-за чего большое значение начинают иметь геометрические особенности регистрации света. Это необходимо учитывать при флуоресцентной диагностике и навигации с использованием данной характеристики.

Ключевые слова: фотосенсибилизатор, концентрация, флуоресценция, математическое моделирование

Контакты: Романишкин И.Д. e-mail: igor.romanishkin@nsc.gpi.ru

Для цитирования: Меерович Г.А., Романишкин И.Д., Ахлюстина Е.В., Лощенов В.Б. О зависимости интенсивности флуоресценции от концентрации растворов фотосенсибилизаторов // Biomedical Photonics. – 2025. – Т. 14, № 2. – С. 21–26. doi: 10.24931/2413–9432–2025–14–2–21–26

Spectral-fluorescent methods for studying photosensitizers (PS) and sensitized biological tissues using local, 2D and 3D methods of fluorescence intensity registration are widely used for fluorescent diagnostics to determine the topology and boundaries of different pathological foci, fluorescent navigation, assessment of the kinetics and level of PS accumulation, what is important for optimizing of photodynamic therapy (PDT) [1–5]. The measurement of integral fluorescence intensity values at different time intervals after administration is used as a pharmacokinetic curve of PS, and the ratio of the values of this parameter in different organs and tissues is used for estimation of the selectivity of PS accumulation [6]. Typically, in such studies, excitation and registration of fluorescence are performed from one side of the examined sample (including a cuvette with a photosensitizer solution) using local (light-guide) or matrix photodetectors equipped with a focusing optics [7]. Fluorescence studies (spectral density distribution in the fluorescence and absorption bands of the working transition of the PS responsible for the photodynamic effect, the shape and features of these spectral characteristics, fluorescence lifetime and spatial distribution of all parameters in biological tissue, and also the integral fluorescence intensity are carried out, as a rule, in a wide range of PS concentrations [2]. However, most of these works do not take into account reabsorption in PS solutions with a significant overlap of absorption and fluorescence spectra in the working band [8], aggregation of PS molecules in solutions, as well as a number of geometric factors associated with the excitation of fluorescence in a volume of a PS solution and its registration at specific dimensions of this volume, that can significantly affect, for example, the dependence of the integral fluorescence intensity on the PS concentration.

The purpose of this work is to evaluate this dependence, taking into account these phenomena, which is important for assessing their influence on the integral fluorescence intensity. For such an assessment, we consider the simplest model (using photophysical characteristics of a tetracationic derivative of synthetic bacteriochlorin for quantitative assessments [9]) with the following assumptions:

- excitation is carried out in a shorter wavelength spectral range, far enough from the fluorescence band (in case of synthetic bacteriochlorin derivatives—in the Q2 band at 532 nm) to exclude the effect of scattered excitation light on the registered fluorescence spectra;
- the scattering in the sensitized liquid is negligible;
- PS is not aggregated;
- the distribution (spectral density) of intensity in the absorption and fluorescence bands is spectrally homogeneous within each of the bands

As a simplified calculation model, consider the scheme of registration of PS fluorescence in an optical cell with length *L* and a cell wall thickness of *l* (Fig. 2). Optical fiber for light irradiation and optical fiber for receiving fluorescence with a diameter D are in contact with this wall (this is a simplified model for studying the fluorescent properties of PS using a fiber-optic spectrometer[1]). The fluorescence of the solution is excited through a transparent wall by a parallel light flux with a power density $P_{0.}$

$$I = \frac{\varepsilon_B D^2 P_0 c}{16} \Gamma \int_l^{l+L} \frac{2.3 \times \exp\left[-\varepsilon_2 (x-l) c - \varepsilon_0 c (1-\gamma)(x-l)\right]}{x^2} dx, \quad (1)$$

where ε_B – PS extinction at a wavelength 532 nm, ε_0 – PS extinction in the spectral maximum of the absorption band of working transition, Γ – quantum yield of photoluminescence in the fluorescent band of working transition upon excitation at a wavelength 532 nm, γ – quantum yield of photoluminescence in fluorescent band upon excitation of absorption band of working

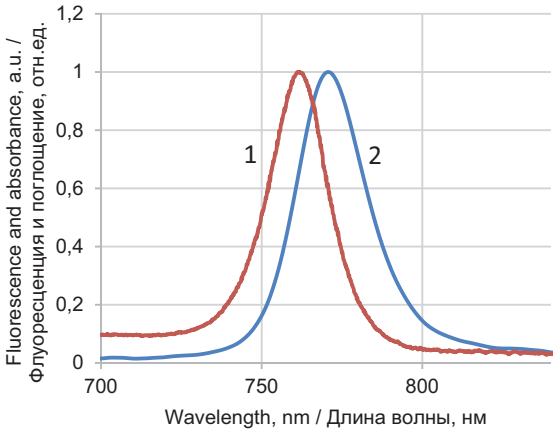

Рис. 1. Спектральные кривые поглощения (1) и флуоресценции (2) тетракационного производного бактериохлорина при концентрации 5 мкМ.
Fig. 1. The spectral contours of absorption (1) and fluorescence (2) bands oftetracationic bacteriochlorin derivative at 5 μM concentration.

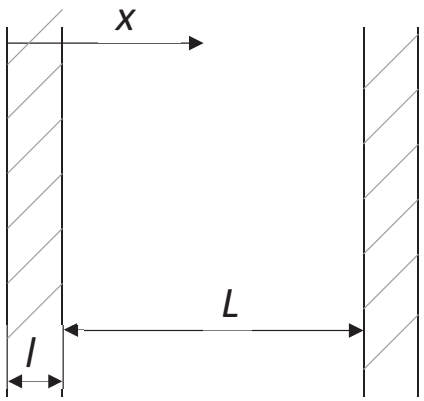

Рис. 2. Схема упрощённой модели.
Fig. 2. Scheme of the simple calculation model.
We take into account that the fluorescence emission from each point is distributed uniformly in all directions.

transition, Δ – "overlapping factor" of the spectral contours of fluorescence and absorption.

$$I = Bc\int_{l}^{l+L} \frac{2.3\times\exp\left[-(x-l)c\left(\varepsilon_2+\varepsilon_0\Delta(1-\gamma)\right)\right]}{x^2}dx$$

$$B = \frac{\varepsilon_2 D^2 P_0}{16}\Gamma,$$

$$a = -b = c\left[\varepsilon_2+\varepsilon_0\Delta(1-\gamma)\right]$$

$$\varepsilon_{\Sigma}=\varepsilon_2+\varepsilon_0\Delta(1-\gamma)$$

$$b = -\varepsilon_{\Sigma}c$$

$$I = Bc\int_{l}^{l+L}\frac{\exp\left(-\varepsilon_{\Sigma}(x-l)c\right)}{x^2}dx$$

$$I = Bc\int_{l}^{l+L}\frac{e^{\varepsilon_{\varepsilon}cl}e^{-\varepsilon_{\Sigma}cx}}{x^2}dx$$

$$I = Bce^{-bl}\int_{l}^{l+L}\frac{e^{bx}}{x^2}dx$$

$$\int\frac{e^{bx}}{x^2}dx = -\frac{e^{bx}}{x}+b\,Ei(bx)\quad \int\frac{e^{bx}}{x^2}dx = -\frac{e^{bx}}{x}+b\,Ei(bx)$$

where $Ei(x)=\int_{-\infty}^{x}\frac{e^t}{t}dt$ – exponential integral. Thus, the dependence of the integral fluorescence intensity the concentration of the photosensitizer for different optical cell lengths can be represented by the formula:

$$I = Bce^{-bl}\left(b\,Ei\left(b(l+L)\right)-b\,Ei(bl)-\frac{e^{b(l+L)}}{l+L}+\frac{e^{bl}}{l}\right). \qquad (2)$$

The "overlapping factor" of the working absorption and fluorescence bands, according to [8], is about 0.4 for a lot of PS. As for the quantum yield of photoluminescence upon its excitation in the working band, its value for an effective PS should be significantly lower than the quantum yield of ROS generation (for example, for phthalocyanines, which have intense fluorescence, according to [10], the quantum yield of ROS generation is 0.60–0.65, and the quantum yield of their fluorescence is 0.03–0.11).

An analysis of ratio (2) shows that in the ranges of PS concentrations of 1–100 μM and cell length (sensitized layer thicknesses) of 1–10 mm, which are relevant for ongoing studies, the dependence of the integrated fluorescence intensity recorded from the excitation side on the PS concentration is sublinear. At low concentrations of PS, a part of the energy of the exciting light, which passes through the absorbing solution, is lost, and, due to local or "one-sided" registration, a part of the fluorescent light, which emits in all directions, is also not registered. Also (especially at high concentrations) the losses of fluorescent light are significantly higher due to the partial reabsorption by PS molecules and subsequent reemission with a quantum yield significantly less than 1 [11].

However, the results of calculations using the above formulas exceed the data obtained experimentally, especially at high concentration, due to a number of simplifying assumptions adopted for making these estimates.

For a more correct assessment of the dependence of the integral fluorescence intensity on PS concentration and its comparison with the experimentally obtained dependence, we will carry out estimates in a modified model with assumptions closer to the experimental conditions. We utilize the real shape of the absorption and fluorescence spectral contours from the experimental data obtained at low concentrations, when PS in solution is not aggregated. We also consider that the delivery of laser light and the reception of a fluorescent signal are carried out via two parallel optical fibers.

An offset of the receiving fiber axis reduces the value of the solid angle at which fluorescence must be emitted to be registered through the receiving fiber, and complicates the calculation form. In the simple case of coaxial transmitter and receiver, the solid angle is defined as

$$\Omega = 2\pi\left(1-\cos\theta\right)\\ \theta = \operatorname{atan}\left(r/d\right), \qquad (3)$$

where θ is the cone angle at the fluorescent light emission point with the base representing the optical fiber core; r – the radius of the base of the cone, d is the height of the cone. Equations (3) is reduced to

$$\Omega = 2\pi\left(1-\frac{1}{\sqrt{\left(\frac{r}{d}\right)^2+1}}\right). \qquad (4)$$

However, in the general case, the calculation of the solid angle is more complicated [12]. It is also necessary to take into account the angle at which the optical fiber is able to receive light, which is determined by its numerical aperture.

Laser light is delivered through an optical fiber directed along the x axis and the center of theend diskof which is located at the point of origin, and its radius is r_{fib}. The laser radiation emerging from the optical fiber propagates at an angle θ not exceeding the critical angle θ_{crit} determined from the numerical aperture of the optical fiber (NA = 0.22). It was determined that in our experiments the sine of the divergence angle of the exciting laser light from the optical fiber was $sin(\theta) = 0.062$, and this value was used in the calculations.

The following model for calculating the fluorescence signal obtained in reverse geometry with offset fiber optic source and receiver has been implemented:

Laser radiation is represented by a set of beams emerging from the point $O = (x_0,0,0)$, where $x_0 = -r_{fib}\,ctg\,(\theta)$, at an angle to the x-axis, less than θ. For each ray r_0, we simulate the absorbed light intensity along its path, calculate the effective intensity of the excited fluorescence at different points in the volume, and calculate the fluorescent signal transmitted through the absorbing photosensitizer medium. The resulting intensity of the fluo-

rescent signal from the beam was calculated using the formula

$$F = \int_{\vec{r}_1}^{\vec{r}_2} A_{exc}(\vec{r}) \cdot f_{eff}(\vec{r}) \cdot T_{fluo}(\vec{r})\, d\vec{r}.$$

Here $\vec{r}_1$ and $\vec{r}_2$ are the radius vectors of the intersection points of the beam r_0 with thefrontandrear innerwalls of the optical cell.

The absorption of exciting light A_{exc} is calculated using the Bouguer-Lambert-Beer law in differential form:

$$A_{exc}(\vec{r}) = -\frac{dT_{exc}(\vec{r})}{d|\vec{r}|}$$

$$T_{exc}(\vec{r}) = e^{-\varepsilon c|\vec{r}-\vec{r}_1|}$$

where ε is the value of the molar absorption of the PS at the wavelength of the exciting light, c is the molar concentration of the PS.

The value of the effective emitted fluorescent signal is determined by the formula

$$f_{eff}(\vec{r}) = \frac{\Omega(\vec{r}_f)}{4\pi} \Phi I_f(\lambda). \qquad (5)$$

Here Φ is the fluorescence quantum yield, $I_f(\lambda)$ is the value of the fluorescence spectrum curveof the photosensitizer, normalized on maximum, measured at a low PS concentration (when aggregation can be neglected), at wavelength λ, $\vec{r}_f$ is the vector between the fluorescence emission point and the center of the receiving fiber face. $\Omega(\vec{r}_f)$ determines the value of the solid angle within which all emitted fluorescence enters the receiving optical fiber.

The factor $T_{fluo}(\vec{r})$ takes into account the absorption of fluorescent light on the way from point $\vec{r}$ to the receiving fiber.

$$T_{fluo}(\vec{r}) = e^{-2.3\times\varepsilon(\lambda)\, c\, |\vec{r}_f| \times \left(1 - \frac{l}{|\vec{r}_f|\cos(\theta_f)}\right)} \qquad (6)$$

Here $\varepsilon(\lambda) = \varepsilon A(\lambda)$ is the value of the molar absorption of the photosensitizer at the fluorescence wavelength, θ_f is the angle between the x-axis and the vector $\vec{r}_f$ (Fig. 3).

The dependence of the integral fluorescence intensity of the PS (obtained numerically using the proposed model with the parameters of tetra-cationic derivative of bacteriochlorin as an example) agrees better with the experimental data (at least in the concentration range under 30 μM, wch is important from a practical point of view) than the dependence obtained in the simplified model (Fig. 4).

This calculation was also carried out in the approximation of a non-aggregated solution corresponding to the Bouguer-Lambert-Beer law. The observed difference between the results of calculations and experiments in the range of concentrations above 30 μM seems to be due to a number of phenomena associated with aggregation. Although the dependence of the PS solution absorption is linear with respect to its concentration, the fluorescence kinetics of its solutions upon excitation by a picosecond laser had features that indicate partial aggregation of solutions with higher concentrations. The values of the fluorescent lifetime of PS molecule aggregates are much shorter than those of non-aggregated molecules [13,14]. If the fluorescence decay kinetics of

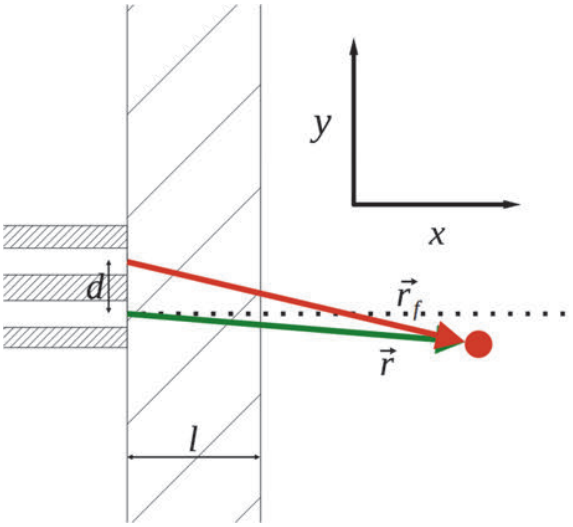

Рис. 3. Диаграмма расширенной модели для расчёта интенсивности флуоресценции раствора ФС в оптической кювете, учитывающая смещение принимающего оптического волокна.
Fig. 3. Diagram of a modified model for calculating the fluorescence intensity of a photosensitizer solution in optical cell, taking into account the shift in the position of the receiving fiber.

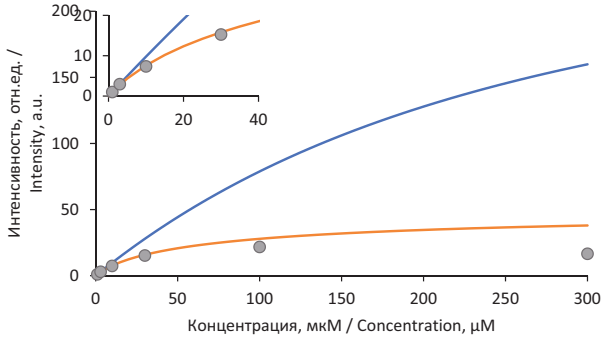

Рис. 4. Зависимость интенсивности интегральной флуоресценции тетракатионного производного бактериохлорина, полученная расчётом с помощью упрощённой модели (синий) и расширенной модели (оранжевый), а также значения (серый), полученные в эксперименте с оптической кюветой длиной 10 мм. Значения нормированы на интенсивность флуоресценции при концентрации 1 мкМ.
Fig. 4. The dependence of the integral fluorescence intensity of tetracationic bacteriochlorin derivative, obtained by calculation using the proposed simplified (blue) and modified (orange) models, and the values (gray markers) obtained in the experiment with the optical cell length of 10 mm. Numerical values are normalized to the fluorescence intensity at a concentration of 1 μM.

a partially aggregated PS is described by the sum of two exponential components with different weight coefficients [13]:

$$I(t) = A_1 \exp\left(-\frac{t}{\tau_1}\right) + A_2 \exp\left(-\frac{t}{\tau_2}\right), \quad (7)$$

then the ratio between the weight coefficients $A_1\tau_1$ for non-aggregated molecules and $A_2\tau_2$ for aggregates can characterize the degree of PS aggregation. Studies using the approach [13] showed that in solutions of the studied PS with a concentration in the range of interest, there are two fluorescent molecular groups: a monomeric PS with a relatively long lifetime (in the range of 1.5–3 ns), and the second group with a significantly shorter time lifetime (< 1 ns), the fluorescence of which is associated with self-aggregated complexes of PS molecules. The ratio of monomeric PS, estimated from the number of photons with such a lifetime among the total number of fluorescence photons, was more than 74% in an aqueous solution, that is, the degree of aggregation is low and does not noticeably affect the efficiency of this PS. but it can lead to a decrease in fluorescence intensity, which and is observed when the experimental data on the integral intensity of the solution deviate from the calculated values. Moreover, at very high concentrations (>100 μM), which go beyond the values observed in biotissues during PDT, the dependence of the integrated fluorescence intensity due to aggregation can saturate or even start decreasing.

The assumption about the partial aggregation of this PS at high concentrations, which affects its fluorescent characteristics, is additionally confirmed by the fact that when studying its fluorescence kinetics of its solution in blood plasma, the fraction of photons emitted by the monomeric component of the PS increases to 85%, and the second component, presumably associated with self-aggregated complexes of PS molecules, correspondingly decreases compared to a solution in water (Table 1). This is typical of tetrapyrroles due to the disaggregating effect of plasma proteins [15,16]but is only now becoming widely used. Originally developed as cancer therapy, some of its most successful applications are for non-malignant disease. The majority of mechanistic research into PDT, however, is still directed towards anti-cancer applications. In the final part of series of three reviews, we will cover

Таблица 1.
Время разрешенные компоненты флуоресценции тетракатионного производного бактериохлорина в воде и плазме крови

Table 1.
Lifetime components of tetracationic bacteriochlorin derivative fluorescence in water and in blood plasma

Раствор Solution	$A_1\tau_1$, %	τ_1, ns	$A_2\tau_2$, %	τ_2, ns
Вода Water	74	1.9–2.9	26	<1
Плазма крови Blood plasma	85	2.4	15	<1

the possible reasons for the well-known tumor localizing properties of photosensitizers (PS. These results confirm the assumption that the deviation of the experimentally obtained dependence of the integral fluorescence intensity from the theoretical (calculated) curve may be associated with PS aggregation at an increased concentration of its solution.

Conclusion

At low concentrations of PS a part of the energy of the exciting light, which goes beyond the volume of the excited solution, is lost, and due to local or "one-sided" registration, a part of the fluorescence light, which propagates in all directions, is also not registered. At higher concentrations, the losses of fluorescence light significantly increase due to the reabsorption of part of fluorescent light by PS molecules and subsequent re-emission with a quantum yield significantly below 1. With a further increase in concentration, partial aggregation of PS also begins to reduce the efficiency of fluorescence. At very high concentrations, the influence of aggregation begins to dominate, and therefore the dependence of the integrated fluorescence intensity on concentration saturates and even starts to decrease. Thus, the dependence of the integral fluorescence intensity on PS concentration is sublinear, and this should be taken into account in fluorescence diagnostics and navigation using this parameter.

This work was supported by RSF grant N 24-45-00020.

REFERENCES

1. Loschenov V.B., Konov V.I., Prokhorov A.M., Photodynamic Therapy and Fluorescence Diagnostics. *Laser Physics*, 2000, Vol. 10, pp.11801207.
2. Budko A.P., Deichman Z.G., Meerovich G.A., Borisova L.M., Meerovich I.G., Lantsova A.V., Yu K.N., Kulbachevskaya N.Yu., Study of pharmacokinetics of liposomal photosensitiser based on hydroxyaluminium tetra-3-phenylthiophthalocyanine on mice. *Biomedical Photonics*, 2019, Vol. 7, pp.16-22. https://doi.org/10.24931/2413-9432-2018-7-4-16-22.
3. Meerovich I.G., Kazachkina N.I., Savitsky A.P., Investigation of the effect of photosensitizer Tiosense on the tumor model

ЛИТЕРАТУРА

1. Loschenov V.B., Konov V.I., Prokhorov A.M., Photodynamic Therapy and Fluorescence Diagnostics // Laser Physics. – 2000. – Vol. 10. – P.11801207.
2. Budko A.P., Deichman Z.G., Meerovich G.A., Borisova L.M., Meerovich I.G., Lantsova A.V., Yu K.N., Kulbachevskaya N.Yu., Study of pharmacokinetics of liposomal photosensitiser based on hydroxyaluminium tetra-3-phenylthiophthalocyanine on mice // Biomedical Photonics. – 2019. – Vol. 7. – P.16-22. https://doi.org/10.24931/2413-9432-2018-7-4-16-22.
3. Meerovich I.G., Kazachkina N.I., Savitsky A.P., Investigation of the effect of photosensitizer Tiosense on the tumor model

mel Kor-TurboRFP expressed red fluorescent protein. *Russ J Gen Chem*, 2015, Vol. 85, pp. 274-279. https://doi.org/10. 1134/S1070363215010429.
4. Savitsky A.P., Meerovich I.G., Zherdeva V.V., Arslanbaeva L.R., Burova O.S., Sokolova D.V., Treshchalina E.M., Baryshnikov A.Y., Fiks I.I., Orlova A.G., Kleshnin M.S., Turchin I.V., Sergeev A.M., Three-Dimensional In Vivo Imaging of Tumors Expressing Red Fluorescent Proteins, in: R.M. Hoffman (Ed.). *In Vivo Cellular Imaging Using Fluorescent Proteins, Humana Press, Totowa, NJ*, 2012, pp. 97-114. https://doi.org/10.1007/978-1-61779-797-2_7.
5. Savelieva T.A., Kuryanova M.N., Akhlyustina E.V., Linkov K.G., Meerovich G.A., Loschenov V.B., Attenuation correction technique for fluorescence analysis of biological tissues with significantly different optical properties. *Front. Optoelectron*, 2020, Vol. 13, pp. 360-370. https://doi.org/10.1007/s12200-020-1094-z.
6. Udeneev A. M. et al. Photo and spectral fluorescence analysis of the spinal cord injury area in animal models, *Biomedical Photonics*, 2023, Vol. 3, pp. 15-20. https://doi.org/10.24931/2413-9432-2023-12-3-16-20.
7. Mironov A.N., ed., Guidelines for conducting preclinical studies of drugs. *Grif*, 2012.
8. Meerovich G., Romanishkin I., Akhlyustina E., Strakhovskaya M., Kogan E., Angelov I., Loschenov V., Borisova E., Photodynamic Action in Thin Sensitized Layers: Estimating the Utilization of Light Energy. *J-BPE*, 2021, Vol. 7, pp. 040301. https://doi.org/10.18287/JBPE21.07.040301.
9. Meerovich G.A., Akhlyustina E.V., Tiganova I.G., Lukyanets E.A., Makarova E.A., Tolordava E.R., Yuzhakova O.A., Romanishkin I.D., Philipova N.I., Zhizhimova Yu.S., Romanova Yu.M., Loschenov V.B., Gintsburg A.L., Novel Polycationic Photosensitizers for Antibacterial Photodynamic Therapy, in: G. Donelli (Ed.). *Advances in Microbiology, Infectious Diseases and Public Health, Springer International Publishing, Cham*, 2019, pp. 1-19. https://doi.org/10.1007/5584_2019_431.
10. Makarov D.A., Kuznetsova N.A., Yuzhakova O.A., Savvina L.P., Kaliya O.L., Lukyanets E.A., Negrimovskii V.M., Strakhovskaya M.G., Effects of the degree of substitution on the physicochemical properties and photodynamic activity of zinc and aluminum phthalocyanine polycations. *Russ. J. Phys. Chem*, 2009, Vol. 83, pp. 1044-1050. https://doi.org/10.1134/S0036024409060326.
11. Silva E.F.F., Serpa C., Dąbrowski J.M., Monteiro C.J.P., Formosinho S.J., Stochel G., Urbanska K., Simões S., Pereira M.M., Arnaut L.G., Mechanisms of Singlet-Oxygen and Superoxide-Ion Generation by Porphyrins and Bacteriochlorins and their Implications in Photodynamic Therapy. *Chem. Eur. J.*, 2010, Vol. 16, pp. 9273-9286. https://doi.org/10.1002/chem.201000111.
12. Paxton F., Solid Angle Calculation for a Circular Disk. *Review of Scientific Instruments*, 1959, Vol. 30, pp. 254-258. https://doi.org/10.1063/1.1716590.
13. Makarov V.I., Pominova D.V., Ryabova A.V., Romanishkin I.D., Voitova A.V., Steiner R.W., Loschenov V.B., Theranostic Properties of Crystalline Aluminum Phthalocyanine Nanoparticles as a Photosensitizer. *Pharmaceutics*, 2022, Vol. 14, pp. 2122. https://doi.org/10.3390/pharmaceutics14102122.
14. Lacey J.A., Phillips D., Fluorescence lifetime measurements of disulfonated aluminium phthalocyanine in the presence of microbial cells. *Photochem Photobiol Sci*, 2002, Vol. 1, pp. 378-383. https://doi.org/10.1039/b108831a.
15. Castano A.P., Demidova T.N., Hamblin M.R., Mechanisms in photodynamic therapy: Part three-Photosensitizer pharmacokinetics, biodistribution, tumor localization and modes of tumor destruction. *Photodiagnosis Photodyn Ther*, 2005, Vol. 2, pp. 91-106. https://doi.org/10.1016/S1572-1000(05)00060-8.
16. Tominaga T.T., Yushmanov V.E., Borissevitch I.E., Imasato H., Tabak M., Aggregation phenomena in the complexes of iron tetraphenylporphine sulfonate with bovine serum albumin. *Journal of Inorganic Biochemistry*, 1997, Vol. 65, pp. 235-244. https://doi.org/10.1016/S0162-0134(96)00137-7.

mel Kor-TurboRFP expressed red fluorescent protein // Russ J Gen Chem. – 2015. – Vol. 85. – P. 274-279. https://doi.org/10.1134/S1070363215010429.
4. Savitsky A.P., Meerovich I.G., Zherdeva V.V., Arslanbaeva L.R., Burova O.S., Sokolova D.V., Treshchalina E.M., Baryshnikov A.Y., Fiks I.I., Orlova A.G., Kleshnin M.S., Turchin I.V., Sergeev A.M., Three-Dimensional In Vivo Imaging of Tumors Expressing Red Fluorescent Proteins, in: R.M. Hoffman (Ed.) // In Vivo Cellular Imaging Using Fluorescent Proteins, Humana Press, Totowa, NJ. – 2012. – P. 97-114. https://doi.org/10.1007/978-1-61779-797-2_7.
5. Savelieva T.A., Kuryanova M.N., Akhlyustina E.V., Linkov K.G., Meerovich G.A., Loschenov V.B., Attenuation correction technique for fluorescence analysis of biological tissues with significantly different optical properties // Front. Optoelectron. – 2020. – Vol. 13. – P. 360-370. https://doi.org/10.1007/s12200-020-1094-z.
6. Udeneev A. M. et al. Photo and spectral fluorescence analysis of the spinal cord injury area in animal models // Biomedical Photonics. – 2023. – T. 12. – №. 3. – C. 15-20. https://doi.org/10.24931/2413-9432-2023-12-3-16-20.
7. Mironov A.N., ed., Guidelines for conducting preclinical studies of drugs // Grif. – 2012.
8. Meerovich G., Romanishkin I., Akhlyustina E., Strakhovskaya M., Kogan E., Angelov I., Loschenov V., Borisova E., Photodynamic Action in Thin Sensitized Layers: Estimating the Utilization of Light Energy // J-BPE. – 2021. – Vol. 7. – P. 040301. https://doi.org/10.18287/JBPE21.07.040301.
9. Meerovich G.A., Akhlyustina E.V., Tiganova I.G., Lukyanets E.A., Makarova E.A., Tolordava E.R., Yuzhakova O.A., Romanishkin I.D., Philipova N.I., Zhizhimova Yu.S., Romanova Yu.M., Loschenov V.B., Gintsburg A.L., Novel Polycationic Photosensitizers for Antibacterial Photodynamic Therapy, in: G. Donelli (Ed.) // Advances in Microbiology, Infectious Diseases and Public Health, Springer International Publishing, Cham. – 2019. – P. 1-19. https://doi.org/10.1007/5584_2019_431.
10. Makarov D.A., Kuznetsova N.A., Yuzhakova O.A., Savvina L.P., Kaliya O.L., Lukyanets E.A., Negrimovskii V.M., Strakhovskaya M.G., Effects of the degree of substitution on the physicochemical properties and photodynamic activity of zinc and aluminum phthalocyanine polycations // Russ. J. Phys. Chem. – 2009. – Vol. 83. – P. 1044-1050. https://doi.org/10.1134/S0036024409060326.
11. Silva E.F.F., Serpa C., Dąbrowski J.M., Monteiro C.J.P., Formosinho S.J., Stochel G., Urbanska K., Simões S., Pereira M.M., Arnaut L.G., Mechanisms of Singlet-Oxygen and Superoxide-Ion Generation by Porphyrins and Bacteriochlorins and their Implications in Photodynamic Therapy // Chem. Eur. J. – 2010. – Vol. 16. – P. 9273-9286. https://doi.org/10.1002/chem.201000111.
12. Paxton F., Solid Angle Calculation for a Circular Disk // Review of Scientific Instruments. – 1959. – Vol. 30. – P. 254-258. https://doi.org/10.1063/1.1716590.
13. Makarov V.I., Pominova D.V., Ryabova A.V., Romanishkin I.D., Voitova A.V., Steiner R.W., Loschenov V.B., Theranostic Properties of Crystalline Aluminum Phthalocyanine Nanoparticles as a Photosensitizer // Pharmaceutics. – 2022. – Vol. 14. – P. 2122. https://doi.org/10.3390/pharmaceutics14102122.
14. Lacey J.A., Phillips D., Fluorescence lifetime measurements of disulfonated aluminium phthalocyanine in the presence of microbial cells // Photochem Photobiol Sci. – 2002. – Vol. 1. – P. 378-383. https://doi.org/10.1039/b108831a.
15. Castano A.P., Demidova T.N., Hamblin M.R., Mechanisms in photodynamic therapy: Part three-Photosensitizer pharmacokinetics, biodistribution, tumor localization and modes of tumor destruction // Photodiagnosis Photodyn Ther. – 2005. – Vol. 2. – P. 91-106. https://doi.org/10.1016/S1572-1000(05)00060-8.
16. Tominaga T.T., Yushmanov V.E., Borissevitch I.E., Imasato H., Tabak M., Aggregation phenomena in the complexes of iron tetraphenylporphine sulfonate with bovine serum albumin // Journal of Inorganic Biochemistry. – 1997. – Vol. 65. – P. 235-244. https://doi.org/10.1016/S0162-0134(96)00137-7.

PHOTODYNAMIC THERAPY OF BASAL CELL CARCINOMA OF THE FACE H-ZONE

Nadkernichnaya E.V.[1], Ermoschenkova M.V.[1,2], Semin V.E.[1], Parts S.A.[1], Galkin V.N.[1], Reshetov I.V.[2]

[1]State Budgetary Healthcare Institution of the City of Moscow "S.S. Yudin City Clinical Hospital of the Moscow City Healthcare Department", Moscow, Russia

[2]First Moscow State Medical University named after I.M. Sechenov, Moscow, Russia

Abstract

This article reviews clinical experience in treating skin neoplasms using photodynamic therapy with combined ultrasound and fluorescence diagnostics for neoplasms in the nose, lateral face, and adjacent areas. Injectable forms of chlorine-type drugs were used as photosensitizers – photoditazine or photoran at a dose of 0.7 to 2.5 mg per kilogram of patient body weight. The drug was administered intravenously for 30 minutes 2.5-3.0 hours before tumor irradiation. Of 107 observations over a 9-month observation period, one case of marginal tumor recurrence in the treatment area was detected. Thus, the recurrence rate was 0.93%. The results show that three-dimensional tumor visualization for the H-zone with complex noninvasive diagnostics allows achieving high efficiency in photodynamic therapy of non-melanoma tumors of the above anatomical localizations.

Keywords: ultrasound navigation; fluorescence diagnostics; laser spectroscopy; non-melanoma skin tumors, laser spectroscopy, non-invasive monitoring.

Contacts: Nadkernichnaya E.V., e-mail: ulena.nadkernichnaya@bk.ru

For citation: Nadkernichnaya E.V., Ermoschenkova M.V., Semin V.E., Parts S.A., Galikin V.N., Reshetov I.V. Photodynamic therapy of basal cell carcinoma of the face H-zone, *Biomedical Photonics*, 2025, vol. 14, no. 2, pp. 27–30. doi: 10.24931/2413–9432–2025–14–2–27–30

ФОТОДИНАМИЧЕСКАЯ ТЕРАПИЯ БАЗАЛЬНОКЛЕТОЧНОГО РАКА КОЖИ Н-ЗОНЫ ЛИЦА

Е.В. Надкерничная[1], М.В. Ермощенкова[1,2], В.Е. Семин[1], С.А. Партс[1], В.Н. Галкин[1], И.В. Решетов[2]

[1]Государственное бюджетное учреждение здравоохранения города Москвы «Городская клиническая больница имени С.С. Юдина Департамента здравоохранения города Москвы», Москва, Россия

[2]Первый Московский государственный медицинский университет им. И.М. Сеченова, Москва, Россия

Резюме

В данной статье рассмотрен клинический опыт лечения новообразований кожи методом фотодинамической терапии с сочетанной ультразвуковой и флуоресцентной диагностикой для новообразований в зоне носа, боковой поверхности лица и смежных областей. В качестве фотосенсибилизатора применяли инъекционные формы препаратов хлоринового ряда, фотодитазин или фоторан, в дозе от 0,7 до 2,5 мг на килограмм массы тела пациента. Препарат вводили внутривенно в течение 30 мин за 2,5-3,0 ч до начала облучения опухоли. Из 107 наблюдений при сроке наблюдения 9 мес выявлен один случай краевого рецидива опухоли в зоне лечения. Таким образом, частота возникновения рецидивов составила 0,93%. Полученные результаты показывают, что трехмерная визуализация опухоли для Н-зоны с комплексной неинвазивной диагностикой позволяет достичь высокой эффективности при фотодинамической терапии немеланомных опухолей вышеуказанных анатомических локализаций.

Ключевые слова: ультразвуковая навигация; флуоресцентная диагностика; лазерная спектроскопия; немеланомные опухоли кожи, лазерная спектроскопия, неинвазивный мониторинг.

Контакты: Надкерничная Е.В., e-mail: yelena.nadkernichnaya@bk.ru

Для цитирования: Надкерничная Е.В., Ермощенкова М.В., Семин В.Е., Партс С.А., Галикин В.Н., Решетов И.В. Фотодинамическая терапия базальноклеточного рака кожи Н-зоны лица // Biomedical Photonics. – 2025. – Т. 14, № 2. – С. 27–30. doi: 10.24931/2413–9432–2025–14–2–27–30

Introduction

In the Russian Federation, for the period from 2013 to 2023, the crude incidence rate (both sexes) of non-melanoma skin cancers increased from 46.09 to 62.79 cases per 100,000 population. The growth rate for the specified period was 15.44% [1]. For non-melanoma tumors, a wide range of surgical and non-surgical treatment methods are used in accordance with clinical guidelines [2]. Photodynamic therapy (PDT) is one of such methods [2-5]. The desire for uniformity and standardization of clinical treatment protocols are key steps to the implementation of current recommendations for the effective use of PDT in oncology. It is known that up to 90% of all non-melanoma skin cancers are localized on the face [2]. The emerging need for gentle, organ-preserving approaches increases the relevance of PDT in the clinical practice of an oncologist. The key objective of therapy is to achieve a good cosmetic result while maintaining antitumor efficacy. It is also necessary to take into account that critical loss of fluorescent radiation (photobleaching) occurs during photodynamic reactions. The practical significance of fluorescence diagnostics (FD) is due to the ability of a photosensitizer (PS) to selectively accumulate in malignant neoplasms relative to surrounding healthy tissues, creating a fluorescent contrast [6]. High-resolution ultrasound with assessment of tumor microvascularization can be a valuable tool for clarifying neoplasm characteristics such as thickness, contours, echostructure, and prevalence [3].

Combining therapeutic and diagnostic capabilities into a single technology will help personalize the selection of energy parameters for laser exposure and monitor PDT in real time.

Materials and methods

A total of 107 cases of clinical observations of ultrasound-guided PDT of epithelial malignant tumors in patients of both sexes and different age groups with basal cell skin cancer were selected for participation in the study. They underwent inpatient treatment in the fluorescence diagnostics and photodynamic therapy room from November 2023 to March 2024. During the ultrasound-guided PDT procedure, injectable forms of chlorine photosensitizers – photoditazine or photoran were used at a dosage of 0.7 to 2.5 mg per kilogram of patient body weight. The drug was administered intravenously for 30 minutes 2.5-3.0 hours before the start of tumor irradiation. The average age of patients was 73 years. The tumors were divided into comparable groups based on indicators regarding high-risk zones of recurrence, ultrasound characteristics, local fluorescence data, and laser exposure parameters. During PDT, high-resolution ultrasound examination was performed on an expert-class Philips Epic 7 device using MFI technology. At the next stage, FD was performed in the blue and red spectrum ranges in real time using PDT apparatus "Harmony" and UFF630/675-01 (video LED phototherapeutic fluorescence devices), as well as a LESA-01 laser fiber-optic spectrometer. For the laser irradiation session, a Lakhta-Milon model 662–2.8 device (OOO Kvalitek, MILON laser LLC group of companies, St. Petersburg, Russia, registration certificate of the Federal Service for Supervision of Health, Safety and Social Development No. FS 02262003/2932-06) with a wavelength of 662 nm was used. Light was delivered to the tumor using a certified light guide with macrolenses (manufactured by OOO Polironik, Moscow, Russia). The light dose and power density were 100-250 J/cm^2. All PDT and FD procedures were performed in specially equipped rooms in accordance with the requirements of the "Sanitary Norms and Rules for the Installation and Operation of Lasers" No. 5804-91. Further clinical observations were carried out 3, 6 and 9 months after PDT under ultrasound navigation in an outpatient care center.

Results

In a retrospective study, cases of non-melanoma skin cancer were analyzed in a group of patients with tumors located in the H-zone of the face. With respect to the anatomical areas, the neoplasms were divided into three groups: group 1 – nasal zone (n=44), group 2 – lateral face surface zone (n=33) and group 3 – adjacent localization zone (n=30). All patients from the studied groups underwent expert-class ultrasound examination with an assessment of the ultrasound characteristics of thickness and prevalence (Fig. 1).

The diagnostic results showed that the thickness of the formations in the nasal area averaged 2.1 mm (minimum 1.5 mm, maximum 3 mm). As for the prevalence of neoplasms in this area, the average value was 9 mm, with a minimum value of 6.38 mm and a maximum value of 12.25 mm. In the area of the lateral surface of the face and adjacent localizations, the thickness of the neoplasms was slightly smaller, averaging 1.8 mm (with a minimum thickness of 1.35 mm and a maximum of 2.6 mm). The prevalence rates in these areas were 9.7–10 mm (minimum 7.5 mm, maximum 13 mm) (Table 1).

After ultrasound navigation, local fluorescence imaging was performed in the blue and red spectral ranges. During local fluorescence spectroscopy (HeNe laser, 632.8 nm), the degree of PS accumulation was assessed using calculations of the fluorescence contrast “tumor/healthy tissue” based on average fluorescence intensity values (Fig. 2).

PDT in combination with ultrasound diagnosis and FD demonstrated high efficiency in dynamic observation of 107 cases of skin neoplasms for 9 months after therapy. The observation periods for patients from the specified groups were divided into time periods in accordance with the schedule. The first period was from 1 week to 3 months, the

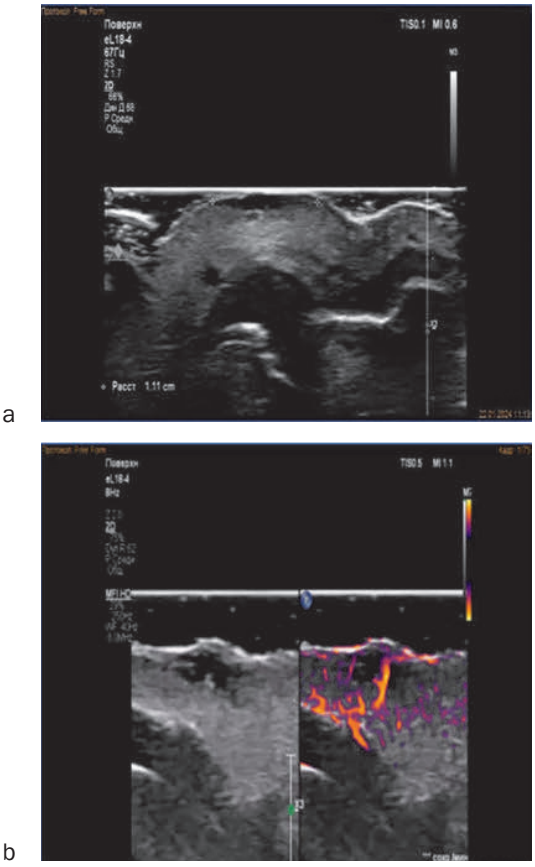

Рис. 1. Пример ультразвукового исследование высокого разрешения на аппарате экспертного класса Philips Epic 7 с использованием технологии MFI перед ФДТ: a – внутрикожное гипоэхогенное неоднородное с неровными нечеткими контурами образование, горизонтальными размерами (протяженность) не менее 11 мм; b – толщина образования 2,8 мм, активный центральный и периферический сосудистый рисунок.
Fig. 1. Example of high-resolution ultrasound examination on the Philips Epic 7 expert class device using MFI technology before PDT: a – intradermal hypoechogenic inhomogeneous formation with uneven fuzzy contours; horizontal dimensions (extent) not less than 11 mm; b – thickness of the formation 2.8 mm, active central and peripheral vascular pattern.

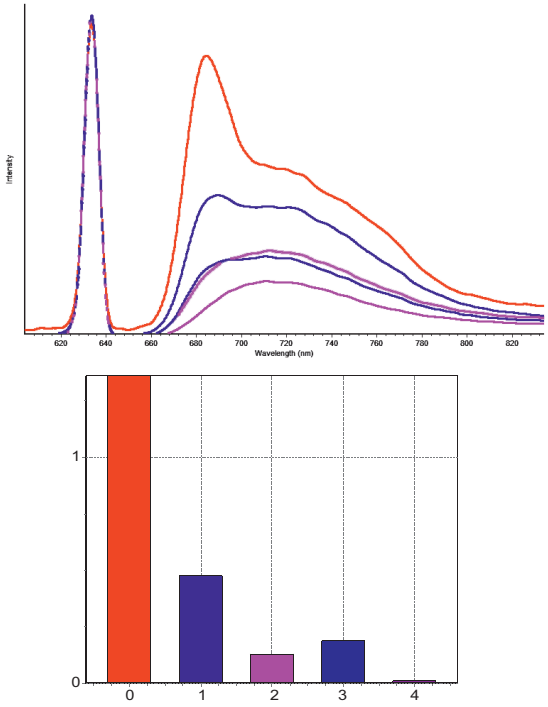

Рис. 2. Спектры флуоресценции и соответствующие им гистограммы, характеризующие интенсивность флюоресценции (возбуждение HeNe-лазер, 632,8 нм): 1 – (красный) – флуоресценция опухоли через 3 часа после введения ФС; 2 – (синий) – флуоресценция опухоли после первого этапа облучения (100 Дж/см^2); 3 – (розовый) – флуоресценция опухоли после второго этапа облучения (50 Дж/см^2); 4 – (темно-синий) – флуоресценция нормальной кожи пациента (контроль 1); 5 – (фиолетовый) – флуоресценция кожи врача (контроль 2).
Фотосенсибилизатор: фотолон, доза 2,0 мг/кг веса. Флуоресцентная контрастность ~6 . Облучение 662 нм, 250 мВт/см^2.
Fig. 2. Fluorescence spectra and their corresponding histograms characterising fluorescence intensity (HeNe-laser excitation, 632.8 nm): 1 – (red) – tumour fluorescence 3 hours after PS injection; 2 – (blue) – tumour fluorescence after the first stage of irradiation (100 J/cm^2); 3 – (pink) – tumour fluorescence after the second stage of irradiation (50 J/cm^2); 4 – (dark blue) – fluorescence of the patient's normal skin (control 1); 5 – (violet) – fluorescence of the doctor's skin (control 2).
Photosensitiser: fotolon, dose 2.0 mg/kg weight. Fluorescence contrast ~6 . Irradiation at 662 nm, 250 mW/cm^2.

Таблица 1.
Характеристики опухолей (толщина и распространенность) и площади лазерного воздействия в зависимости от локализации опухоли

Table 1.
Tumor characteristics (thickness and extent) and laser treatment areas depending on tumor location

Группа Group	n	Толщина образования, мм Formation thickness, mm		Размеры (протяженность), мм Dimensions (length), mm		Общая площадь лазерного воздействия Total laser treatment area	
		Me	$Q_1 – Q_3$	Me	$Q_1 – Q_3$	Me	$Q_1 – Q_3$
Область боковой поверхности лица Lateral facial surface area	33	1,8	1,35 – 2,60	9,7	7,50 – 13,00	3	3 – 5
Область носа Nasal region	44	2,1	1,51 – 3,00	9	6,38 – 12,25	3	3– 5
Область смежных локализаций Area of related localisations	30	1,8	1,32 – 2,50	10	7,70 – 12,00	3	3 – 5

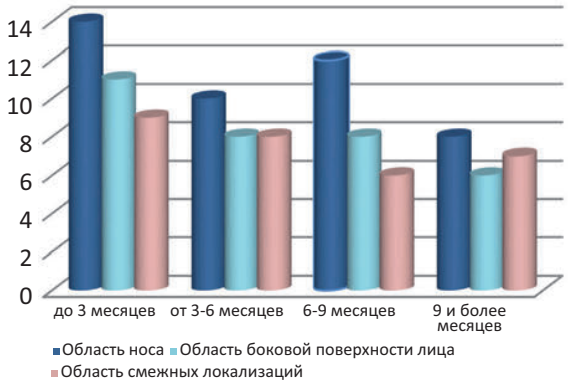

Рис. 3. Распределение новообразований кожи для исследуемых групп согласно графику динамического наблюдения.
Fig. 3. Distribution of skin neoplasms for the studied groups according to the dynamic observation schedule.

second – from 3 to 6 months, the third – from 6 to 9 months, and the fourth – from 9 months and more (Fig. 3).

All patients underwent regular monitoring, which allowed for timely detection of relapse and provision of the necessary subsequent treatment. Of the 107 observations, 106 cases of relapse-free observation and one case of marginal tumor relapse in the treatment area 9 months after PDT were identified. Thus, the relapse rate was 0.93%. Registration of one relapse of the disease (0.93%) during the specified observation period indicates the high therapeutic efficiency of PDT.

Fig. 4 shows an example of the result obtained 9 months after PDT under ultrasound navigation of a skin neoplasm on the bridge of the nose.

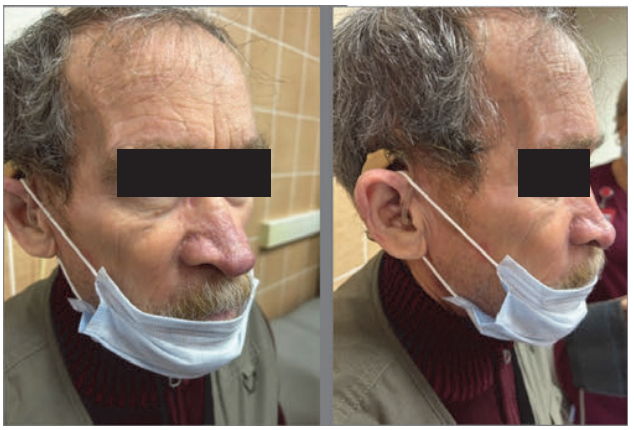

Рис. 4. Результат лечения пациента через 9 мес после ФДТ под УЗ-навигацией новообразования кожи спинки носа. Фотосенсибилизатор: фотолон, доза 2,0 мг/кг веса. Облучение 662 нм, 250 мВт/см^2.
Fig. 4. Patient's treatment result 9 months after PDT under ultrasound guidance of dorsal nasal skin neoplasm. Photosensitiser: Fotolon, dose 2.0 mg/kg body weight. Irradiation at 662 nm, 250 mW/cm^2.

Conclusion

The study confirmed that PDT is a highly effective method for treating basal cell skin cancer, including tumor foci localized on the skin of the H-zone of the face. At the same time, three-dimensional visualization of the tumor for the H-zone with complex non-invasive diagnostics had an advantage in PDT of non-melanoma tumors of the above anatomical localizations.

REFERENCES

1. The state of oncological care for the Russian population in 2023. Edited by Kaprina A.D., Starinsky V.V., Shakhzadova A.O. Malignant neoplasms in Russia in 2023 (morbidity and mortality) – Moscow: P.A. Herzen Moscow Medical Research Institute – branch of the Federal State Budgetary Institution «NMITS of Radiology» of the Ministry of Health of the Russian Federation. Moscow, 2024, pp.14.
2. Basal cell carcinoma of the skin. Clinical recommendations. Association of Oncologists of Russia. Association of Melanoma Specialists. All-Russian public organization «Russian Society of Clinical Oncology». All-Russian public organization «Association of Ophthalmologists». Russian Federation 2024 (Russia), pp. 26-47.
3. Kapinus V.N., Kaplan M.A., Sokol N.I. Predictors of recurrence of basal cell carcinoma of the skin after photodynamic therapy with photolon photosensitizer. *Laser medicine,* 2019, pp. 28-37.
4. Filonenko E.V., Ivanova-Radkevich V.I. Fluorescence diagnostics in non-melanocytic skin tumors. *Biomedical Photonics*, 2022, pp. 32-40.
5. Kapinus V.N., Kaplan M.A., Yaroslavtseva-Isaeva E.V. [et al.] Photodynamic therapy as a treatment option for skin cancer that has developed on scars. *Laser medicine*, 2020, Vol. 24(4), pp. 54-61.
6. Khoruzhaya S.S., Vasiliev A.Yu., Semin V.E., Nechaev V.A. High – resolution ultrasound examination during photodynamic therapy of basal cell carcinoma of the head and neck. *Radiology – practice*, 2025, pp.12-26.

ЛИТЕРАТУРА

1. Состояние онкологической помощи населению России в 2023 году. Под ред. А.Д. Каприна, В.В. Старинского, А.О. Шахзадовой. Злокачественные новообразования в России в 2023 году (заболеваемость и смертность) – М.: МНИОИ им. П.А. Герцена – филиал ФГБУ «НМИЦ радиологии» Минздрава России. Москва. – 2024. – С.14.
2. Базальноклеточный рак кожи. Клинические рекомендации. Ассоциация онкологов России. Ассоциация специалистов по проблемам меланомы. Общероссийская общественная организация «Российское общество клинической онкологии». Общероссийская общественная организация «Ассоциация врачей-офтальмологов». РФ 2024 г. (Россия). – С. 26-47.
3. Капинус В.Н., Каплан М.А., Сокол Н.И. Предикторы рецидивов базальноклеточного рака кожи после проведения фотодинамической терапии с фотосенсибилизатором фотолон // Лазерная медицина. – 2019. – С. 28-37.
4. Филоненко Е.В., Иванова-Радкевич В.И. Флуоресцентная диагностика при немеланоцитарных опухолях кожи // Biomedical Photonics. – 2022 г. – С. 32-40.
5. Капинус В.Н., Каплан М.А., Ярославцева-Исаева Е.В. [др.] Фотодинамическая терапия как вариант лечения рака кожи, развившегося на рубцах // Лазерная медицина. – 2020. – Т. 24, № 4. – С. 54-61.
6. Хоружая С.С., Васильев А.Ю., Семин В.Е., Нечаев В.А. Ультразвуковое исследование высокого разрешения при проведении фотодинамической терапии базальноклеточного рака головы и шеи // Радиология — практика. – 2025 г. – С.12-26.

CLINICAL RESEARCH OF PHOTODYNAMIC THERAPY WITH 5-ALA FOR CERVICAL INTRAEPITHELIAL NEOPLASMS: FROM PRELIMINARY STUDIES TO CURRENT DEVELOPMENTS

Shanazarov N.A.[1], Aitkaliyev A.D.[1], Grishacheva T.G.[2], Kissikova S.D.[1], Zinchenko S.V.[3], Kassiyeva B.S.[1], Smailova S.B.[1], Salmagambetova Zh.Zh.[1], Seitbekova K.[1]

[1]Medical Center Hospital of the President's Affairs Administration of the Republic of Kazakhstan, Astana, Kazakhstan

[2]Pavlov First Saint-Petersburg State Medical University, Saint-Petersburg, Russian Federation

[3]Kazan (Volga Region) Federal University, Kazan, Russia

Abstract

Non-surgical therapies are essential for reducing the progression rate of human papillomavirus-associated cervical intraepithelial neoplasia (CIN) from low-grade (CIN 1) to high-grade CIN (CIN 2/3) and subsequently to cervical cancer with minimal adverse reactions and complications in women, such as haemorrhaging, cervical stenosis, spontaneous abortion, and preterm birth.

Photodynamic therapy (PDT) has garnered considerable attention as a non-invasive approach to CIN treatment in recent years. PDT works by applying photoactive compounds, known as photosensitizers, that accumulate in target cells. Subsequent exposure of these cells to light of a specific wavelength (photoactivation) occurs. This paper aims to review the clinical development of clinical research on the effectiveness of PDT with a 5-Aminolevulinic acid (5-ALA) photosensitiser for treating CIN 1-3 from the early preliminary studies to recent reports.

Early PDT studies using lower concentrations of 5-ALA showed poor effectiveness, but recent research with a 20% concentration of 5-ALA demonstrated better outcomes. Larger studies, preferably conducted across multiple centres, are needed to establish the optimal number of PDT sessions required to eliminate HPV.

Keywords: cervical intraepithelial neoplasia, photodynamic therapy, human papillomavirus, 5-aminolevulinic acid, squamous intraepithelial lesions.

Contacts: Aitkaliyev A., e-mail: aitkaliyev1998@gmail.com

For citations: Shanazarov N.A., Aitkaliyev A.D., Grishacheva T.G., Kissikova S.D., Zinchenko S.V., Kassiyeva B.S., Smailova S.B., Salmagambetova Zh.Zh., Seitbekova K. Clinical research of photodynamic therapy with 5-ALA for cervical intraepithelial neoplasms: from preliminary studies to current developments, *Biomedical Photonics*, 2025, vol. 14, no. 2, pp. 31–39. doi: 10.24931/2413–9432–2025–14–2–31–39

КЛИНИЧЕСКИЕ ИССЛЕДОВАНИЯ ФОТОДИНАМИЧЕСКОЙ ТЕРАПИИ С 5-АЛК ПРИ ДИСПЛАЗИИ ШЕЙКИ МАТКИ: ОТ ПИЛОТНЫХ ИССЛЕДОВАНИЙ ДО СОВРЕМЕННЫХ РАЗРАБОТОК

Н.А. Шаназаров[1], А.Д. Айткалиев[1], Т.Г. Гришачева[2], С.Д. Кисикова[1], С.В. Зинченко[3], Б.С. Касиева[1], С.Б. Смаилова[1], Ж.Ж. Сальмагамбетова[1], К. Сейтбекова[1]

[1]Больница Медицинского центра Управления делами Президента Республики Казахстан, Астана, Казахстан

[2]Первый Санкт-Петербургский государственный медицинский университет имени академика И. П. Павлова, Санкт-Петербург, Россия

[3]Казанский (Приволжский) федеральный университет, Казань, Россия

Резюме

Неоперативные методы терапии имеют важное значение для снижения скорости прогрессирования дисплазий шейки матки, ассоциированных с вирусом папилломы человека (ВПЧ), от CIN 1 до CIN 2/3, а затем до рака шейки матки, при минимальных побочных эффектах и осложнениях у женщин, таких как кровотечения, сужение шейки матки, спонтанные аборты и преждевременные роды.

Фотодинамическая терапия (ФДТ) привлекла значительное внимание как неинвазивный метод лечения CIN в последние годы. ФДТ

основана на применении фотоактивных соединений, известных как фотосенсибилизаторы, которые накапливаются в целевых клетках. Затем эти клетки подвергаются воздействию света с определенной длиной волны. Цель данной работы — обзор клинического развития и исследования эффективности ФДТ с фотосенсибилизатором 5-аминолевулиновой кислоты (5-АЛК) для лечения CIN 1–3, начиная с ранних пилотных исследований и заканчивая последними отчетами.
Ранние исследования ФДТ с использованием низких концентраций 5-АЛК показали низкую эффективность, но недавние исследования с концентрацией 20% 5-АЛК продемонстрировали лучшие результаты. Для установления оптимального количества сеансов ФДТ, необходимых для устранения ВПЧ, требуются более крупные исследования, желательно проводимые в нескольких центрах.

Ключевые слова: дисплазия шейки матки, фотодинамическая терапия, вирус папилломы человека, 5-аминолевулиновая кислота, плоскоклеточное интраэпителиальное поражение.

Контакты: Айткалиев А. Д., e-mail: aitkaliyev1998@gmail.com

Для цитирования: Шаназаров Н.А., Айткалиев А.Д., Гришачева Т.Г., Кисикова С.Д., Зинченко С.В., Касиева Б.С., Смаилова С.Б., Сальмагамбетова Ж.Ж., Сейтбекова К. Клинические исследования фотодинамической терапии с 5-АЛК при дисплазии шейки матки: от пилотных исследований до современных разработок // Biomedical Photonics. – 2025. – Т. 14, № 2. – С. 31–39. doi: 10.24931/2413–9432–2025–14–2–31–39

Introduction

Among all human cancer cases worldwide, approximately 15% to 20% are associated with viral infections, thus making oncogenic viruses recognized as significant risk factors for cancer development [1]. One of the most prominent infectious oncogenic agents worldwide is human papillomavirus (HPV) which is responsible for 31.1% of all infectious disease-induced cancer cases and the development of 99.7% of cervical cancer in women [1, 2]. Particularly, HPV types 16 and 18 are the most virulent and are responsible for about 70% of all pre-cancerous cervical lesions and cervical cancers [3]. While 90% of HPV infections are transient and get cleared up by the immune systems within 12 to 24 months of exposure, some persistent HPV strains can prompt infected cells to proliferate uncontrollably, therefore inducing precancerous or tumorous changes in the host organism [4].

Cervical cancer is a progression of a prolonged phase of pre-invasive disease known as cervical intraepithelial neoplasia (CIN). CIN is further categorized into CIN 1, 2, or 3, reflecting increasing severity based on the proportion of abnormal cells within the cervical epithelium. Although CIN is classified as a precancerous condition, only about 9% of CIN 1 lesions progress to CIN 3 over approximately 2 to 3 years [5], and only 30% of CIN 3 lesions progress to cancer in 10-25 years [6]. According to the Lower Anogenital Squamous Terminology (LAST) standardization, low-grade squamous intraepithelial lesions (LSIL or CIN 1/2) are an instantaneous expression of HPV infection, exhibiting distinct biological properties from malignant tumours and featuring a high natural regression rate, – about 60%-90% of LSIL cases undergo natural reversal within 2 years, and only 1% may advance to cervical cancer [7], whereas high-grade squamous intraepithelial lesions (HSIL or CIN 3) a more dangerous category with the risk of progression to invasive carcinoma of the cervix in the absence of appropriate treatment.

Generally, the mortality rate in underdeveloped countries from cervical cancer is 18 times higher than the wealthier Western countries due to their lack of public awareness, socioeconomic factors, no HPV vaccination, limited access to screening programs, and subsequent delayed or inadequate treatments [8].

Conventional treatment methods for CINs and HPV infection, such as radiation, chemotherapy, cryotherapy, and surgical excision using laser or loop electrosurgical excision procedures, are all invasive in their application. These invasive treatments can lead to various adverse reactions and complications, including haemorrhaging, cervical stenosis, and serious issues in subsequent pregnancies like spontaneous abortion, preterm birth, and overall fertility [9, 10]. Hence, there is a crucial need to develop alternative treatment approaches that effectively address CIN and cervical HPV infection without compromising a patient's fertility and health [11, 12].

Photodynamic therapy (PDT) stands out as a promising and highly selective therapeutic method in this context. PDT involves the use of photoactive compounds (photosensitizers) that accumulate in target cells, and its therapeutic effect is not limited to the direct destruction of these cells. The photodynamic action also includes damage to local vasculature and modulation of the immune response, making PDT a multifaceted treatment modality [13, 14]. 5-Aminolevulinic acid (5-ALA), a precursor to the potent sensitizer protoporphyrin IX (PpIX), has been utilised in PDT treatments for cervical condyloma, cervical intraepithelial neoplasia (CIN), and other diseases of the female reproductive tract. The sensitiser selectively accumulates in abnormal tissues and, upon exposure to light at specific wavelengths induced, induces cellular oxidative stress by generating reactive oxygen species that kill pre-cancerous cells [15]. PDT has found utility across various medical domains as a non-invasive, highly selective, and locally applied treatment.

Our study seeks to review the development and evolution of clinical research assessing the effectiveness of PDT with 5-ALA with some parallels with similar

photosensitisers as a therapeutic option for women diagnosed with cervical dysplasia induced by an HPV virus.

PDT-5-ALA Mode of Action

PDT consists of three essential components: a photosensitiser, an optical wavelength of light, and a reactive oxygen species [11, 15]. Early clinical trials of PDT utilized first-generation photosensitisers, such as hematoporphyrin derivative and its purified form photofrin II, demonstrating effectiveness against various cancers including brain, lung, and skin carcinomas [16-18]. However, first-generation photosensitisers were limited by their complex composition and structure, which negatively impacted tissue selectivity and the stability of photodynamic damage intensity. In contrast, second-generation photosensitisers have a clear composition and structure, with significantly improved photosensitivity, absorption spectrum, and tissue selectivity [16]. Many second-generation photosensitisers are based on the porphyrin structure, including benzoporphyrins, purpurins, texaphyrins, and protoporphyrin IX (PpIX)[16].

5-ALA, and its more hydrophobic ester derivatives, methyl aminolevulinate (MAL) and hexaminolevulinate, is a natural amino acid and a precursor of PpIX. When externally administered, 5-ALA enters normal cells and participates in the porphyrin metabolism pathway, contributing to haem synthesis. However, in cancer cells, PpIX accumulates selectively and acts as a photosensitizer due to the reduced activity of the enzyme ferrochelatase (FECH), which is responsible for converting PpIX into haem [19, 20]. Cells infected with HPV can selectively take up ALA upon exposure, leading to the accumulation of PpIX within these infected cells [21, 22]. During irradiation, specifically ultraviolet or blue light, PpIX exhibits distinct red fluorescence, simultaneously initiating the generation of cytotoxic reactive oxidative species that eliminate the cells, inhibiting viral replication through oxygen-dependent cytotoxic reactions, viral nucleic acid strand breaking, or base site disappearance [23]. Unlike typical fluorescent agents used solely for imaging, these prodrugs serve a dual purpose by labelling cancer cells for easy detection and cancer cell death, which is employed by PDT [24].

Early feasibility studies of 5-ALA-PDT in treating cervical dysplasia

Hillemanns et al. were one of the pioneers in employing 5-ALA for fluorescence-based diagnosis of CIN, revealing promising prospects for the 5-ALA-mediated PDT (5-ALA-PDT) of CIN [25, 26]. In their study, it was the topical application of 1% 5-ALA that exhibited distinctive porphyrin fluorescence specifically in CIN, while the lesser concentration of 5-ALA (0.5%) was proven ineffective due to rapid photobleaching [26].

In a retrospective analysis involving clinical data from 115 patients with CIN (53 in a control group and 62 in an experimental group treated with 5-ALA-PDT), Yi Chen et al. found that the PDT treatment achieved HPV clearance and disease reversal at significantly higher rates (79.0% and 80.6%, respectively) than the one-time CO_2 laser therapy (62.3% and 64.2%, respectively) ($p<0.05$) at the 6-month follow-up. Furthermore, the PDT therapy achieved a better therapeutic effect with no significant difference in the cure rate of different parts, indicating that 5-ALA-PDT can reach a target site without causing scarring and preserving fertility function, thus demonstrating the ability to target localized HPV infections [27].

HPV is a highly epitheliotropic virus, – it adheres to basal cells, and the released viral DNA integrates into the host cell genome [28]. This integration results in elevated protein expression levels of E6 and E7 with synergistic effects, enhancing the proliferation capacity of cells and contributing to the transformation into cancerous cells [28]. Yi Chen et al. hypothesized that eradication of HPV from a host happens through 5-ALA-PDT-induced inhibition of the expression of E6 and E7, which in turn creates conditions in which the host cells cannot support the complete life cycle of HPV [27]. However, it is worth noting that in this study both control and case groups consisted of patients only with low-grade squamous intraepithelial lesions (LSIL).

In a similar prospective study with 76 patients with persistent cervical HPV infection, a randomly allocated treatment group (39 patients) underwent three sessions of topical 5-ALA–PDT at two-week intervals, while the control group (37 patients) received no treatment [29]. After being monitored for 9 months, the treatment group exhibited an overall HPV remission rate of 76.92%, while the control group's natural remission rate was 32.4%. A statistical analysis comparing remission rates between the two groups revealed a significant difference ($p<0.01$). The findings in a comparative study between cold-knife conization and ALA–PDT treatment for CIN 2 associated with HR-HPV infection were consistent with previous research findings where Bodner et al. found negative viral detection in 73% of patients after a 3-month treatment [30].

Contrastingly, upon the investigation of the ameliorative effects of topical 5-ALA-PDT in a clinical trial involving 40 women diagnosed with CIN 2 and 3, Keefe et al. reported that locally applied 5-ALA–PDT showed non-significant effects in the treatment of cervical CIN 2 and CIN 3 [31]. Colposcopy, followed by morphological examination of cervical biopsy material at 4, 8, and 12 months after PDT, confirmed complete regression in 15 (4-month checkpoint), 13 (8-month checkpoint), and 9 patients 1 year after PDT. Three patients experienced disease progression immediately after treatment [31]. Notably, the efficacy of PDT for the irradiation of neoplastic lesions did not show dependence on the varying light

doses (50—150 J/cm^2) used for irradiation [31]. Barnett et al. reported similar results from their randomized, double-blind, placebo-controlled trial with topical 3% 5-ALA-PDT treatment against placebo (13 women each, 26 total) for the treatment of CIN [32]. Histologic examination at the 3-month post-PDT mark revealed that 33% showed no evidence of CIN 3 (31% in the placebo arm), 42% displayed CIN of the same grade observed before PDT (38% in the placebo arm), 25% presented evidence of a higher-grade CIN than before the treatment (31% in the placebo arm), thus concluding there was no significant difference in response observed between the groups receiving 5-ALA-PDT and those undergoing placebo treatment [32]. The limited success of PDT in treating CIN, as reported by these authors, might be attributed to the topical application of photosensitizers. More promising outcomes were observed with the systemic administration of photosensitizers for CIN treatment through PDT.

The non-specific, selective absorption of 5-ALA and its derivatives by cervical mucosa and urethral mucosa, coupled with the predominant location of PPIX in the epidermal layer of cervical mucosa (rather than the dermis), ensured the safety of 5-ALA-PDT treatment in addressing cervical HPV infection. The dose increase of 5-ALA did not result in an increased accumulation of 5-ALA in the cells of the cervical epithelium [25]. Notably, 5-ALA-PDT exhibits selective action on rapidly proliferating cells, resulting in a specific killing effect with little or no damage to normal tissues and cells [33]. Side effects observed in the studies observing topically applied 5-ALA mostly included local burning and vaginal discharge, which did not require treatment or pain relief [29, 30, 32, 34]. Notably, it produced minimal local scarring compared to procedures like laser or LEEP, effectively preserved cervical function, and minimised the impact on fertility. Topically applied 5-ALA's small content in normal cells does not induce photosensitivity. However, depending on the sensitizer used, when applied intravenously or orally, patients are advised to restrict sunlight exposure to their eyes and skin for up to thirty days or more after treatment, due to the significant likelihood of skin photosensitivity, despite the dye having greater affinity for tumour tissues [35, 36].

These clinical studies had common limitations, such as a small sample size, a relatively short duration for observing the curative effects, and a lack of extensive research on long-term negative conversion rates and recurrence rates.

Current clinical studies of 5-ALA-PDT in treating cervical dysplasia

The most recent studies indicated that 5-ALA-PDT is an effective treatment for LSIL with a regression rate of 84.88%-94.81% with no significantly different rates among different age groups [37, 38]. However, patients with normal vaginal microecology might elicit a significantly higher remission rate compared to those with vaginal microecological imbalance [38]. Moreover, Liyiong Gu et al. reported women older than 50 years had a higher progression rate than the <50 years old women after the PDT treatment (12.20 % and 0.46 %, respectively). It is worth noting that women above 50 years had an increased risk of spontaneous progression than women of age >50 (31.4 % and 21.98 %, respectively) [39]. Therefore, Liyiong Gu et al. recommended patients over 50 still need close follow-up monitoring.

A single-centre, prospective cohort study by L. Ma et al. compared the clinical efficacy of 5-ALA-PDT and cryotherapy for CIN2: the regression rate after PDT was significantly higher than cryotherapy (91.7% vs 81.4%) but with no difference in HPV clearance rate [40]. Moreover, the study used a 20% concentration of 5-ALA with two follow-up treatments while suggesting increasing the frequency if patients have multicentric lesions in the cervix and inflammation in the genital tract to achieve a better outcome. The 20% concentration could be more suitable since 12-20% 5-ALA reached 91% of efficacy [41, 42], compared to 30.8-63% with 5-10% 5-ALA [43, 44].

Xiaoyun Wang et al. noticed that most women with LSIL had cervical ectropion, a condition that might expose the host to various sexually transmitted diseases, including HPV infection [45]. Interestingly, Xiaoyun Wang et al. unexpectedly discovered a significant reduction in cervical erosion and a decrease in vaginal discharge in 78% of the cases following treatment, indicating the benefits of 5-ALA-PDT not only as an organ-preserving alternative but also a simultaneous treatment of LSIL and cervical ectropion [45].

The systemic review and meta-analysis of data from 45,000 women with CIN reported that the high-risk HPV was associated with a 28.4% treatment failure rate [46]. After the integration of HPV DNA into a host genome, viral oncoproteins promote the hypermethylation of CpG islands of tumour suppressor genes, consequently silencing them and allowing the progression of cervical lesions [47, 48]. Particularly, PAX1 methylation is strongly linked to the development of cervical lesions [49, 50]. As was reported by Y. Tang *et al.* during the 5-ALA-PDT study on treating HSIL, the HPV clearance and complete remission (CR) rates in the PAX1^{lm} group were 71.3% and 92.5%, respectively, which were significantly higher than the rates of 36.8% and 73.7% observed in the PAX1^{hm} group, suggesting that the PAX1 methylation status may influence the effectiveness of 5-ALA-PDT [51]. The findings imply that patients with higher PAX1 methylation levels are more likely to progress toward cervical cancer rather than experience regression, although the exact mechanisms behind this effect remain unclear.

Nonetheless, the virus clearance rate is of great importance to avoid the risk of disease remission. A systematic review and meta-analysis of randomised

clinical trials reported promising outcomes: 62.3% of patients (48 out of 77) who underwent PDT achieved complete remission at the 3-month follow-up [52]. More recent studies reported similar results, with a 64.34%-75.32% HPV remission rate at 3 months, 64.6%-88.54% at 6 months, and 81.3-81.82% at 12 months post-treatment [37, 38, 51, 53], or a 63.64% HPV remission rate following six treatment sessions [54]. These remission rates are considerably higher than the conization (57-59.1%) [55, 56]. A minimum of two years of follow-up is required to confirm the effectiveness of the treatment for HR-HPV clearance, although the complete response rate of 75% and 90% was achieved in CIN1 and CIN2/3 patients, respectively, during the one to two-year long-term effectiveness of topical PDT for CIN1 and CIN2/3 study [41].

The recent retrospective study revealed that small cervical intraepithelial lesions responded more positively to 5-ALA-PDT, while larger lesions had a higher failure rate, implying that factors such as "HSIL/ASC-H on cytological tests" and lesion characteristics were linked to the effectiveness of 5-ALA PDT [57]. Z. Qu suggested that the severity of the lesion increases with the extent of the SIL [57], and large cervical lesions may lead to micro invasion or invasion [58]. The research showed that patients with visible lesions covering less than one cervical quadrant had a higher HSIL regression rate after 5-ALA PDT [57]. Therefore, the authors expressed the importance of the use of appropriate cytological tests, endocervical curettage, and colposcopic examinations to assess the severity of HSIL, and strict criteria when selecting patients for 5-ALA PDT.

There are several potential reasons for the failure of 5-ALA PDT. First, 5-ALA may not adhere tightly to the cervical surface, resulting in insufficient absorption by some of the target cervical cells, thus failing to accumulate the photosensitizer [57]. Second, if the lesion is located near the external os of the exocervix, the LED light may have difficulty reaching the lesion due to the direct path the light travels [57]. Lastly, if the intraepithelial lesion is too deep, the 635nm red light may not penetrate effectively to activate the photosensitiser.

As far as safety is concerned, the primary side effects of 5-ALA-PDT were reported to be local discomfort, burning sensations, and increased vaginal discharge [59], or abdominal pain, increased vaginal discharge, and itching sensations, while the incidence of increased vaginal discharge was significantly lower in the PDT group compared to the cryotherapy group [40].

As 5-ALA-PDT is a tissue-preserving treatment that doesn't result in visible scarring, the preservation of the reproductive abilities of women remains a high priority. 5-ALA PDT has not caused cutaneous phototoxic reactions to the cervix, and studies on reproductive and developmental toxicity have indicated that it is relatively safe for the embryo and fetus [60]. There have been no reports of pregnancy failure resulting from PDT. Conversely, some patients were able to conceive successfully within 6 months after treatment [53], and one patient delivered a healthy baby vaginally at full term after becoming pregnant within three months post-5-ALA-PDT [38]. Out of 29 patients who attempted pregnancy after undergoing 5-ALA-PDT, 18 became pregnant, and none of the fetuses experienced death due to cervical insufficiency [34].

The main advantage of PDT with 5-ALA that was indicated by all researchers is that it clears oncogenic HPV, selectively targets epithelial tissues or CIN lesions, avoiding surgery, hospitalization, or even interference with follow-up colposcopies, and in some studies, it avoids the risk of preterm birth in later pregnancies. Additionally, the devices used for the PDT application were easily administered by the gynaecologist and removed by the subjects. In many countries, such as Germany, conization is often performed under general anaesthesia, and hospitalization and disability are significant cost drivers [61]. Pregnancy-related morbidity linked to surgical procedures is substantial, with the average incremental cost per preterm birth (all causes) estimated to be $51,600 in the United States [62]. This highlights the potential for economic advantages by reducing the number of surgical interventions in patients with cervical high-grade disease using tissue-preserving treatments like PDT.

Conclusion

Multiple clinical studies suggest that 5-ALA-PDT is particularly attractive as an alternative treatment for its minimally invasive application, high tissue selectivity, reduced risk of adverse events compared to conventional methods, and lower likelihood of severe complications. Moreover, 5-ALA PDT can shrink cervical ectropion and reduce vaginal discharge, making it a potential treatment for cervical ectropion and chronic cervicitis. These advantages make PDT a potentially effective approach for managing CIN and cervical HPV infection, particularly among young women who plan for pregnancy. Regulating vaginal microflora during PDT can improve the remission rate of HPV for patients with vaginal microecological imbalance. For patients over 50, close follow-up monitoring after treatment may be necessary.

Early studies with smaller concentrations of 5-ALA showed poor effectiveness rates; however, 5-ALA with a concentration of 20% has shown better results in recent research. Larger studies, ideally from multiple centres, are needed to determine the optimal number of PDT sessions required to eradicate HPV.

This research is funded by the Science Committee of the Ministry of Science and Higher Education of the Republic of Kazakhstan (Grant №BR18574160).

REFERENCES

1. McLaughlin-Drubin M. E., Munger K. Viruses associated with human cancer. *Biochimica et Biophysica Acta (BBA)-Molecular Basis of Disease*, 2008, vol. 1782, pp. 127-150.
2. Plummer M., de Martel C., Vignat J., Ferlay J., Bray F., Franceschi S. Global burden of cancers attributable to infections in 2012: a synthetic analysis. *The Lancet Global Health*, 2016, vol. 9, P. e609-e616.
3. Kotsopoulos J., Lubinski J., Gronwald J. Updates to the National Cancer Institute's PDQ Information from Recently Published Oncology Research. *Cancer*, 2017, vol. 9, vol. 303.
4. Asiaf A., Ahmad S. T., Mohammad S. O., Zargar M. A. Review of the current knowledge on the epidemiology, pathogenesis, and prevention of human papillomavirus infection. *European Journal of Cancer Prevention*, 2014, vol. 3, pp. 206-224.
5. McCredie M. R., Sharples K. J., Paul C., Baranyai J., Medley G., Jones R. W., Skegg D. C. Natural history of cervical neoplasia and risk of invasive cancer in women with cervical intraepithelial neoplasia 3: a retrospective cohort study. *The Lancet Oncology*, 2008, vol. 5, pp. 425-434.
6. Munk A. C., Gudlaugsson E., Ovestad I. T., Lovslett K., Fiane B., van Diermen Hidle B., Kruse A.-J., Skaland I., Janssen E. A., Baak J. P. Interaction of epithelial biomarkers, local immune response and condom use in cervical intraepithelial neoplasia 2–3 regression. *Gynecologic oncology*, 2012, vol. 3, pp. 489-494.
7. Segura S. E., Ramos-Rivera G., Hakima L., Suhrland M., Khader S. Low-grade squamous intraepithelial lesion, cannot rule out high-grade lesion: Diagnosis, histological outcomes and human papillomavirus results. *Cytopathology*, 2019, vol.1, pp. 99-104.
8. Ferlay J., Colombet M., Soerjomataram I., Siegel R., Torre L., Jemal A. Global and regional estimates of the incidence and mortality for 38 cancers: GLOBOCAN 2018. *Lyon: International Agency for Research on Cancer. World Health Organization*, 2018, vol. 394, pp. 424.
9. Nene B. M., Hiremath P. S., Kane S., Fayette J.-M., Shastri S. S., Sankaranarayanan R. Effectiveness, safety, and acceptability of cryotherapy by midwives for cervical intraepithelial neoplasia in Maharashtra, India. *International Journal of Gynecology & Obstetrics*, 2008, vol 3, pp. 232-236.
10. Rema P., Suchetha S., Thara S., Fayette J. M., Wesley R., Sankaranarayanan R. Effectiveness and safety of loop electrosurgical excision procedure in a low-resource setting. *International Journal of Gynecology & Obstetrics*, 2008, vol. 2, pp. 105-110.
11. Shanazarov N. A., Zinchenko S. V., Kisikova S. D., Rizvanov A. A., Smailova S., Petukhov K. A., Salmaganbetova Z. Z. Photodynamic Therapy In The Treatment Of Hpv-Associated Cervical Cancer: Mechanisms, Challenges And Future Prospects. *Biomedical Photonics*, 2024, vol. 1, pp. 47-55.
12. Tzerkovsky D. A., Dunaevskaya V. V. Laser technologies in treatment of cervical intraepytelial neoplasia (review). *Biomedical Photonics*, 2020, vol. 3, pp. 30-39.
13. Szpringer E., Lutnicki K., Marciniak A. Photodynamic therapy--mechanism and employment. Annales Universitatis Mariae Curie-Sklodowska, Sectio D: Medicina, 2004, vol. 59, pp. 498-502.
14. Trushina O. I., Filonenko E. V., Novikova E. G., Mukhtarulina S. V. Photodynamic therapy in the prevention of hpv-induced recurrences of precancer and initial cancer of the cervix. *Biomedical Photonics*, 2024, vol. 13, pp. 42-46.
15. Dobson J., de Queiroz G. F., Golding J. P. Photodynamic therapy and diagnosis: Principles and comparative aspects. *The Veterinary Journal*, 2018, vol. 233, pp. 8-18.
16. Kou J., Dou D., Yang L. Porphyrin photosensitizers in photodynamic therapy and its applications. *Oncotarget*, 2017, vol. 46, pp. 81591.
17. Stylli S. S., Howes M., MacGregor L., Rajendra P., Kaye A. H. Photodynamic therapy of brain tumours: evaluation of porphyrin uptake versus clinical outcome. *Journal of Clinical Neuroscience*, 2004, vol. № 6, pp. 584-596.
18. Yoshida T., Saeki T., Ohashi S., Okudaira T., Lee M., Yoshida H., Maruoka H., Ito H., Funasaka S., Kato H. Clinical study of photodynamic therapy for laryngeal cancer, *Nippon Jibiinkoka Gakkai Kaiho*, 1995, vol. 5, pp. 795-804,927.
19. Koizumi N., Harada Y., Minamikawa T., Tanaka H., Otsuji E.,

ЛИТЕРАТУРА

1. McLaughlin-Drubin M. E., Munger K. Viruses associated with human cancer // Biochimica et Biophysica Acta (BBA)-Molecular Basis of Disease. – 2008. – Vol. 1782. – P. 127-150.
2. Plummer M., de Martel C., Vignat J., Ferlay J., Bray F., Franceschi S. Global burden of cancers attributable to infections in 2012: a synthetic analysis // The Lancet Global Health. – 2016. – Vol. 9. – P. e609-e616.
3. Kotsopoulos J., Lubinski J., Gronwald J. Updates to the National Cancer Institute's PDQ Information from Recently Published Oncology Research. – 2017. – Vol. 9. – P. 303.
4. Asiaf A., Ahmad S. T., Mohammad S. O., Zargar M. A. Review of the current knowledge on the epidemiology, pathogenesis, and prevention of human papillomavirus infection // European Journal of Cancer Prevention. – 2014. – Vol. 3. – P. 206-224.
5. McCredie M. R., Sharples K. J., Paul C., Baranyai J., Medley G., Jones R. W., Skegg D. C. Natural history of cervical neoplasia and risk of invasive cancer in women with cervical intraepithelial neoplasia 3: a retrospective cohort study // The lancet oncology. – 2008. – Vol. 5. – P. 425-434.
6. Munk A. C., Gudlaugsson E., Ovestad I. T., Lovslett K., Fiane B., van Diermen Hidle B., Kruse A.-J., Skaland I., Janssen E. A., Baak J. P. Interaction of epithelial biomarkers, local immune response and condom use in cervical intraepithelial neoplasia 2–3 regression // Gynecologic oncology. – 2012. – Vol. 3. ¬– P. 489-494.
7. Segura S. E., Ramos-Rivera G., Hakima L., Suhrland M., Khader S. Low-grade squamous intraepithelial lesion, cannot rule out high-grade lesion: Diagnosis, histological outcomes and human papillomavirus results // Cytopathology. – 2019. – Vol. 1. – P. 99-104.
8. Ferlay J., Colombet M., Soerjomataram I., Siegel R., Torre L., Jemal A. Global and regional estimates of the incidence and mortality for 38 cancers: GLOBOCAN 2018. Lyon: International Agency for Research on Cancer // World Health Organization. – 2018. – Vol. 394. – P. 424.
9. Nene B. M., Hiremath P. S., Kane S., Fayette J.-M., Shastri S. S., Sankaranarayanan R. Effectiveness, safety, and acceptability of cryotherapy by midwives for cervical intraepithelial neoplasia in Maharashtra, India // International Journal of Gynecology & Obstetrics. – 2008. – Vol. 3. – P. 232-236.
10. Rema P., Suchetha S., Thara S., Fayette J. M., Wesley R., Sankaranarayanan R. Effectiveness and safety of loop electrosurgical excision procedure in a low-resource setting // International Journal of Gynecology & Obstetrics. – 2008. – Vol. 2. – P. 105-110.
11. Shanazarov N. A., Zinchenko S. V., Kisikova S. D., Rizvanov A. A., Smailova S., Petukhov K. A., Salmaganbetova Z. Z. Photodynamic Therapy In The Treatment Of Hpv-Associated Cervical Cancer: Mechanisms, Challenges And Future Prospects // Biomedical Photonics. – 2024. – Vol. 13. ¬– P. 47-55.
12. Tzerkovsky D. A., Dunaevskaya V. V. Laser technologies in treatment of cervical intraepytelial neoplasia (review) // Biomedical Photonics. – 2020. – Vol 3. – P. 30-39.
13. Szpringer E., Lutnicki K., Marciniak A. Photodynamic therapy--mechanism and employment // Annales Universitatis Mariae Curie-Sklodowska. Sectio D: Medicina. – 2004. – Vol. 59. – P. 498-502.
14. Trushina O. I., Filonenko E. V., Novikova E. G., Mukhtarulina S. V. Photodynamic therapy in the prevention of hpv-induced recurrences of precancer and initial cancer of the cervix // Biomedical Photonics. – 2024. – Vol. 13. – P. 42-46.
15. Dobson J., de Queiroz G. F., Golding J. P. Photodynamic therapy and diagnosis: Principles and comparative aspects // The Veterinary Journal. – 2018. – Vol. 233. – P. 8-18.
16. Kou J., Dou D., Yang L. Porphyrin photosensitizers in photodynamic therapy and its applications // Oncotarget. – 2017. – Vol 46. – P. 81591.
17. Stylli S. S., Howes M., MacGregor L., Rajendra P., Kaye A. H. Photodynamic therapy of brain tumours: evaluation of porphyrin uptake versus clinical outcome // Journal of Clinical Neuroscience. – 2004. – Vol. 6. – P. 584-596.
18. Yoshida T., Saeki T., Ohashi S., Okudaira T., Lee M., Yoshida H., Maruoka H., Ito H., Funasaka S., Kato H. Clinical study of photodynamic therapy for laryngeal cancer // Nippon Jibiinkoka Gakkai Kaiho. – 1995. – Vol. 5. – P. 795-804,927.
19. Koizumi N., Harada Y., Minamikawa T., Tanaka H., Otsuji E., Takamatsu T. Recent advances in photodynamic diagnosis of gastric cancer

Takamatsu T. Recent advances in photodynamic diagnosis of gastric cancer using 5-aminolevulinic acid, *World Journal of Gastroenterology*, 2016, vol. 22, pp. 1289.
20. Harada Y., Murayama Y., Takamatsu T., Otsuji E., Tanaka H. 5-aminolevulinic acid-induced protoporphyrin IX fluorescence imaging for tumor detection: Recent advances and challenges. *International journal of molecular sciences*, 2022, vol. 12, pp. 6478.
21. Zavedeeva V. E., Efendiev K. T., Kustov D. M., Loschenova L. Y., Loschenov V. B. Dual-Wavelength Fluorescence Study Of In Vivo Accumulation And Formation Of 5-Ala-Induced Porphyrins. *Biomedical Photonics*, 2025, vol. 14, pp. 36-46.
22. Ivanova-Radkevich V. I., Kuznetsova O. M., Filonenko E. V. The Role Of Membrane Transport Proteins In 5-Alk-Induced Accumulation Of Protoporphyrin Ix In Tumor Cells, *Biomedical Photonics*, 2024, vol. 13, pp. 43-48.
23. Akbarzadeh A., Rezaei-Sadabady R., Davaran S., Joo S. W., Zarghami N., Hanifehpour Y., Samiei M., Kouhi M., Nejati-Koshki K. Liposome: classification, preparation, and applications. *Nanoscale Research Letters*, 2013, vol. 8, pp.102.
24. Rkein A. M., Ozog D. M. Photodynamic Therapy. *Dermatologic Clinics*, 2014, vol. 32, pp. 415-425.
25. Hillemanns P., Soergel P., Löning M. Fluorescence diagnosis and photodynamic therapy for lower genital tract diseases – A review, *Medical Laser Application*, 2009, vol. 24, pp. 10-17.
26. Hillemanns P., Weingandt H., Baumgartner R., Diebold J., Xiang W., Stepp H. Photodetection of cervical intraepithelial neoplasia using 5-aminolevulinic acid–induced porphyrin fluorescence. *Cancer*, 2000. vol. 10. pp. 2275-2282.
27. Chen Y., Xu Y., Zhang Z., Xiong Z., Wu D. 5-aminolevulinic acid-mediated photodynamic therapy effectively ameliorates HPV-infected cervical intraepithelial neoplasia. *American Journal of Translational Research*, 2022, vol. № 4, pp. 2443.
28. Poreba E., Broniarczyk J. K., Gozdzicka-Jozefiak A. Epigenetic mechanisms in virus-induced tumorigenesis. *Clinical epigenetics*, 2011, vol. 2, pp. 233-247.
29. Fu Y., Bao Y., Hui Y., Gao X., Yang M., Chang J. Topical photodynamic therapy with 5-aminolevulinic acid for cervical high-risk HPV infection. *Photodiagnosis and photodynamic therapy*, 2016, vol. 13, pp. 29-33.
30. Bodner K., Bodner-Adler B., Wierrani F., Kubin A., Szölts-Szölts J., Spängler B., Grünberger W. Cold-knife conization versus photodynamic therapy with topical 5-aminolevulinic acid (5-ALA) in cervical intraepithelial neoplasia (CIN) II with associated human papillomavirus infection: a comparison of preliminary results. *Anticancer Res*., 2003, vol. 23, pp. 1785-8.
31. Keefe K. A., Tadir Y., Tromberg B., Berns M., Osann K., Hashad R., Monk B. J. Photodynamic therapy of high-grade cervical intraepithelial neoplasia with 5-aminolevulinic acid. *Lasers Surg Med*., 2002, vol. 31, pp. 289-93.
32. Barnett A. A., Haller J. C., Cairnduff F., Lane G., Brown S. B., Roberts D. J. H. A randomised, double-blind, placebo-controlled trial of photodynamic therapy using 5-aminolaevulinic acid for the treatment of cervical intraepithelial neoplasia. *International Journal of Cancer*, 2003, vol. 103, pp. 829-832.
33. Inoue K. 5-Aminolevulinic acid-mediated photodynamic therapy for bladder cancer. *International Journal of Urology*, 2017, vol. 24, pp. 97-101.
34. Choi M. C., Jung S. G., Park H., Lee S. Y., Lee C., Hwang Y. Y., Kim S. J. Photodynamic therapy for management of cervical intraepithelial neoplasia II and III in young patients and obstetric outcomes. *Lasers in Surgery and Medicine*, 2013, vol. 45, pp. 564-572.
35. Bellnier D. A., Greco W. R., Loewen G. M., Nava H., Oseroff A. R., Pandey R. K., Tsuchida T., Dougherty T. J. Population pharmacokinetics of the photodynamic therapy agent 2-[1-hexyloxyethyl]-2-devinyl pyropheophorbide-a in cancer patients. *Cancer research*, 2003, vol. 63, pp. 1806-1813.
36. Istomin Y. P., Lapzevich T. P., Chalau V. N., Shliakhtsin S. V., Trukhachova T. V. Photodynamic therapy of cervical intraepithelial neoplasia grades II and III with Photolon®. *Photodiagnosis and Photodynamic Therapy*, 2010, vol. 7, pp. 144-151.
37. Gu L., Cheng M., Hong Z., Di W., Qiu L. The effect of local photodynamic therapy with 5-aminolevulinic acid for the

using 5-aminolevulinic acid // World Journal of Gastroenterology. – 2016. – Vol. 3. – P. 1289.
20. Harada Y., Murayama Y., Takamatsu T., Otsuji E., Tanaka H. 5-aminolevulinic acid-induced protoporphyrin IX fluorescence imaging for tumor detection: Recent advances and challenges // International journal of molecular sciences. – 2022. – Vol. 12. – P. 6478.
21. Zavedeeva V. E., Efendiev K. T., Kustov D. M., Loschenova L. Y., Loschenov V. B. Dual-Wavelength Fluorescence Study Of In Vivo Accumulation And Formation Of 5-Ala-Induced Porphyrins // Biomedical Photonics. – 2025. – Vol. 1. – P. 36-46.
22. Ivanova-Radkevich V. I., Kuznetsova O. M., Filonenko E. V. The Role Of Membrane Transport Proteins In 5-Alk-Induced Accumulation Of Protoporphyrin Ix In Tumor Cells // Biomedical Photonics. – 2024. – Vol. 2. – P. 43-48.
23. Akbarzadeh A., Rezaei-Sadabady R., Davaran S., Joo S. W., Zarghami N., Hanifehpour Y., Samiei M., Kouhi M., Nejati-Koshki K. Liposome: classification, preparation, and applications // Nanoscale Research Letters. – 2013. – Vol. 1. – P. 102.
24. Rkein A. M., Ozog D. M. Photodynamic Therapy // Dermatologic Clinics. – 2014. – Vol. 3. – P. 415-425.
25. Hillemanns P., Soergel P., Löning M. Fluorescence diagnosis and photodynamic therapy for lower genital tract diseases – A review // Medical Laser Application. – 2009. – Vol. 24. – P. 10-17.
26. Hillemanns P., Weingandt H., Baumgartner R., Diebold J., Xiang W., Stepp H. Photodetection of cervical intraepithelial neoplasia using 5-aminolevulinic acid–induced porphyrin fluorescence // Cancer. – 2000. – Vol. 10. – P. 2275-2282.
27. Chen Y., Xu Y., Zhang Z., Xiong Z., Wu D. 5-aminolevulinic acid-mediated photodynamic therapy effectively ameliorates HPV-infected cervical intraepithelial neoplasia // American Journal of Translational Research. – 2022. – Vol. 4. – P. 2443.
28. Poreba E., Broniarczyk J. K., Gozdzicka-Jozefiak A. Epigenetic mechanisms in virus-induced tumorigenesis // Clinical epigenetics. – 2011. – Vol. 2. – P. 233-247.
29. Fu Y., Bao Y., Hui Y., Gao X., Yang M., Chang J. Topical photodynamic therapy with 5-aminolevulinic acid for cervical high-risk HPV infection // Photodiagnosis and photodynamic therapy. – 2016. – Vol. 13. – P. 29-33.
30. Bodner K., Bodner-Adler B., Wierrani F., Kubin A., Szölts-Szölts J., Spängler B., Grünberger W. Cold-knife conization versus photodynamic therapy with topical 5-aminolevulinic acid (5-ALA) in cervical intraepithelial neoplasia (CIN) II with associated human papillomavirus infection: a comparison of preliminary results // Anticancer Res. – 2003. – Vol. 2c. – P. 1785-8.
31. Keefe K. A., Tadir Y., Tromberg B., Berns M., Osann K., Hashad R., Monk B. J. Photodynamic therapy of high-grade cervical intraepithelial neoplasia with 5-aminolevulinic acid // Lasers Surg Med. – 2002. – Vol. 4. – P. 289-93.
32. Barnett A. A., Haller J. C., Cairnduff F., Lane G., Brown S. B., Roberts D. J. H. A randomised, double-blind, placebo-controlled trial of photodynamic therapy using 5-aminolaevulinic acid for the treatment of cervical intraepithelial neoplasia // International Journal of Cancer. – 2003. – Vol. 6. – P. 829-832.
33. Inoue K. 5-Aminolevulinic acid-mediated photodynamic therapy for bladder cancer // International Journal of Urology. – 2017. – Vol. 2. – P. 97-101.
34. Choi M. C., Jung S. G., Park H., Lee S. Y., Lee C., Hwang Y. Y., Kim S. J. Photodynamic therapy for management of cervical intraepithelial neoplasia II and III in young patients and obstetric outcomes // Lasers in Surgery and Medicine. – 2013. – Vol. 9. – P. 564-572.
35. Bellnier D. A., Greco W. R., Loewen G. M., Nava H., Oseroff A. R., Pandey R. K., Tsuchida T., Dougherty T. J. Population pharmacokinetics of the photodynamic therapy agent 2-[1-hexyloxyethyl]-2-devinyl pyropheophorbide-a in cancer patients // Cancer research. – 2003. – Vol. 8. – P. 1806-1813.
36. Istomin Y. P., Lapzevich T. P., Chalau V. N., Shliakhtsin S. V., Trukhachova T. V. Photodynamic therapy of cervical intraepithelial neoplasia grades II and III with Photolon® // Photodiagnosis and Photodynamic Therapy. – 2010. – Vol. 3. – P. 144-151.
37. Gu L., Cheng M., Hong Z., Di W., Qiu L. The effect of local photodynamic therapy with 5-aminolevulinic acid for the

treatment of cervical low-grade squamous intraepithelial lesions with high-risk HPV infection: A retrospective study. *Photodiagnosis and Photodynamic Therapy*, 2021. vol. 33, pp. 102172.
38. Li D., Zhang F., Shi L., Lin L., Cai Q., Xu Y. Treatment of HPV Infection-Associated Low Grade Cervical Intraepithelial Neoplasia with 5-Aminolevulinic Acid-Mediated Photodynamic Therapy. *Photodiagnosis and Photodynamic Therapy*, 2020, vol. 32, pp. 101974.
39. Quint K. D., de Koning M. N. C., Quint W. G. V., Pirog E. C. Progression of cervical low grade squamous intraepithelial lesions: in search of prognostic biomarkers. *European Journal of Obstetrics & Gynecology and Reproductive Biology*, 2013, vol. 170, pp. 501-506.
40. Ma L., Gao X., Geng L., You K., Wu Z., Li Y., Han Q., Wang Y., Guo H. Efficacy and safety of photodynamic therapy mediated by 5-aminolevulinic acid for the treatment of cervical intraepithelial neoplasia 2: a single-center, prospective, cohort study. *Photodiagnosis and photodynamic therapy*, 2021, vol. 36, pp. 102472.
41. Inada N. M., Buzzá H. H., Leite M. F. M., Kurachi C., Trujillo J. R., de Castro C. A., Carbinatto F. M., Lombardi W., Bagnato V. S. Long term effectiveness of photodynamic therapy for CIN treatment. *Pharmaceuticals*, 2019, vol. 12, pp. 107.
42. Mizuno M., Mitsui H., Kajiyama H., Teshigawara T., Inoue K., Takahashi K., Ishii T., Ishizuka M., Nakajima M., Kikkawa F. Efficacy of 5-aminolevulinic acid and LED photodynamic therapy in cervical intraepithelial neoplasia: A clinical trial. *Photodiagnosis and photodynamic therapy*, 2020, vol. 32, pp. 102004.
43. Keefe K. A., Tadir Y., Tromberg B., Berns M., Osann K., Hashad R., Monk B. J. Photodynamic therapy of high-grade cervical intraepithelial neoplasia with 5-aminolevulinic acid. Lasers in Surgery and Medicine: *The Official Journal of the American Society for Laser Medicine and Surgery*, 2002. vol. 31, pp. 289-293.
44. Soergel P., Wang X., Stepp H., Hertel H., Hillemanns P. Photodynamic therapy of cervical intraepithelial neoplasia with hexaminolevulinate. *Lasers in Surgery and Medicine: The Official Journal of the American Society for Laser Medicine and Surgery*, 2008, vol. 40, pp. 611-615.
45. Hwang L. Y., Ma Y., Shiboski S. C., Farhat S., Jonte J., Moscicki A.-B. Active Squamous Metaplasia of the Cervical Epithelium Is Associated With Subsequent Acquisition of Human Papillomavirus 16 Infection Among Healthy Young Women. *The Journal of Infectious Diseases*, 2012, vol. 206, pp. 504-511.
46. Arbyn M., Redman C. W. E., Verdoodt F., Kyrgiou M., Tzafetas M., Ghaem-Maghami S., Petry K.-U., Leeson S., Bergeron C., Nieminen P., Gondry J., Reich O., Moss E. L. Incomplete excision of cervical precancer as a predictor of treatment failure: a systematic review and meta-analysis. *The Lancet Oncology*, 2017, vol. 18, pp. 1665-1679.
47. Sen P., Ganguly P., Ganguly N. Modulation of DNA methylation by human papillomavirus E6 and E7 oncoproteins in cervical cancer. *Oncology letters*, 2018, vol. 15, pp. 11-22.
48. Jacquin E., Baraquin A., Ramanah R., Carcopino X., Morel A., Valmary-Degano S., Bravo I. G., De Sanjosé S., Riethmuller D., Mougin C. Methylation of human papillomavirus type 16 CpG sites at E2-binding site 1 (E2BS1), E2BS2, and the Sp1-binding site in cervical cancer samples as determined by high-resolution melting analysis–PCR. *Journal of clinical microbiology*, vol. 51, pp. 3207-3215.
49. Chang C.-L., Ho S.-C., Su Y.-F., Juan Y.-C., Huang C.-Y., Chao A.-S., Hsu Z.-S., Chang C.-F., Fwu C.-W., Chang T.-C. DNA methylation marker for the triage of hrHPV positive women in cervical cancer screening: real-world evidence in Taiwan. *Gynecologic oncology*, 2021, vol. 161, pp. 429-435.
50. Kim M.-K., Lee I.-H., Lee K.-H., Lee Y. K., So K. A., Hong S. R., Hwang C.-S., Kee M.-K., Rhee J. E., Kang C. DNA methylation in human papillomavirus-infected cervical cells is elevated in high-grade squamous intraepithelial lesions and cancer. *Journal of gynecologic oncology*, 2016, vol. 27, pp. 25-28.
51. Tang Y., Su Y., Xu Y., Zhang Y., Shen Y., Qin L., Zhang L., Cao L., Zhou Y., Zhang T. Therapeutic effects of topical photodynamic therapy with 5-aminolevulinic acid on cervical high-grade squamous intraepithelial lesions. *Photodiagnosis and Photodynamic Therapy*, 2022, vol. 39. pp. 102884.

treatment of cervical low-grade squamous intraepithelial lesions with high-risk HPV infection: A retrospective study // Photodiagnosis and Photodynamic Therapy. – 2021. – Vol. 33. – P. 102172.
38. Li D., Zhang F., Shi L., Lin L., Cai Q., Xu Y. Treatment of HPV Infection-Associated Low Grade Cervical Intraepithelial Neoplasia with 5-Aminolevulinic Acid-Mediated Photodynamic Therapy // Photodiagnosis and Photodynamic Therapy. – 2020. – Vol. 32. – P. 101974.
39. Quint K. D., de Koning M. N. C., Quint W. G. V., Pirog E. C. Progression of cervical low grade squamous intraepithelial lesions: in search of prognostic biomarkers // European Journal of Obstetrics & Gynecology and Reproductive Biology. – 2013. – Vol. 2. – P. 501-506.
40. Ma L., Gao X., Geng L., You K., Wu Z., Li Y., Han Q., Wang Y., Guo H. Efficacy and safety of photodynamic therapy mediated by 5-aminolevulinic acid for the treatment of cervical intraepithelial neoplasia 2: a single-center, prospective, cohort study // Photodiagnosis and photodynamic therapy. – 2021. – Vol. 36. – P. 102472.
41. Inada N. M., Buzzá H. H., Leite M. F. M., Kurachi C., Trujillo J. R., de Castro C. A., Carbinatto F. M., Lombardi W., Bagnato V. S. Long term effectiveness of photodynamic therapy for CIN treatment // Pharmaceuticals. – 2019. – Vol. 3. – P. 107.
42. Mizuno M., Mitsui H., Kajiyama H., Teshigawara T., Inoue K., Takahashi K., Ishii T., Ishizuka M., Nakajima M., Kikkawa F. Efficacy of 5-aminolevulinic acid and LED photodynamic therapy in cervical intraepithelial neoplasia: A clinical trial // Photodiagnosis and photodynamic therapy. – 2020. – Vol. 32. – P. 102004.
43. Keefe K. A., Tadir Y., Tromberg B., Berns M., Osann K., Hashad R., Monk B. J. Photodynamic therapy of high-grade cervical intraepithelial neoplasia with 5-aminolevulinic acid // Lasers in Surgery and Medicine: The Official Journal of the American Society for Laser Medicine and Surgery. – 2002. – Vol. 4. – P. 289-293.
44. Soergel P., Wang X., Stepp H., Hertel H., Hillemanns P. Photodynamic therapy of cervical intraepithelial neoplasia with hexaminolevulinate // Lasers in Surgery and Medicine: The Official Journal of the American Society for Laser Medicine and Surgery. – 2008. – Vol. 9. – P. 611-615.
45. Hwang L. Y., Ma Y., Shiboski S. C., Farhat S., Jonte J., Moscicki A.-B. Active Squamous Metaplasia of the Cervical Epithelium Is Associated With Subsequent Acquisition of Human Papillomavirus 16 Infection Among Healthy Young Women // The Journal of Infectious Diseases. – 2012. – Vol. 4. – P. 504-511.
46. Arbyn M., Redman C. W. E., Verdoodt F., Kyrgiou M., Tzafetas M., Ghaem-Maghami S., Petry K.-U., Leeson S., Bergeron C., Nieminen P., Gondry J., Reich O., Moss E. L. Incomplete excision of cervical precancer as a predictor of treatment failure: a systematic review and meta-analysis // The Lancet Oncology. – 2017. – Vol. 12. – P. 1665-1679.
47. Sen P., Ganguly P., Ganguly N. Modulation of DNA methylation by human papillomavirus E6 and E7 oncoproteins in cervical cancer // Oncology letters. – 2018. – Vol. 15. – P. 11-22.
48. Jacquin E., Baraquin A., Ramanah R., Carcopino X., Morel A., Valmary-Degano S., Bravo I. G., De Sanjosé S., Riethmuller D., Mougin C. Methylation of human papillomavirus type 16 CpG sites at E2-binding site 1 (E2BS1), E2BS2, and the Sp1-binding site in cervical cancer samples as determined by high-resolution melting analysis–PCR // Journal of clinical microbiology. – 2013. – Vol. 10. – P. 3207-3215.
49. Chang C.-L., Ho S.-C., Su Y.-F., Juan Y.-C., Huang C.-Y., Chao A.-S., Hsu Z.-S., Chang C.-F., Fwu C.-W., Chang T.-C. DNA methylation marker for the triage of hrHPV positive women in cervical cancer screening: real-world evidence in Taiwan // Gynecologic oncology. – 2021. – Vol. 2. – P. 429-435.
50. Kim M.-K., Lee I.-H., Lee K.-H., Lee Y. K., So K. A., Hong S. R., Hwang C.-S., Kee M.-K., Rhee J. E., Kang C. DNA methylation in human papillomavirus-infected cervical cells is elevated in high-grade squamous intraepithelial lesions and cancer // Journal of gynecologic oncology. – 2016. – Vol. 2. – P. 24-27.
51. Tang Y., Su Y., Xu Y., Zhang Y., Shen Y., Qin L., Zhang L., Cao L., Zhou Y., Zhang T. Therapeutic effects of topical photodynamic therapy with 5-aminolevulinic acid on cervical high-grade squamous intraepithelial lesions // Photodiagnosis and Photodynamic Therapy. – 2022. – Vol. 39. – P. 102884.

52. Zhang W., Zhang A., Sun W., Yue Y., Li H. Efficacy and safety of photodynamic therapy for cervical intraepithelial neoplasia and human papilloma virus infection: A systematic review and meta-analysis of randomized clinical trials. *Medicine*, 2018, vol. 97, pp. e10864.
53. Wang X., You L., Zhang W., Ma Y., Tang Y., Xu W. Evaluation of 5-aminolevulinic acid-mediated photodynamic therapy on cervical low-grade squamous intraepithelial lesions with high-risk HPV infection. *Photodiagnosis and Photodynamic Therapy*, 2022, vol. 38, pp. 102807.
54. Ran R., Wang M., Li X., Liu Q. A prospective study of photodynamic therapy for cervical squamous intraepithelial lesion. *Photodiagnosis and Photodynamic therapy*, 2021, vol. 34, pp. 102185.
55. Kim Y.-T., Lee J. M., Hur S.-Y., Cho C.-H., Kim Y. T., Kim S. C., Kang S. B. Clearance of human papillomavirus infection after successful conization in patients with cervical intraepithelial neoplasia. *International Journal of Cancer*, 2010, vol. 126, pp. 1903-1909.
56. Kim H. S., Kwon J. E., Kim J. H., Kim A., Lee N. R., Kim M., Lee M., Suh D. H., Kim Y. B. Efficacy of loop electrosurgical excision procedure with cold coagulation for treating cervical intraepithelial neoplasia: A two center cohort study. *Obstet Gynecol Sci*., 2017, vol. 60, pp. 200-206.
57. Qu Z., Wang Z., Qiu S., Cui G., Li C. Efficacy of photodynamic therapy with 5-aminolevulinic acid for the treatment of cervical high-grade squamous intraepithelial lesions with high-risk HPV infection: A retrospective study. *Photodiagnosis and Photodynamic Therapy*, 2022, vol. 40, pp. 103068.
58. Pretorius R. G., Belinson J. L., Peterson P., Azizi F., Lo A. Yield and mode of diagnosis of cervical intraepithelial neoplasia 3 or cancer among women with negative cervical cytology and positive high-risk human papillomavirus test results. *Journal of lower genital tract disease*, 2013, vol. 17, pp. 430-439.
59. Zhang W., Zhang A., Sun W., Yue Y., Li H. Efficacy and safety of photodynamic therapy for cervical intraepithelial neoplasia and human papilloma virus infection: A systematic review and meta-analysis of randomized clinical trials. *Medicine*, 2018, vol. 97, pp. 47-54.
60. Maździarz A. Successful pregnancy and delivery following selective use of photodynamic therapy in treatment of cervix and vulvar diseases. *Photodiagnosis and photodynamic therapy*, 2019, vol. 28, pp. 65-68.
61. Hillemanns P., Garcia F., Petry K. U., Dvorak V., Sadovsky O., Iversen O.-E., Einstein M. H. A randomized study of hexaminolevulinate photodynamic therapy in patients with cervical intraepithelial neoplasia 1/2. *American journal of obstetrics and gynecology*, 2015, vol. 212, pp. 465. e1-465. e7.
62. Waitzman N. J., Jalali A., Grosse S. D. Preterm birth lifetime costs in the United States in 2016: *An update. Seminars in Perinatology*, 2021, vol. 45, pp. 151390.

52. Zhang W., Zhang A., Sun W., Yue Y., Li H. Efficacy and safety of photodynamic therapy for cervical intraepithelial neoplasia and human papilloma virus infection: A systematic review and meta-analysis of randomized clinical trials // Medicine. – 2018. – Vol. 21. – P. e10864.
53. Wang X., You L., Zhang W., Ma Y., Tang Y., Xu W. Evaluation of 5-aminolevulinic acid-mediated photodynamic therapy on cervical low-grade squamous intraepithelial lesions with high-risk HPV infection // Photodiagnosis and Photodynamic Therapy. – 2022. – Vol. 38. – P. 102807.
54. Ran R., Wang M., Li X., Liu Q. A prospective study of photodynamic therapy for cervical squamous intraepithelial lesion // Photodiagnosis and Photodynamic therapy. – 2021. – Vol. 34. – P. 102185.
55. Kim Y.-T., Lee J. M., Hur S.-Y., Cho C.-H., Kim Y. T., Kim S. C., Kang S. B. Clearance of human papillomavirus infection after successful conization in patients with cervical intraepithelial neoplasia // International Journal of Cancer. – 2010. – Vol. 8. – P. 1903-1909.
56. Kim H. S., Kwon J. E., Kim J. H., Kim A., Lee N. R., Kim M., Lee M., Suh D. H., Kim Y. B. Efficacy of loop electrosurgical excision procedure with cold coagulation for treating cervical intraepithelial neoplasia: A two center cohort study // Obstet Gynecol Sci. – 2017. – Vol. 2. – P. 200-206.
57. Qu Z., Wang Z., Qiu S., Cui G., Li C. Efficacy of photodynamic therapy with 5-aminolevulinic acid for the treatment of cervical high-grade squamous intraepithelial lesions with high-risk HPV infection: A retrospective study // Photodiagnosis and Photodynamic Therapy. – 2022. – Vol. 40. – P. 103068.
58. Pretorius R. G., Belinson J. L., Peterson P., Azizi F., Lo A. Yield and mode of diagnosis of cervical intraepithelial neoplasia 3 or cancer among women with negative cervical cytology and positive high-risk human papillomavirus test results // Journal of lower genital tract disease. – 2013. – Vol. 4. – P. 430-439.
59. Zhang W., Zhang A., Sun W., Yue Y., Li H. Efficacy and safety of photodynamic therapy for cervical intraepithelial neoplasia and human papilloma virus infection: A systematic review and meta-analysis of randomized clinical trials // Medicine. – 2018. – Vol. 21. – P. 47-54.
60. Maździarz A. Successful pregnancy and delivery following selective use of photodynamic therapy in treatment of cervix and vulvar diseases // Photodiagnosis and photodynamic therapy. – 2019. – Vol. 28. – P. 65-68.
61. Hillemanns P., Garcia F., Petry K. U., Dvorak V., Sadovsky O., Iversen O.-E., Einstein M. H. A randomized study of hexaminolevulinate photodynamic therapy in patients with cervical intraepithelial neoplasia 1/2 // American journal of obstetrics and gynecology. – 2015. – Vol. 4. – P. 465. e1-465. e7.
62. Waitzman N. J., Jalali A., Grosse S. D. Preterm birth lifetime costs in the United States in 2016: An update // seminars in Perinatology. – 2021. – Vol. 45. – P. 151390.

AUTOMATIZATION OF PLANNING AND CONTROL OF PHOTODYNAMIC THERAPY OF GASTROINTESTINAL ORGANS

Krivetskaya A.A.[1,2], **Savelieva T.A.**[1,2], **Kustov D.M.**[1], **Levkin V.V.**[3], **Kharnas S.S.**[3], **Loschenov V.B.**[1,2]
[1]Prokhorov General Physics Institute of the Russian Academy of Sciences, Moscow, Russia
[2]Institute of Engineering Physics for Biomedicine, National Research Nuclear University MEPhI, Moscow, Russia
[3]Department of Faculty Surgery No. 1, I.M. Sechenov First Moscow State Medical University, Moscow, Russia

Abstract

The main aspects of automatization of photodynamic therapy (PDT) planning include several key areas related to improving accuracy, efficiency and personalization of treatment. Mathematical modeling of light propagation makes it possible to calculate the distribution of light energy in biotissues taking into account their optical characteristics and pathology geometry. At the same time the use of optical diagnostic methods allows not only to plan but also to control in real time the photodynamic effect with parameters adjustment depending on the degree of photosensitizer photobleaching and the hemoglobin oxygen saturation, as well as to determine the optical properties of tissues exactly in the exposure area. These methods also make it possible to personalize the effect, since it is based not on a priori information about averaged properties of organs and tissues, but on dynamically changing and measurable parameters. The use of photodynamic therapy for tumor diseases of the gastrointestinal tract has shown effectiveness as an adjunct to surgical treatment, as well as for tumors of small size and as a method of palliative treatment. At the same time from the point of view of light propagation in tissues the walls of gastrointestinal tract organs represent rather complex multilayer structures, optical properties of which depend on physiological state and pathologies developing in the organ. These circumstances make the task of automation of planning of photodynamic therapy of GI organs urgent and nontrivial. In this paper we review the methods that solve this problem.

Key words: photodynamic therapy, optical spectroscopy, photosensitizer, hemoglobin, optical properties, gastrointestinal tract

Contacts: Krivetskaya A.A., e-mail: annakrivetskaya1998@gmail.com

For citations: Krivetskaya A.A., Savelieva T.A., Kustov D.M., Levkin V.V., Kharnas S.S., Loschenov V.B. Automatization of planning and control of photodynamic therapy of gastrointestinal organs, *Biomedical Photonics*, 2025, vol. 14, no. 2, pp. 40–54. doi: 10.24931/2413–9432–2025–14-2-40–54

АВТОМАТИЗАЦИЯ ПЛАНИРОВАНИЯ И КОНТРОЛЯ ФОТОДИНАМИЧЕСКОЙ ТЕРАПИИ ОРГАНОВ ЖЕЛУДОЧНО-КИШЕЧНОГО ТРАКТА

А.А. Кривецкая[1,2], **Т.А. Савельева**[1,2], **Д.М. Кустов**[1], **В.В. Левкин**[3], **С.С. Харнас**[3], **В.Б. Лощенов**[1,2]
[1]Институт общей физики им. А.М. Прохорова Российской академии наук, Москва, Россия
[2]Национальный исследовательский ядерный университет «МИФИ», Москва, Россия
[3]Университетская Клиническая больница №1 Первого МГМУ им. Сеченова, Москва, Россия

Резюме

Основные аспекты автоматизации планирования фотодинамической терапии (ФДТ) включают несколько ключевых направлений, связанных с повышением точности, эффективности и персонализации лечения. Математическое моделирование распространения излучения позволяет рассчитать распределение световой энергии в биотканях с учетом их оптических характеристик и геометрии патологии. При этом использование оптических методов диагностики позволяет не только планировать, но и контролировать в реальном времени фотодинамическое воздействие с корректировкой параметров в зависимости от степени выгорания фотосенсибилизатора и степени насыщения гемоглобина кислородом, а также определять оптические свойства тканей именно в зоне воз-

действия. Эти методы обуславливают также и возможность персонализации воздействия, поскольку оно при этом основано не на априорной информации об усредненных свойствах органов и тканей, а на динамически меняющихся и измеряемых параметрах. Использование фотодинамической терапии для опухолевых заболеваний желудочно-кишечного тракта показало эффективность в качестве дополнения к хирургическому лечению, а также для опухолей небольшого размера и в качестве метода паллиативного лечения. При этом с точки зрения распространения света в тканях стенки органов желудочно-кишечного тракта представляют достаточно сложные многослойные структуры, оптические свойства которых зависят от физиологического состояния и развивающихся в органе патологий. Эти обстоятельства делают задачу автоматизации планирования фотодинамической терапии органов ЖКТ актуальной и нетривиальной. В настоящей статье проведен обзор методов, которые решают эту задачу.

Ключевые слова: фотодинамическая терапия, оптическая спектроскопия, фотосенсибилизатор, гемоглобин, оптические свойства, желудочно-кишечный тракт.

Контакты: Кривецкая А.А., e-mail: annakrivetslaya1998@gmail.com

Для цитирования: Кривецкая А.А., Савельева Т.А., Кустов Д.М., Левкин В.В., Харнас С.С., Лощенов В.Б. Автоматизация планирования и контроля фотодинамической терапии органов желудочно-кишечного тракта // Biomedical Photonics. – 2025. – Т. 14, № 2. – С. 40–54. doi: 10.24931/2413–9432–2025–14-2-40–54

Introduction

Photodynamic therapy (PDT) is a progressive method of treatment of various diseases, including malignant neoplasms [1, 2] and precancerous conditions [3] of the gastrointestinal (GI) organs. To implement photodynamic action, a combination of light-sensitive substances (photosensitizers) and light radiation of a certain wavelength is necessary. In this case, PDT can either directly form free radicals through a substrate (Type I) or generate singlet oxygen through the transfer of energy to oxygen (Type II). The effectiveness of PDT depends on personalized treatment planning and dosimetric control during the procedure, which necessitates the development and application of techniques to achieve these goals.

The main limitation of traditional PDT protocols is the standardized approach, which does not take into account the variability of tissue optical properties, the degree of photosensitizer accumulation and heterogeneity of biological tissues. This leads to the risk of damage to healthy tissues or insufficient therapeutic effect. For example, the absorbed dose varies depending on the light penetration depth and the local concentration of the photosensitizer. The absorbed dose is mainly determined by the light power density, energy dose, photosensitizer and oxygen concentration in the irradiated tissue, which makes it necessary to take into account the optical properties of tissues and individual characteristics of patients [4]. Therefore, control of PDT by dosimetry and automatic treatment planning, as well as personalization of the procedure, are important factors to maximize the effectiveness of therapy. Fig. 1 presents a scheme showing the sequence of dosimetric techniques applied during the photodynamic therapy procedure.

Personalization of PDT is carried out by adapting the radiation dose and exposure time to the specific biological characteristics of the patient. This review is devoted to the consideration of existing methods of automated planning of photodynamic treatment and various techniques of

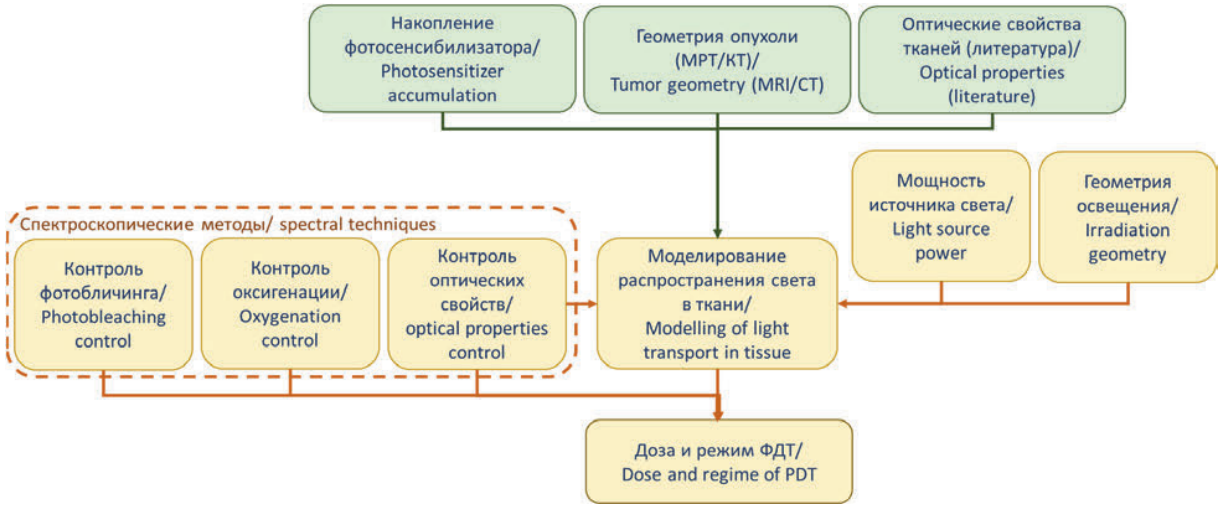

Рис. 1. Последовательность процесса дозиметрического контроля ФДТ.
Fig. 1. Sequence of the process of dosimetric control of PDT.

dosimetric control, as well as the influence of taking into account the optical properties of exposed biological tissues on the effectiveness of treatment.

Review of PDT methodology for GI organs

In this paragraph we provide an analysis of the methodology of photodynamic therapy on gastrointestinal organs, the key aspects of which are summarized in two tables, with Tab. 1 shows the studies for which the method of PDT efficacy control was not specified in the papers, and in Tab. 2 are those for which the efficacy control was performed. Tab. 1 includes data from 34 studies, and Tab. 2 nine, so we can conclude that only every fifth PDT protocol for gastrointestinal neoplasms is accompanied by a control procedure.

Tables 1 and 2 compare different methodologies of photodynamic therapy of various diseases of gastrointestinal tract organs. In some works instead of dose (J/cm^2) and power (W/cm^2) per unit area the dose per unit diffuser length (J/cm) and power per unit diffuser length (W/cm) are given. These values are convenient for certain applications, but for comparing studies using different photosensitizers and illumination geometries, the values per unit area are more informative because they provide information on the absolute measure of light illuminating the surface of the area being treated [45]. One of the most common pathologies for which this treatment method is used is Barrett's esophagus also abbreviated CELLO (columnar epithelium lined lower oesophagus). In this disease in the epithelial lining of the esophageal mucosa is found atypical for the normal intestinal type epithelium instead of flat multilayer epithelium. If untreated, Barrett's esophagus can progress to the malignant pathology of adenocarcinoma, which has the fastest growing incidence of any solid tumor in most of the world [62]. When treatment is performed according to standardized protocols that do not take into account the tissue characteristics of a particular patient, there is variability in the response to PDT, in the case of Barrett's esophagus it consists of residual Barrett's syndrome and stricture formation. One of the reasons for the different outcome of therapy is the difference in the delivered dose, as the actual dose of light absorbed by tissue depends not only on the energy of light, but also on the optical properties and geometry of the sample, which is especially significant for hollow organs [46] and, consequently, for GI organs. Accordingly, in order to increase the probability of a positive treatment outcome, it is necessary to carry out personalized laser-induced exposure depending on the tissue characteristics of each specific patient. This task can be accomplished using methods of automatic planning and dosimetric measurements directly during the PDT procedure.

Таблица 1.
Сопоставление протоколов проведения фотодинамической терапии различных заболеваний желудочно-кишечного тракта – без контроля эффективности

Table 1.
Comparison of protocols for photodynamic therapy of various gastrointestinal diseases – without effectiveness control

№	Источник Source	Диагноз Diagnosis	Фотосенсибилизатор Photosensitizer	Длина волны (нм) Wavelength (nm)	Вид облучателя The type of light delivery	Доза (плотность мощности) Energy (fluence rate)
1	[1]	КРР CRC	Фотофрин Photofrin	630	ПТ FC	200 J/cm^2 (-)
2	[2]	АП EA	Фотофрин Photofrin	630	ЦД CD	300 J/cm (400 mW/cm)
3	[3]	ПБ, АП CELLO, EA	Фотофрин Photofrin	632	ЦД CD	150-250 J/cm (400 mW/cm)
4	[5]	ПБ CELLO	Фотофрин Photofrin	630	ЦД, баллон CD, balloon	130 J/cm (400 mW/cm)
5	[6]	ПБ, АП CELLO, EA	Фотофрин, 5-АЛК Photofrin, 5-ALA	630	ЦД, баллон CD, balloon	50 – 75 J/cm (400 mW/cm)
6	[7]	ПБ, АП CELLO, EA	Фотофрин Photofrin		ЦД CD	150 – 225 J/cm (-)
7	[8]	ПБ, АП CELLO, EA	Фотофрин II, ПГП Photofrin II, HPD	630	ЦД CD	200 J/cm, 32 J/cm^2 (400 mW/cm)
8	[9]	ПБ CELLO	Фотофрин Photofrin	630	ЦД CD	150 J/cm (-)
9	[10]	ПБ CELLO	5-АЛК, фотофрин 5-ALA (a), photofrin (b)	635	(a): ПТ, (b): ЦД (a): FC, (b): CD	(a): 200J/cm^2 (b): 130 J/cm, 28 J/cm^2 (-)
10	[11]	ПБ CELLO	5-АЛК 5-ALA	635	ЦД CD	500-1000 J/cm

11	[12]	ПБ, АП CELLO, EA	5-АЛК 5-ALA	635	ПТ FC	150 J/cm^2 (100 mW/cm^2)
12	[13]	ПБ, АП CELLO, EA	5-АЛК 5-ALA	630	ЦД CD	100 – 200 J/cm^2 90 – 150 mW/cm^2
13	[14]	АП EA	5-АЛК 5-ALA	580 – 720, 1250 – 1600	ПТ FC	100 J/cm^2 (-)
14	[15]	ПБ CELLO	mTHPC	514	ЦД CD	75 J/cm^2 (100 mW/cm^2)
15	[16]	ПБ CELLO	mTHPC	511 (a), 652 (b)	ЦД CD	(a): 75 J/cm^2 (b): 7 J/cm^2 (60-100 mW/cm^2)
16	[17]	АП, РП EA, ESCC	5-АЛК (a), mTHPC (b) 5-ALA (a) mTHPC (b)	635, 652	ЦД, баллон CD, balloon	(a): 150J/cm^2, (b): 20 J/cm^2 100 mW/cm
17	[18]	ПБ, АП CELLO, EA	mTHPC	652	ЦД CD	8 – 20 J/cm^2 (200 mW/cm)
18	[19]	ОП ET	Фотофрин Photofrin	630	Волокно с микролинзой Microlens fiber	75 J/cm^2 (-)
19	[20]	ОП ET	Фотофрин, талапорфин натрия Photofrin, talaporfn sodium	630, 664	ПТ FC	75-100 J/cm^2 (150 mW/cm^2)
20	[21]	ОП ET	Талапорфин натрия Talaporfin sodium	664	-	100 J/cm^2 (-)
21	[22]	АП EA	HPPH	665	ЦД CD	150-175 J/cm (100- 400 mW/cm^2)
22	[23]	РП ESCC	Фотофрин Photofrin	630	ПТ, микролинза, ЦД FC, microlens, CD	75 J/cm^2 (-)
23	[24]	РП ESCC	Фотофрин Photofrin	630	Волокно с микролинзой Microlens fiber	75 J/cm^2 (160 mW/cm^2)
24	[25]	ОП ET	Талапорфин натрия Talaporfin sodium	664	ПТ FC	50 J/cm^2 (150 mW/cm^2)
25	[26]	ОП ET	Фотофрин Photofrin	630	Баллон Balloon	100 J/cm (-)
26	[27]	РП ESCC	Талапорфин натрия Talaporfin sodium	664	ПТ FC	100 J/cm^2 (150 mW/cm^2)
27	[28]	ПБ, АП CELLO, EA	Фотофрин Photofrin	630	ЦД CD	- (-)
28	[29]	ПБ CELLO	Фотофрин Photofrin	630	ЦД CD	100 – 200 J/cm (-)
29	[30]	ПБ, АП CELLO, EA	ПГП, фотофрин HPD, photofrin	630	ЦД CD	300 J/cm, 32 J/cm^2 (400 mW/cm)
30	[31]	РП ESCC	Фотофрин Photofrin	630	ПТ FC	75 J/cm^2 (-)
31	[32]	АП, РП EA, ESCC	Фотофрин Photofrin	630	ЦД CD	300 J/cm (400 mW/cm)
32	[33]	ОП ET	Фотофрин II Photofrin II	630	ЦД CD	300 – 400 J/cm (-)
33	[34]	ПБ CELLO	ПГП, фотофрин HPD, photofrin	630	ЦД, баллон CD, balloon	200 J/cm (400 mW/cm)
34	[35]	РЖ GC	Фотофрин, талапорфин натрия Photofrin, talaporfin sodium	405, 630	ПТ FC	60 J/cm^2 (150 mW/cm^2) 60 J/cm^2

КРР – колоректальный рак, АП – аденокарцинома пищевода, ОП – опухоли пищевода, ПБ – пищевод Баретта, РП – плоскоклеточный рак пищевода, РЖ – рак желудка, ПГП – производные гематопорфирина, 5-АЛК – 5-аминолевулиновая кислота, hTHPC – 5,10,15,20-тетра(м -гидроксифенил)хлорин, HPPH (2-[1-гексилоксиэтил]-2-девинил пирофеофорбид-а), ЦД – цилиндрический диффузор, ПТ – плоский торец.
CRC – Colorectal Cancer, EA – Esophageal Adenocarcinoma, ET – Esophageal Tumors, CELLO – Columnar Epithelium Lined Lower Oesophagus, ESCC – Esophageal Squamous Cell Carcinoma, GC – Gastric Cancer, HPD – Hematoporphyrin Derivatives, 5-ALA – 5-aminolevulinic acid, hTHPC – 5,10,15,20-tetra(m-hydroxyphenyl)chlorin, HPPH (2-[1-hexyloxyethyl]-2-devinyl pyropheophorbide-a), CD – Cylindrical Diffuser, FC – Flat Cut.

Таблица 2.
Сопоставление протоколов проведения фотодинамической терапии различных заболеваний желудочно-кишечного тракта с контролем эффективности

Table 2.
Comparison of protocols for photodynamic therapy of various gastrointestinal diseases with monitoring of effectiveness

№	Источник Source	Диагноз Diagnosis	Фотосенсибилизатор Photosensitizer	Длина волны (нм) Wavelength (nm)	Вид облучателя The type of light delivery	Доза (плотность мощности) Energy (fluence rate)	Контроль эффективности Effectiveness control
1	[36]	ПБ CELLO	5-АЛК 5-ALA	635	CD, balloon	150 J/cm^2 (150 mW/cm^2)	Дозиметрия ФС, фотовыцветание Photosensitizer concentration, photobleaching
2	[37]	РЖ GC	5-АЛК 5-ALA	635	FC	- (30 W/cm^2)	Фотовыцветание Photobleaching
3	[38]	CRR	Фотофрин Photofrin	532	FC	- (-)	Сатурация, концентрация гемоглобина, концентрация ф/с Blood oxygenation, hemoglobin concentration, drug concentration
4	[39]	ПБ, АП CELLO, EA	Фотофрин Photofrin	630	CD	- (400 mW/cm)	Флуоресцентная спектроскопия Fluorescence spectroscopy
5	[40]	EC	Талапорфин натрия Talaporfin sodium	664	-	100 J/cm^2 (150mW/cm^2)	Визуализация оксигенации Oxygensaturation imaging
6	[41]	ПБ CELLO	5-АЛК 5-ALA	505	-	- (-)	Флуоресцентная спектроскопия Fluorescence spectroscopy
7	[42]	АП EA	5-АЛК 5-ALA	630	CD	100 – 200 J/cm^2 (90 – 150 mW/cm^2)	Флуоресцентная спектроскопия Fluorescence spectroscopy
8	[43]	ПБ CELLO	Фотофрин Photofrin	635	CD	37 J/cm^2 (45 mW/cm^2)	Допплеровская ОКТ Doppler OCT
9	[44]	ПБ CELLO	5-АЛК 5-ALA	630	CD	100 J/cm^2 (100 mW/cm^2)	Контроль мощности излучения Fluence rate measurements

КРР – колоректальный рак, АП – аденокарцинома пищевода, ПБ – пищевод Баретта, РЖ – рак желудка, 5-АЛК – 5-аминолевулиновая кислота, ЦД – цилиндрический диффузор, ПТ – плоский торец, ФС – фотосенсибилизатор.
CRC – Colorectal Cancer, EA – Esophageal Adenocarcinoma, CELLO – Columnar Epithelium Lined Lower Oesophagus, GC – Gastric Cancer, 5-ALA – 5-aminolevulinic acid, CD – Cylindrical Diffuser, FC – Flat Cut.

Automated planning of photodynamic therapy

Automating PDT planning addresses key challenges such as tumor irregularity, patient movements, and the need for accurate light dosimetry in complex anatomical areas, and includes several key components. First, computer-aided design algorithms determine the optimal placement, power, and configuration of light sources (e.g., fiber-optic probes or LED arrays) based on 3D imaging data (e.g., MRI or CT) to adjust the distribution of light absorption in tissues to the tumor shape and minimize the impact on organs at risk. Second, the automation of PDT planning usually implements dynamic dosimetry and light dose monitoring. Automated systems can adjust light output in real time to account for patient movement or changes in tissue optical properties. Third, machine learning techniques, which are now being widely adopted in clinical practice, are also being used for this task to adapt to individual variations in tissue optical properties, making treatment plans more reliable and personalized.

Automated planning of photodynamic therapy (PDT) uses advanced mathematical and technical methods to

optimize the light dose, minimize damage to healthy tissue, and maximize tumor destruction. PDT planning must take into account irradiation geometry, separating the cases of intrathecal and superficial irradiation schemes. Intrathecal PDT has evolved as a response to the clinical demand for therapy of deep-seated tumors, the effect on which is limited by the depth of light penetration during surface irradiation.

Modeling of light propagation is the main tool for estimating the absorbed light dose in tissues [47]. Monte Carlo methods numerically simulate light transport in three-dimensional models of pathologies, including complex geometry [48], in the volume of surrounding tissues, the geometric parameters of which are obtained using MRI or CT [49]. Dose-volume histograms derived from modeling reduce computational costs and allow iterative improvement of the plan. This modeling takes into account the optical properties of tissues (absorption, scattering), generates the distribution of the absorbed dose in the tissue volume for different illumination geometries, allows iteratively refining the position of sources and taking into account the change of optical properties during the PDT procedure.

The clinical implementation of these PDT planning techniques is represented, for example, by PDT-SPACE (open source software combining machine learning for planning that takes into account individual patient differences, adaptive optimization for bone metastases and brain gliomas, damage reduction (>70% compared to previous methods) while achieving >98% tumor destruction) [47]. The approach implemented in the FullMonte software package for tetrahedral 3-D Monte Carlo simulation, visualization, and analysis of light propagation in inhomogeneous turbid media is also of interest [50].

Analysis of oxygen concentration in the photodynamic treatment zone is another critical component of planning and implementation of photodynamic therapy (PDT), along with dosimetry of absorbed radiation, because the efficacy of PDT depends on the simultaneous presence of photosensitizer, light, and oxygen. The generation of cytotoxic reactive oxygen species (ROS), especially singlet oxygen, is central to the mechanism of PDT, and insufficient oxygen in tissues can limit therapeutic results [51]. Maintaining adequate oxygenation throughout treatment is essential for optimal ROS formation and exposure control. Monitoring methods are represented by several approaches. Direct measurement methods include oxygen electrodes and fluorescent optodes. They provide a direct, spot measurement of tissue partial pressure of oxygen (pO_2), but are invasive and not always suitable for clinical settings [51].

Optical spectroscopy also allows us to determine oxygen concentration indirectly, since it is closely related to the level of hemoglobin oxygen saturation. At the same time, this approach provides noninvasive assessment of oxygenation status and is the most widely used at present [51, 52].

Another important aspect of PDT planning that is often overlooked in clinical application is modeling of the biological response. It is necessary to take into account the dynamics of oxygen transport during PDT and singlet oxygen-mediated cell death kinetics [53], binary models of cell fate decision making [54].

The use of photodynamic therapy for tumor diseases of the gastrointestinal tract has shown efficacy as an adjunct to surgical treatment, as well as for tumors of small size and as a method of palliative treatment [55-57]. Consider in more detail such aspects of PDT planning automation as the use of mathematical models of treated organs and tissues for numerical simulation of light propagation in the medium and consideration of optical properties of these organs and tissues.

PDT control

The transition to personalized PDT dosimetry is a non-trivial task due to the difficulty in accounting for the nonlinear interaction between light dose, irradiation time, and the concentration of photosensitizer and molecular oxygen [58].

PDT dosimetry

The main three components of photodynamic therapy are photosensitizer, laser light and oxygen. Accordingly, in order to transition to personalized treatment, it is necessary to monitor the parameters related to these three components. PDT dosimetry can be divided into four types: explicit and implicit dosimetry, monitoring of biological tissue response, and direct dosimetry [59].

Explicit dosimetry takes into account the entire PDT pathway, from light absorption to singlet oxygen production. This type of dosimetry involves direct control of the power density of the light source, photosensitizer concentration, and oxygen content [60]. This type of dosimetry works well in conditions of high tissue oxygen saturation, when the PDT dose, which is proportional to the time integral of the product of local photosensitizer concentration and light flux intensity, is the most accurately defined dosimetric value and a good indicator of treatment outcome [61]. Using explicit dosimetry, initial PDT parameters are measured and incorporated into a dose calculation model to estimate singlet oxygen production [62]. Even under static conditions, it is technically difficult to measure all three parameters and, given that they are also dynamically interdependent, it is difficult to achieve accurate dose determination [62].

Taking into account the interdependence of light intensity, photosensitizer concentration, and oxygen content, the parameters controlled by direct dosimetry, is a difficult task in determining the photodynamic dose. The dependence of the photosensitizer decay on

the radiation intensity cannot be expressed as a simple exponential expression [63]. Since it is extremely difficult to track all changes using explicit dosimetry, implicit dosimetry is often used, which aims to measure a value that depends on all or at least most of the above factors [63].

Implicit dosimetry measures parameters that depend on several of the three components of PDT, such as photobleaching and photoproduct formation [64]. The main goal of implicit dosimetry is to quantify all relevant individual parameters, the aggregate of which can be represented as an integral parameter closely correlating with the therapeutic dose [65].

Monitoring the response of biological tissues involves adjusting the parameters of photodynamic treatment depending on its effect on the tissues of the treated organ, which is monitored by avoiding the occurrence of necrosis area or blockage of the vascular channel [66].

In order to control the PDT procedure using direct dosimetry, it is necessary to measure the presence and amount of reactive oxygen species in the tissues under study [67]. The technique is based on the assumption that the PDT effect is mainly achieved through photochemical reactions of the second type.

Currently, the main methods used for PDT dosimetry are optical imaging, including techniques based on fluorescent and diffusely reflected signal registration, and modeling [65]. A comparison of techniques for monitoring the effectiveness of PDT and types of dosimetry is shown in Table 3. Optical imaging is a broad concept that includes such techniques as video fluorescence imaging, fluorescence spectroscopy, optical diffusion spectroscopy (mainly in diffuse reflection geometry), Raman spectroscopy, and optical coherence tomography [65]. Video fluorescence imaging and fluorescence spectroscopy make it possible to determine the areas of photosensitizer accumulation, as well as to evaluate photobleaching. Accordingly, these methods can be referred to implicit dosimetry. Diffuse reflectance spectroscopy can be used to estimate oxygen content, which allows this method to be classified as explicit dosimetry. This method can also be used to determine the optical properties of tissues to personalize photodynamic treatment. Raman spectroscopy allows to determine the concentration of photosensitizer [68, 69], therefore, it is a method of explicit dosimetry. Optical coherence tomography [70] refers to methods of monitoring the response of biological tissues. Singlet oxygen dosimetry [71], which refers to direct dosimetry, is also used as a method to monitor photodynamic effects. It is also possible to use several techniques together, for example, diffuse reflectance spectroscopy and fluorescence spectroscopy [52, 72] or singlet oxygen photobleaching and luminescence measurements [62], for simultaneous monitoring of a larger number of parameters.

Таблица 3.
Сопоставление вида дозиметрии и методик контроля эффективности ФДТ

Table 3.
Comparison of the type of dosimetry and methods for monitoring the PDT effectiveness

Вид дозиметрии Type of dosimetry	Контролируемые параметры Controlled parameters	Методы Methods
Явная Explicit	Плотность энергии источника, концентрация фотосенсибилизатора, содержание кислорода Source energy density, photosensitizer concentration, oxygen content	Спектроскопия диффузного отражения Diffuse reflectance spectroscopy
Неявная Implicit	Фотобличинг или образование фотопродуктов Photobleaching or photoproduct formation	Флуоресцентная диагностика Fluorescent diagnostics
Контроль реакции биологических тканей Control of biological tissue reactions	Недопущение некроза и блокировки сосудистого русла Preventing necrosis and blockage of the vascular bed	Оптическая когерентная томография Optical coherence tomography
Прямая Direct	Количество активных форм кислорода Active oxygen forms	Люминесценция синглетного кислорода Singlet oxygen luminescence

Determination of optical properties as a method of PDT control

Regardless of the choice of the type of dosimetry for more accurate realization of PDT it is necessary to take into account the optical properties of tissues. When performing explicit dosimetry, this is possible by introducing a correction factor that allows taking into account the optical properties when recording fluorescence; this methodology is presented in [73]. In this paper, optical properties were determined not directly during photodynamic treatment, but beforehand using optical phantoms imitating biological tissues.

When calculating the required dose from the light source during photodynamic therapy, the dose that will be delivered to tissues is most often calculated. However, not the entire volume of this dose will be absorbed by biological objects, including due to incomplete overlap of the light source spectra and absorption of the photosensitizer [74]. Accordingly, for more accurate control of the PDT procedure, it is necessary to make measurements of the absorbed dose in each case. In addition to influencing the absorbed

dose, the optical properties of tissues also affect the spectral characteristics of the fluorescence signal, including the detectable signal depends on the oxygen concentration [75]. Consequently, determination of the optical characteristics of the studied objects is important not only for personalization of photodynamic therapy, but also for increasing the accuracy of fluorescence diagnostics.

The interaction of optical radiation with tissues can be described using various analytical models, including modified Beer-Lambert law [76], Jacques [77] and Yudovsky [78] models. Also, light propagation in tissues can be investigated using Monte Carlo simulations. In [79], a comparison of the three mentioned analytical models is presented with respect to their applicability for estimating tissue parameters. The comparison was carried out using data obtained by Monte Carlo simulation and measurements on optical phantoms with known optical properties. The simulation results are best matched by the Yudovsky model. The empirical data are closest to the calculations performed with the Jacques model.

There are various methods that allow to determine the optical properties of biological objects by processing the data obtained from spectral measurements. The most common are the inverse Monte Carlo method and the inverse addition-doubling method [80]. These techniques involve registration of spectra in several geometries. Conducting measurements of diffuse reflectance and transmittance spectra allows the determination of two parameters: absorption coefficient and reduced scattering coefficient. To recover three optical properties: absorption coefficient, scattering coefficient and anisotropy factor, it is necessary to register spectra in three geometries. Globally, modern algorithms for recovering optical properties of biological tissues are based either on integrating sphere measurements, which are based on reflectance and transmittance measurements of thin slices of dissected tissue [81], and techniques based on the registration of diffusely reflected signal using point sources and detectors [82-84], which aim to characterize the spatial, temporal, and spectral dependence of the recorded signal. The recovery of information about optical properties from measured signals can be based on empirical calibration based on tables with a representative set of reference phantoms with known characteristics [83], as well as on models with analytical approximation, such as diffusion theory [84], or Monte Carlo simulations [82]. Currently, data on optical properties have been obtained for such localizations as bone, nerve, muscle, and adipose tissue [85], white and gray matter of the brain [86], esophagus [87], stomach [88, 89], colon [90, 91], and small intestine [89]. In all the works cited in this paragraph, the optical properties were determined not during surgery.

Currently, several scientific groups are working on the task of taking into account the optical properties of tissues during clinical photodynamic treatment. They propose to take into account the optical properties of tissues during fluorescence registration by applying the Monte Carlo method for modeling the propagation of radiation in biological media, with the values of optical properties either determined using optical phantoms [92, 93] or taken from literature data [94].

The article [95] is devoted to the development and demonstration of a noninvasive method for quantitative determination of optical properties of turbid media (including biological tissues) in the wavelength range from 430 to 1050 nm. The method is called spatially modulated quantitative spectroscopy and is based on the measurement of reflected light from the sample under study when it is illuminated at different spatial frequencies. This allows to calculate absorption and scattering coefficients without preliminary assumptions about the composition of chromophores in the sample. The method was tested on liquid phantoms with known concentrations of absorbers and scatterers. The obtained values of optical properties had good agreement with the expected results. As a demonstration of the feasibility of the *in vivo* method, an experiment was performed on human skin. The obtained skin absorption spectrum was described with good accuracy using models taking into account the contribution of oxy- and deoxyhemoglobin, water and melanin, and the quantitative values of these components corresponded to the data for skin from literature sources.

The authors of the study [38] developed a technique for transforming the diffuse reflectance signal in a wide spectral range into parameters of human skin, such as light penetration depth, blood oxygen saturation, hemoglobin concentration, and epidermis thickness. The diffusion approximation of the radiative transfer theory was used to analyze the data. The obtained values of blood oxygen saturation and hemoglobin concentration are in good agreement with published physiological data, the epidermis thickness measured optically coincides with the results of histologic studies. The proposed approach can be used to monitor skin condition, diagnose diseases and evaluate the efficacy of photodynamic therapy.

In the article [96], modeling of photodynamic therapy of the esophagus was carried out taking into account the absorption and scattering coefficients determined by measuring a porcine esophagus sample on integrating spheres. PDT modeling was performed by Monte Carlo method taking into account tissue multilayers. The introduction of photosensitizer was taken into account by changing the values of optical properties: both absorption and scattering increased. The depth of tissue damage was determined for different values of light

dose. The obtained values were compared with clinical results in other literature sources.

In [97], the control of PDT efficiency was determined using fluorescence spectroscopy and light dose measurements. Depending on the *in vivo* determined concentration of the photosensitizer (Photofrin), a correction for the optical properties of the object under study was introduced. The method of correction of irradiation procedure depending on optical properties was developed by means of Monte Carlo simulation and tested on optical phantoms. The presented system allows simultaneous examination of eight areas in real time.

In [98], the determination of tissue optical properties is carried out to optimize the implicit dosimetry technique. The method consisted in measuring the fluorescence and reflected signal, which were used to estimate blood volume, reduced scattering coefficient and photosensitizer concentration. Validation of the methodology was performed on optical phantoms using least squares nonlinear regression analysis and *in vivo* on mice. Diffuse reflectance spectroscopy was used as a reference method to independently measure the properties of biological tissues and compare the results. The blood volume and scattering coefficient measured by the developed method were compared with the results obtained by diffuse reflectance spectroscopy. Hemoglobin oxygen saturation was also measured in the tumor using diffuse reflectance spectroscopy.

The work [99] is devoted to the application of machine learning methods (neural networks and gradient boosting regression trees) to restore the optical properties of biological tissues during intrathecal PDT in real time by adapting the power of light sources. Optical properties of tissues (absorption coefficient μ_a and scattering coefficient μ_s) can change during treatment due to changes in blood flow, edema or cell swelling, which affects the light dose distribution. Traditional methods to account for optical properties based on analytical models (e.g., diffusion approximation) are not accurate enough for deep-seated tumors. Using machine learning (gradient bousting and neural networks), with training on simulation data to predict tumor μ_a and μ_s based on light dose measurements using cylindrical diffusers, it is possible to optimize emitter location and power distribution by pre-planning based on average tissue optical properties. The light dose is also measured in real time using receiving optical fibers, the actual μ_a and μ_s are reconstructed using machine learning techniques, and then the power of the emitters is recalculated to minimize errors in the delivered dose magnitude. The methodology has been validated on 3D glioblastoma models. Results indicate that optical property restoration followed by power reoptimization reduces the uncertainty in dose prediction by 75% for healthy tissues. The method enhances treatment personalization by adapting to tissue changes during therapy, which may improve clinical outcomes in deep-seated tumors such as glioblastoma.

Conclusion

This review has considered the actual works devoted to the task of automation of planning and control of photodynamic therapy of gastrointestinal organs and highlighted several main directions for solving this task. First of all, automation is realized due to more effective calculation of the absorbed dose of therapeutic radiation using algorithms of numerical modeling of light propagation in tissues, information about the geometry of pathological inclusions and optical properties of normal and tumor tissues, determination of which is possible both at the preoperative stage and during the exposure itself. Two other important aspects of PDT planning and control are the control of photosensitizer photobleaching and oxygen concentration in the treatment zone, because without these components it is impossible for the photodynamic reaction to proceed according to type II. The methods of machine learning and artificial intelligence, which are currently primarily associated with automation of various processes, are just coming to the field of photodynamic treatment planning, as they require a sufficiently large amount of unified data for training classification models. However, their use already makes it possible to increase the accuracy and efficiency of determining the optical properties of tissues in order to optimize the location of emitters and the distribution of absorbed dose in the tissue volume by means of preliminary planning. Thus, we can conclude that automation of photodynamic treatment planning includes a number of important components, both algorithmic and technical, and represents an actively developing area of scientific research.

The work was funded by the Russian Science Foundation, grant No. 25-25-00516.

REFERENCES

1. Sun B., Li W., Liu N. Curative effect of the recent Porfimer sodium photodynamic adjuvant treatment on young patients with advanced colorectal cancer. *Oncol. Lett*, 2016, vol. 11, pp. 2071–2074. https://doi.org/ 10.3892/ol.2016.4179.
2. McGarrity T., Peiffer L., Granville D., Carthy C., Levy J., Khandelwal M., Hunt D. Apoptosis associated with esophageal adenocarcinoma:

ЛИТЕРАТУРА

1. Sun B., Li W., Liu N. Curative effect of the recent Porfimer sodium photodynamic adjuvant treatment on young patients with advanced colorectal cancer // Oncol Lett. – 2016. – T. 11. – C. 2071–2074. https://doi.org/10.3892/ol.2016.4179.
2. McGarrity T., Peiffer L., Granville D., Carthy C., Levy J., Khandelwal M., Hunt D. Apoptosis associated with esophageal adenocarcinoma:

influence of photodynamic therapy. *Cancer Lett.*, 2001, vol. 163, pp. 33–41. https://doi.org/ 10.1016/S0304-3835(00)00663-7.
3. Wolfsen H.C., Woodward T.A., Raimondo M. Photodynamic therapy for dysplastic Barrett esophagus and early esophageal adenocarcinoma. *Mayo Clin. Proc.*, 2002, vol. 77, no. 11, pp. 1176–1181. https://doi.org/ 10.4065/77.11.1176.
4. Liu H. Editorial: dosimetry study in photodynamic therapy for diagnosis, precision treatment and treatment evaluation. *Front. Phys.*, 2020, vol. 8. https://doi.org/ 10.3389/fphy.2020.588484.
5. Overholt B.F., Wang K.K., Burdick J.S. et al. Five-year efficacy and safety of photodynamic therapy with Porfimer sodium in Barrett's high-grade dysplasia. *Gastrointest. Endosc.*, 2007, vol. 66, no. 3, pp. 460–468. https://doi.org/ 10.1016/j.gie.2006.12.037.
6. Overholt B.F., Panjehpour M., Halberg D.L. Photodynamic therapy for Barrett's esophagus with dysplasia and/or early stage carcinoma: long-term results. *Gastrointest. Endosc.*, 2003, vol. 58, no. 2, pp. 183–188. https://doi.org/ 10.1067/mge.2003.327.
7. Wolfsen H.C., Hemminger L.L., Wallace M.B., DeVault K.R. Clinical experience of patients undergoing photodynamic therapy for Barrett's dysplasia or cancer. *Aliment Pharmacol. Ther.*, 2004, vol. 20, pp. 1125–1131. https://doi.org/ 10.1111/j.1365-2036.2004.02209.x.
8. Buttar N.S., Wang K.K., Lutzke L.S., Krishnadath K.K., Anderson M.A. Combined endoscopic mucosal resection and photodynamic therapy for esophageal neoplasia within Barrett's esophagus. *Gastrointest. Endosc.*, 2001, vol. 54, no. 6, pp. 682–688. https://doi.org/ 10.1067/gien.2001.0003.
9. Yachimski P., Puricelli W.P., Nishioka N.S. Patient predictors of histopathologic response after photodynamic therapy of Barrett's esophagus with high-grade dysplasia or intramucosal carcinoma. *Gastrointest. Endosc.*, 2009, vol. 69, no. 2, pp. 205–212. https://doi.org/ 10.1016/j.gie.2008.05.032.
10. Dunn J.M., Mackenzie G.D., Banks M.R. et al. A randomised controlled trial of ALA vs. Porfimer sodium photodynamic therapy for high-grade dysplasia arising in Barrett's oesophagus. *Lasers Med. Sci.*, 2013, vol. 28, pp. 707–715. https://doi.org/ 10.1007/s10103-012-1132-1.
11. Mackenzie G.D., Jamieson N.F., Novelli M.R. et al. How light dosimetry influences the efficacy of photodynamic therapy with 5-aminolaevulinic acid for ablation of high-grade dysplasia in Barrett's esophagus. *Lasers Med. Sci.*, 2008, vol. 23, no. 2, pp. 203–210. https://doi.org/ 10.1007/s10103-007-0473-7.
12. Pech O., Gossner L., May A. et al. Long-term results of photodynamic therapy with 5-aminolevulinic acid for superficial Barrett's cancer and high-grade intraepithelial neoplasia. *Gastrointest. Endosc.*, 2005, vol. 62, no. 1, pp. 24–30. https://doi.org/ 10.1016/s0016-5107(05)00333-0.
13. Tan W.C., Fulljames C., Stone N., Dix A.J., Shepherd N., Roberts D.J., Brown S.B., Krasner N., Barr H. Photodynamic therapy using 5-aminolaevulinic acid for oesophageal adenocarcinoma associated with Barrett's metaplasia. *J. Photochem. Photobiol. B*, 1999, vol. 53, no. 1-3, pp. 75–80. https://doi.org/ 10.1016/s1011-1344(99)00129-3.
14. Kashtan H., Konikoff F., Haddad R., Skornick Y. Photodynamic therapy of cancer of the esophagus using systemic aminolevulinic acid and a non laser light source: a phase I/II study. *Gastrointest. Endosc.*, 1999, vol. 49, no. 6, pp. 760–764. https://doi.org/ 10.1016/s0016-5107(99)70297-x.
15. Etienne J., Dorme N., Bourg-Heckly G., Raimbert P., Fléjou J.F. Photodynamic therapy with green light and m-tetrahydroxyphenyl chlorin for intramucosal adenocarcinoma and high-grade dysplasia in Barrett's esophagus. *Gastrointest. Endosc.*, 2004, vol. 59, no. 7, pp. 880–889. https://doi.org/ 10.1016/s0016-5107(04)01271-4.
16. Lovat L.B., Jamieson N.F., Novelli M.R., Mosse C.A., Selvasekar C., Mackenzie G.D., Thorpe S.M., Bown S.G. Photodynamic therapy with m-tetrahydroxyphenyl chlorin for high-grade dysplasia and early cancer in Barrett's columnar lined esophagus. *Gastrointest. Endosc.*, 2005, vol. 62, no. 4, pp. 617–623. https://doi.org/ 10.1016/j.gie.2005.04.043.
17. Gossner L., May A., Sroka R., Ell C. A new long-range through-the-scope balloon applicator for photodynamic therapy in the esophagus and cardia. *Endoscopy*, 1999, vol. 31, no. 5, pp. 370–376. https://doi.org/ 10.1055/s-1999-31.
18. Javaid B., Watt P., Krasner N. Photodynamic therapy (PDT) for oesophageal dysplasia and early carcinoma with mTHPC (m-tetrahydroxyphenyl chlorin): a preliminary study. *Lasers Med. Sci.,*

influence of photodynamic therapy // Cancer Lett. – 2001. – Т. 163. – С. 33–41. https://doi.org/10.1016/S0304-3835(00)00663-7.
3. Wolfsen H.C., Woodward T.A., Raimondo M. Photodynamic therapy for dysplastic Barrett esophagus and early esophageal adenocarcinoma // Mayo Clin Proc. – 2002. – Т. 77, № 11. – С. 1176–1181. https://doi.org/10.4065/77.11.1176.
4. Liu H. Editorial: dosimetry study in photodynamic therapy for diagnosis, precision treatment and treatment evaluation // Front Phys. – 2020. – Т. 8. https://doi.org/10.3389/fphy.2020.588484.
5. Overholt B.F., Wang K.K., Burdick J.S. и соавт. Five-year efficacy and safety of photodynamic therapy with Porfimer sodium in Barrett's high-grade dysplasia // Gastrointest Endosc. – 2007. – Т. 66, № 3. – С. 460–468. https://doi.org/10.1016/j.gie.2006.12.037.
6. Overholt B.F., Panjehpour M., Halberg D.L. Photodynamic therapy for Barrett's esophagus with dysplasia and/or early stage carcinoma: long-term results // Gastrointest Endosc. – 2003. – Т. 58, № 2. – С. 183–188. https://doi.org/10.1067/mge.2003.327.
7. Wolfsen H.C., Hemminger L.L., Wallace M.B., DeVault K.R. Clinical experience of patients undergoing photodynamic therapy for Barrett's dysplasia or cancer // Aliment Pharmacol Ther. – 2004. – Т. 20. – С. 1125–1131. https://doi.org/10.1111/j.1365-2036.2004.02209.x.
8. Buttar N.S., Wang K.K., Lutzke L.S., Krishnadath K.K., Anderson M.A. Combined endoscopic mucosal resection and photodynamic therapy for esophageal neoplasia within Barrett's esophagus // Gastrointest Endosc. – 2001. – Т. 54, № 6. – С. 682–688. https://doi.org/10.1067/gien.2001.0003.
9. Yachimski P., Puricelli W.P., Nishioka N.S. Patient predictors of histopathologic response after photodynamic therapy of Barrett's esophagus with high-grade dysplasia or intramucosal carcinoma // Gastrointest Endosc. – 2009. – Т. 69, № 2. – С. 205–212. https://doi.org/10.1016/j.gie.2008.05.032.
10. Dunn J.M., Mackenzie G.D., Banks M.R. и соавт. A randomised controlled trial of ALA vs. Porfimer sodium photodynamic therapy for high-grade dysplasia arising in Barrett's oesophagus // Lasers Med Sci. – 2013. – Т. 28. – С. 707–715. https://doi.org/10.1007/s10103-012-1132-1.
11. Mackenzie G.D., Jamieson N.F., Novelli M.R. и соавт. How light dosimetry influences the efficacy of photodynamic therapy with 5-aminolaevulinic acid for ablation of high-grade dysplasia in Barrett's esophagus // Lasers Med Sci. – 2008. – Т. 23, № 2. – С. 203–210. https://doi.org/10.1007/s10103-007-0473-7.
12. Pech O., Gossner L., May A. и соавт. Long-term results of photodynamic therapy with 5-aminolevulinic acid for superficial Barrett's cancer and high-grade intraepithelial neoplasia // Gastrointest Endosc. – 2005. – Т. 62, № 1. – С. 24–30. https://doi.org/10.1016/s0016-5107(05)00333-0.
13. Tan W.C., Fulljames C., Stone N., Dix A.J., Shepherd N., Roberts D.J., Brown S.B., Krasner N., Barr H. Photodynamic therapy using 5-aminolaevulinic acid for oesophageal adenocarcinoma associated with Barrett's metaplasia // Journal of Photochemistry and Photobiology. B, Biology. – 1999. – Т. 53, № 1-3. – С. 75–80. https://doi.org/10.1016/s1011-1344(99)00129-3.
14. Kashtan H., Konikoff F., Haddad R., Skornick Y. Photodynamic therapy of cancer of the esophagus using systemic aminolevulinic acid and a non laser light source: a phase I/II study // Gastrointestinal Endoscopy. – 1999. – Т. 49, № 6. – С. 760–764. https://doi.org/10.1016/s0016-5107(99)70297-x.
15. Etienne J., Dorme N., Bourg-Heckly G., Raimbert P., Fléjou J.F. Photodynamic therapy with green light and m-tetrahydroxyphenyl chlorin for intramucosal adenocarcinoma and high-grade dysplasia in Barrett's esophagus // Gastrointestinal Endoscopy. – 2004. – Т. 59, № 7. – С. 880–889. https://doi.org/10.1016/s0016-5107(04)01271-4.
16. Lovat L.B., Jamieson N.F., Novelli M.R., Mosse C.A., Selvasekar C., Mackenzie G.D., Thorpe S.M., Bown S.G. Photodynamic therapy with m-tetrahydroxyphenyl chlorin for high-grade dysplasia and early cancer in Barrett's columnar lined esophagus // Gastrointestinal Endoscopy. – 2005. – Т. 62, № 4. – С. 617–623. https://doi.org/10.1016/j.gie.2005.04.043.
17. Gossner L., May A., Sroka R., Ell C. A new long-range through-the-scope balloon applicator for photodynamic therapy in the esophagus and cardia // Endoscopy. – 1999. – Т. 31, № 5. – С. 370–376. https://doi.org/10.1055/s-1999-31.
18. Javaid B., Watt P., Krasner N. Photodynamic therapy (PDT) for oesophageal dysplasia and early carcinoma with mTHPC (m-tetrahydroxyphenyl chlorin): a preliminary study // Lasers in Medical Science. – 2002. – Т. 17, № 1. – С. 51–56. https://doi.org/10.1007/s10103-002-8266-5.

2002, vol. 17, no. 1, pp. 51–56. https://doi.org/ 10.1007/s10103-002-8266-5.
19. Yano T., Muto M., Minashi K., Ohtsu A., Yoshida S. Photodynamic therapy as salvage treatment for local failures after definitive chemoradiotherapy for esophageal cancer. *Gastrointest. Endosc.*, 2005, vol. 62, no. 1, pp. 31–36. https://doi.org/ 10.1016/s0016-5107(05)00545-6.
20. Minamide T., Yoda Y., Hori K., Shinmura K., Oono Y., Ikematsu H., Yano T. Advantages of salvage photodynamic therapy using talaporfin sodium for local failure after chemoradiotherapy or radiotherapy for esophageal cancer. *Surg. Endosc.*, 2020, vol. 34, no. 2, pp. 899–906. https://doi.org/ 10.1007/s00464-019-06846-3.
21. Ishida N., Osawa S., Miyazu T., Kaneko M., Tamura S., Tani S., Yamade M., Iwaizumi M., Hamaya Y., Furuta T., Sugimoto K. Photodynamic Therapy Using Talaporfin Sodium for Local Failure after Chemoradiotherapy or Radiotherapy for Esophageal Cancer: A Single Center Experience. *J. Clin. Med.*, 2020, vol. 9, no. 5, p. 1509. https://doi.org/ 10.3390/jcm9051509.
22. Nava H.R., Allamaneni S.S., Dougherty T.J., Cooper M.T., Tan W., Wilding G., Henderson B.W. Photodynamic therapy (PDT) using HPPH for the treatment of precancerous lesions associated with Barrett's esophagus. *Lasers Surg. Med.*, 2011, vol. 43, pp. 705–712. https://doi.org/ 10.1002/lsm.21112.
23. Tanaka T., Matono S., Nagano T., Murata K., Sueyoshi S., Yamana H., Shirouzu K., Fujita H. Photodynamic therapy for large superficial squamous cell carcinoma of the esophagus. *Gastrointest. Endosc.*, 2011, vol. 73, no. 1, pp. 1–6. https://doi.org/ 10.1016/j.gie.2010.08.049.
24. Yano T., Muto M., Minashi K., Iwasaki J., Kojima T., Fuse N., Doi T., Kaneko K., Ohtsu A. Photodynamic therapy as salvage treatment for local failure after chemoradiotherapy in patients with esophageal squamous cell carcinoma: A phase II study. *Int. J. Cancer*, 2012, vol. 131, pp. 1228–1234. https://doi.org/ 10.1002/ijc.27320.
25. Yano T., Muto M., Yoshimura K. et al. Phase I study of photodynamic therapy using talaporfin sodium and diode laser for local failure after chemoradiotherapy for esophageal cancer. *Radiat. Oncol.*, 2012, vol. 7, p. 113. https://doi.org/ 10.1186/1748-717X-7-113.
26. Lindenmann J., Matzi V., Neuboeck N., Anegg U., Baumgartner E., Maier A., Smolle J., Smolle-Juettner F.M. Individualized, multimodal palliative treatment of inoperable esophageal cancer: Clinical impact of photodynamic therapy resulting in prolonged survival. *Lasers Surg. Med.*, 2012, vol. 44, pp. 189–198. https://doi.org/ 10.1002/lsm.22006.
27. Yano T., Kasai H., Horimatsu T., Yoshimura K., Teramukai S., Morita S., Tada H., Yamamoto Y., Kataoka H., Kakushima N., Ishihara R., Isomoto H., Muto M. et al. A multicenter phase II study of salvage photodynamic therapy using talaporfin sodium (ME2906) and a diode laser (PNL6405EPG) for local failure after chemoradiotherapy or radiotherapy for esophageal cancer. *Oncotarget*, 2017, vol. 8, pp. 22135–22144.
28. Foroulis Ch.N., Thorpe J.A.C. Photodynamic therapy (PDT) in Barrett's esophagus with dysplasia or early cancer. *Eur. J. Cardiothorac. Surg.*, 2006, vol. 29, no. 1, pp. 30–34. https://doi.org/ 10.1016/j.ejcts.2005.10.033.
29. Gray J., Fullarton G.M. Long term efficacy of photodynamic therapy (PDT) as an ablative therapy of high grade dysplasia in Barrett's oesophagus. *Photodiagnosis Photodyn. Ther.*, 2013, vol. 10, no. 4, pp. 561–565. https://doi.org/ 10.1016/j.pdpdt.2013.06.002.
30. Pacifico R.J., Wang K.K., Wongkeesong L.M., Buttar N.S., Lutzke L.S. Combined endoscopic mucosal resection and photodynamic therapy versus esophagectomy for management of early adenocarcinoma in Barrett's esophagus. *Clin. Gastroenterol. Hepatol.*, 2003, vol. 1, no. 4, pp. 252–257.
31. Hatogai K., Yano T., Kojima T., Onozawa M., Daiko H., Nomura S., Yoda Y., Doi T., Kaneko K., Ohtsu A. Salvage photodynamic therapy for local failure after chemoradiotherapy for esophageal squamous cell carcinoma. *Gastrointest. Endosc.*, 2016, vol. 83, no. 6, pp. 1130–1139. e3. https://doi.org/ 10.1016/j.gie.2015.11.016.
32. Lightdale C.J., Heier S.K., Marcon N.E., McCaughan J.S. Jr, Gerdes H., Overholt B.F., Sivak M.V. Jr, Stiegmann G.V., Nava H.R. Photodynamic therapy with porfimer sodium versus thermal ablation therapy with Nd:YAG laser for palliation of esophageal cancer: a multicenter randomized trial. *Gastrointest. Endosc.*, 1995, vol. 42, no. 6, pp. 507–512. https://doi.org/ 10.1016/s0016-5107(95)70002-1.
33. Litle V.R., Luketich J.D., Christie N.A., Buenaventura P.O., Alvelo-Rivera M., McCaughan J.S., Nguyen N.T., Fernando H.C. Photodynamic

19. Yano T., Muto M., Minashi K., Ohtsu A., Yoshida S. Photodynamic therapy as salvage treatment for local failures after definitive chemoradiotherapy for esophageal cancer // Gastrointestinal Endoscopy. – 2005. – T. 62, № 1. – C. 31–36. https://doi.org/10.1016/s0016-5107(05)00545-6.
20. Minamide T., Yoda Y., Hori K., Shinmura K., Oono Y., Ikematsu H., Yano T. Advantages of salvage photodynamic therapy using talaporfin sodium for local failure after chemoradiotherapy or radiotherapy for esophageal cancer // Surgical Endoscopy. – 2020. – T. 34, № 2. – C. 899–906. https://doi.org/10.1007/s00464-019-06846-3.
21. Ishida N., Osawa S., Miyazu T., Kaneko M., Tamura S., Tani S., Yamade M., Iwaizumi M., Hamaya Y., Furuta T., Sugimoto K. Photodynamic Therapy Using Talaporfin Sodium for Local Failure after Chemoradiotherapy or Radiotherapy for Esophageal Cancer: A Single Center Experience // Journal of Clinical Medicine. – 2020. – T. 9, № 5. – C. 1509. https://doi.org/10.3390/jcm9051509.
22. Nava H.R., Allamaneni S.S., Dougherty T.J., Cooper M.T., Tan W., Wilding G., Henderson B.W. Photodynamic therapy (PDT) using HPPH for the treatment of precancerous lesions associated with Barrett's esophagus // Lasers in Surgery and Medicine. – 2011. – T. 43. – C. 705–712. https://doi.org/10.1002/lsm.21112.
23. Tanaka T., Matono S., Nagano T., Murata K., Sueyoshi S., Yamana H., Shirouzu K., Fujita H. Photodynamic therapy for large superficial squamous cell carcinoma of the esophagus // Gastrointestinal Endoscopy. – 2011. – T. 73, № 1. – C. 1–6. https://doi.org/10.1016/j.gie.2010.08.049.
24. Yano T., Muto M., Minashi K., Iwasaki J., Kojima T., Fuse N., Doi T., Kaneko K., Ohtsu A. Photodynamic therapy as salvage treatment for local failure after chemoradiotherapy in patients with esophageal squamous cell carcinoma: A phase II study // International Journal of Cancer. – 2012. – T. 131. – C. 1228–1234. https://doi.org/10.1002/ijc.27320.
25. Yano T., Muto M., Yoshimura K. и соавт. Phase I study of photodynamic therapy using talaporfin sodium and diode laser for local failure after chemoradiotherapy for esophageal cancer // Radiation Oncology. – 2012. – T. 7. – C. 113. https://doi.org/10.1186/1748-717X-7-113.
26. Lindenmann J., Matzi V., Neuboeck N., Anegg U., Baumgartner E., Maier A., Smolle J., Smolle-Juettner F.M. Individualized, multimodal palliative treatment of inoperable esophageal cancer: Clinical impact of photodynamic therapy resulting in prolonged survival // Lasers in Surgery and Medicine. – 2012. – T. 44. – C. 189–198. https://doi.org/10.1002/lsm.22006.
27. Yano T., Kasai H., Horimatsu T., Yoshimura K., Teramukai S., Morita S., Tada H., Yamamoto Y., Kataoka H., Kakushima N., Ishihara R., Isomoto H., Muto M. и др. A multicenter phase II study of salvage photodynamic therapy using talaporfin sodium (ME2906) and a diode laser (PNL6405EPG) for local failure after chemoradiotherapy or radiotherapy for esophageal cancer // Oncotarget. – 2017. – T. 8. – C. 22135–22144.
28. Foroulis Ch.N., Thorpe J.A.C. Photodynamic therapy (PDT) in Barrett's esophagus with dysplasia or early cancer // European Journal of Cardio-Thoracic Surgery. – 2006. – T. 29, № 1. – C. 30–34. https://doi.org/10.1016/j.ejcts.2005.10.033.
29. Gray J., Fullarton G.M. Long term efficacy of photodynamic therapy (PDT) as an ablative therapy of high grade dysplasia in Barrett's oesophagus // Photodiagnosis and Photodynamic Therapy. – 2013. – T. 10, № 4. – C. 561–565. https://doi.org/10.1016/j.pdpdt.2013.06.002.
30. Pacifico R.J., Wang K.K., Wongkeesong L.M., Buttar N.S., Lutzke L.S. Combined endoscopic mucosal resection and photodynamic therapy versus esophagectomy for management of early adenocarcinoma in Barrett's esophagus // Clinical Gastroenterology and Hepatology. – 2003. – T. 1, № 4. – C. 252–257.
31. Hatogai K., Yano T., Kojima T., Onozawa M., Daiko H., Nomura S., Yoda Y., Doi T., Kaneko K., Ohtsu A. Salvage photodynamic therapy for local failure after chemoradiotherapy for esophageal squamous cell carcinoma // Gastrointestinal Endoscopy. – 2016. – T. 83, № 6. – C. 1130–1139.e3. https://doi.org/10.1016/j.gie.2015.11.016.
32. Lightdale C.J., Heier S.K., Marcon N.E., McCaughan J.S. Jr, Gerdes H., Overholt B.F., Sivak M.V. Jr, Stiegmann G.V., Nava H.R. Photodynamic therapy with porfimer sodium versus thermal ablation therapy with Nd:YAG laser for palliation of esophageal cancer: a multicenter randomized trial // Gastrointestinal Endoscopy. – 1995. – T. 42, № 6. – C. 507–512. https://doi.org/10.1016/s0016-5107(95)70002-1.
33. Litle V.R., Luketich J.D., Christie N.A., Buenaventura P.O., Alvelo-Rivera M., McCaughan J.S., Nguyen N.T., Fernando H.C. Photody-

therapy as palliation for esophageal cancer: experience in 215 patients. *Ann. Thorac. Surg.*, 2003, vol. 76, no. 5, pp. 1687–1693. https://doi.org/ 10.1016/s0003-4975(03)01299-2.

34. Prasad G.A., Wang K.K., Buttar N.S., Wongkeesong L.M., Lutzke L.S., Borkenhagen L.S. Predictors of stricture formation after photodynamic therapy for high-grade dysplasia in Barrett's esophagus. *Gastrointest. Endosc.*, 2007, vol. 65, no. 1, pp. 60–66. https://doi.org/ 10.1016/j.gie.2006.04.028.
35. Nakamura T., Oinuma T. Usefulness of photodynamic diagnosis and therapy using talaporfin sodium for an advanced-aged patient with inoperable gastric cancer. *Laser Ther.*, 2014, vol. 23, no. 3, pp. 201–210. https://doi.org/ 10.5978/islsm.14-OR-16.
36. Pogue B.W., Sheng C., Benevides J., Forcione D., Puricelli B., Nishioka N., Hasan T. Protoporphyrin IX fluorescence photobleaching increases with the use of fractionated irradiation in the esophagus. *J. Biomed. Opt.*, 2008, vol. 13, no. 3, p. 034009. https://doi.org/ 10.1117/1.2937476.
37. Loshchenov M., Levkin V., Kalyagina N., Linkov K., Kharnas S., Efendiev K., Kharnas P., Loschenov V. Laser-induced fluorescence diagnosis of stomach tumor. *Lasers Med. Sci.*, 2020, vol. 35. https://doi.org/ 10.1007/s10103-020-02963-x.
38. Wang H.-W., Zhu T.C., Putt M.P., Solonenko M.G., Metz J.M., Dimofte A., Miles J.D., Fraker D.L., Glatstein E., Hahn S.M., Yodh A.G. Broadband reflectance measurements of light penetration, blood oxygenation, hemoglobin concentration, and drug concentration in human intraperitoneal tissues before and after photodynamic therapy. *J. Biomed. Opt.*, 2005, vol. 10, no. 1, p. 014004. https://doi.org/ 10.1117/1.1854679.
39. Pfefer T.J., Schomacker K.T., Nishioka N.S. Long-term effects of photodynamic therapy on fluorescence spectroscopy in the human esophagus. *Photochem. Photobiol.*, 2001, vol. 73, no. 6, pp. 664–668. https://doi.org/ 10.1562/0031-8655(2001)073<0664:lteopt>2.0.co;2.
40. Masayuki PhD, Yoda Y., Yamamoto Y., Sunakawa H., Minamide T., Hori K., Ikematsu H., Yano T. Oxygen saturation imaging as a useful tool for visualizing the mode of action of photodynamic therapy for esophageal cancer. *VideoGIE*, 2020, vol. 5. https://doi.org/ 10.1016/j.vgie.2020.07.003.
41. Ortner M.A., Ebert B., Hein E., Zumbusch K., Nolte D., Sukowski U., Weber-Eibel J., Fleige B., Dietel M., Stolte M., Oberhuber G., Porschen R., Klump B., Hörtnagl H., Lochs H., Rinneberg H. Time gated fluorescence spectroscopy in Barrett's oesophagus. *Gut.*, 2003, vol. 52, no. 1, pp. 28–33. https://doi.org/ 10.1136/gut.52.1.28.
42. Tan W.C., Fulljames C., Stone N., Dix A.J., Shepherd N., Roberts D.J., Brown S.B., Krasner N., Barr H. Photodynamic therapy using 5-aminolaevulinic acid for oesophageal adenocarcinoma associated with Barrett's metaplasia. *J. Photochem. Photobiol.* B, 1999, vol. 53, no. 1-3, pp. 75–80. https://doi.org/ 10.1016/s1011-1344(99)00129-3.
43. Standish B.A., Yang V.X., Munce N.R., Wong Kee Song L.M., Gardiner G., Lin A., Mao Y.I., Vitkin A., Marcon N.E., Wilson B.C. Doppler optical coherence tomography monitoring of microvascular tissue response during photodynamic therapy in an animal model of Barrett's esophagus. *Gastrointest. Endosc.*, 2007, vol. 66, no. 2, pp. 326–333. https://doi.org/ 10.1016/j.gie.2007.02.040.
44. van Veen R.L., Aalders M.C., Pasma K.L., Siersema P.D., Haringsma J., van de Vrie W., Gabeler E.E., Robinson D.J., Sterenborg H.J. In situ light dosimetry during photodynamic therapy of Barrett's esophagus with 5-aminolevulinic acid. *Lasers Surg. Med.*, 2002, vol. 31, no. 5, pp. 299–304. https://doi.org/ 10.1002/lsm.10129.
45. Stone N. Standardizing dosimetry in esophageal PDT: an argument for use of centering devices and removal of misleading units. *Technol. Cancer Res. Treat.*, 2003, vol. 2, no. 4, pp. 333–338. https://doi.org/ 10.1177/153303460300200408.
46. Veen R., Robinson D., Siersema P., Sterenborg H. The importance of in situ dosimetry during photodynamic therapy of Barrett's esophagus. *Gastrointest. Endosc.*, 2006, vol. 64, pp. 786–788. https://doi.org/ 10.1016/j.gie.2006.06.056.
47. Wang S., Dai X.Y., Ji S., Saeidi T., Schwiegelshohn F., Yassine A.A., Lilge L., Betz V. Scalable and accessible personalized photodynamic therapy optimization with FullMonte and PDT-SPACE. *J. Biomed. Opt.*, 2022, vol. 27, no. 8, p. 083006.
48. Tran A.P., Jacques S. Modeling voxel-based Monte Carlo light transport with curved and oblique boundary surfaces. *J. Biomed. Opt.*, 2020, vol. 25, no. 2, pp. 1–13.

namic therapy as palliation for esophageal cancer: experience in 215 patients // Annals of Thoracic Surgery. – 2003. – T. 76, № 5. – C. 1687–1693. https://doi.org/10.1016/s0003-4975(03)01299-2.

34. Prasad G.A., Wang K.K., Buttar N.S., Wongkeesong L.M., Lutzke L.S., Borkenhagen L.S. Predictors of stricture formation after photodynamic therapy for high-grade dysplasia in Barrett's esophagus // Gastrointestinal Endoscopy. – 2007. – T. 65, № 1. – C. 60–66. https://doi.org/10.1016/j.gie.2006.04.028.
35. Nakamura T., Oinuma T. Usefulness of photodynamic diagnosis and therapy using talaporfin sodium for an advanced-aged patient with inoperable gastric cancer // Laser Therapy. – 2014. – T. 23, № 3. – C. 201–210. https://doi.org/10.5978/islsm.14-OR-16.
36. Pogue B.W., Sheng C., Benevides J., Forcione D., Puricelli B., Nishioka N., Hasan T. Protoporphyrin IX fluorescence photobleaching increases with the use of fractionated irradiation in the esophagus // Journal of Biomedical Optics. – 2008. – T. 13, № 3. – C. 034009. https://doi.org/10.1117/1.2937476.
37. Loshchenov M., Levkin V., Kalyagina N., Linkov K., Kharnas S., Efendiev K., Kharnas P., Loschenov V. Laser-induced fluorescence diagnosis of stomach tumor // Lasers in Medical Science. – 2020. – T. 35. https://doi.org/10.1007/s10103-020-02963-x.
38. Wang H.-W., Zhu T.C., Putt M.P., Solonenko M.G., Metz J.M., Dimofte A., Miles J.D., Fraker D.L., Glatstein E., Hahn S.M., Yodh A.G. Broadband reflectance measurements of light penetration, blood oxygenation, hemoglobin concentration, and drug concentration in human intraperitoneal tissues before and after photodynamic therapy // J. Biomed. Opt. – 2005. – T. 10, № 1. – C. 014004. https://doi.org/10.1117/1.1854679.
39. Pfefer T.J., Schomacker K.T., Nishioka N.S. Long-term effects of photodynamic therapy on fluorescence spectroscopy in the human esophagus // Photochemistry and photobiology. – 2001. – T. 73, № 6. – C. 664–668. https://doi.org/10.1562/0031-8655(2001)073<0664:lteopt>2.0.co;2.
40. Masayuki PhD, Yoda Y., Yamamoto Y., Sunakawa H., Minamide T., Hori K., Ikematsu H., Yano T. Oxygen saturation imaging as a useful tool for visualizing the mode of action of photodynamic therapy for esophageal cancer // VideoGIE. – 2020. – T. 5. https://doi.org/10.1016/j.vgie.2020.07.003.
41. Ortner M.A., Ebert B., Hein E., Zumbusch K., Nolte D., Sukowski U., Weber-Eibel J., Fleige B., Dietel M., Stolte M., Oberhuber G., Porschen R., Klump B., Hörtnagl H., Lochs H., Rinneberg H. Time gated fluorescence spectroscopy in Barrett's oesophagus // Gut. – 2003. – T. 52, № 1. – C. 28–33. https://doi.org/10.1136/gut.52.1.28.
42. Tan W.C., Fulljames C., Stone N., Dix A.J., Shepherd N., Roberts D.J., Brown S.B., Krasner N., Barr H. Photodynamic therapy using 5-aminolaevulinic acid for oesophageal adenocarcinoma associated with Barrett's metaplasia // Journal of photochemistry and photobiology. B, Biology. – 1999. – T. 53, № 1-3. – C. 75–80. https://doi.org/10.1016/s1011-1344(99)00129-3.
43. Standish B.A., Yang V.X., Munce N.R., Wong Kee Song L.M., Gardiner G., Lin A., Mao Y.I., Vitkin A., Marcon N.E., Wilson B.C. Doppler optical coherence tomography monitoring of microvascular tissue response during photodynamic therapy in an animal model of Barrett's esophagus // Gastrointestinal endoscopy. – 2007. – T. 66, № 2. – C. 326–333. https://doi.org/10.1016/j.gie.2007.02.040.
44. van Veen R.L., Aalders M.C., Pasma K.L., Siersema P.D., Haringsma J., van de Vrie W., Gabeler E.E., Robinson D.J., Sterenborg H.J. In situ light dosimetry during photodynamic therapy of Barrett's esophagus with 5-aminolevulinic acid // Lasers in surgery and medicine. – 2002. – T. 31, № 5. – C. 299–304. https://doi.org/10.1002/lsm.10129.
45. Stone N. Standardizing dosimetry in esophageal PDT: an argument for use of centering devices and removal of misleading units // Technology in Cancer Research & Treatment. – 2003. – T. 2, № 4. – C. 333–338. https://doi.org/10.1177/153303460300200408.
46. Veen R., Robinson D., Siersema P., Sterenborg H. The importance of in situ dosimetry during photodynamic therapy of Barrett's esophagus // Gastrointestinal endoscopy. – 2006. – T. 64. – C. 786–788. https://doi.org/10.1016/j.gie.2006.06.056.
47. Wang S., Dai X.Y., Ji S., Saeidi T., Schwiegelshohn F., Yassine A.A., Lilge L., Betz V. Scalable and accessible personalized photodynamic therapy optimization with FullMonte and PDT-SPACE // J Biomed Opt. – 2022. – T. 27, № 8. – C. 083006.
48. Tran A.P., Jacques S. Modeling voxel-based Monte Carlo light transport with curved and oblique boundary surfaces // J Biomed Opt. – 2020. – T. 25, № 2. – C. 1–13.

49. Guo S., Kang J.U. Convolutional neural network-based common-path optical coherence tomography A-scan boundary-tracking training and validation using a parallel Monte Carlo synthetic dataset. *Opt. Express*, 2022, vol. 30, no. 14, pp. 25876–25890.
50. Cassidy J., Nouri A., Betz V., Lilge L. High-performance, robustly verified Monte Carlo simulation with FullMonte. *J. Biomed. Opt.*, 2018, vol. 23, no. 8, pp. 1–11.
51. Woodhams J.H., Macrobert A.J., Bown S.G. The role of oxygen monitoring during photodynamic therapy and its potential for treatment dosimetry. *Photochem. Photobiol. Sci.*, 2007, vol. 6, no. 12, pp. 1246–1256.
52. Efendiev K., Alekseeva P., Linkov K., Shiryaev A., Pisareva T., Gilyadova A., Reshetov I., Voitova A., Loschenov V. Tumor fluorescence and oxygenation monitoring during photodynamic therapy with chlorin e6 photosensitizer. *Photodiagnosis Photodyn. Ther.*, 2024, vol. 45, p. 103969.
53. Gkigkitzis I., Feng Y., Yang C., Lu J.Q., Hu X. Modeling of Oxygen Transport and Cell Killing in Type-II Photodynamic Therapy. *Photochem. Photobiol.*, 2012, vol. 88.
54. Porter J.R., Andrews B.W., Iglesias P.A. A framework for designing and analyzing binary decision-making strategies in cellular systems. *Integr. Biol. (Camb.)*, 2012, vol. 4, no. 3, pp. 310–317.
55. Странадко Е.Ф., Баранов А.В., Дуванский В.А., Лобаков А.И., Морохотов В.А., Рябов М.В. Фотодинамическая терапия рака большого дуоденального сосочка и внепеченочных желчных протоков. *Biomedical Photonics*, 2020, vol. 9, no. 2, pp. 18–28. https://doi.org/ 10.24931/2413-9432-2020-9-2-18-28.
56. Wang H., Ewetse M.P., Ma C., Pu W., Xu B., He P., Wang Y., Zhu J., Chen H. The "Light Knife" for Gastric Cancer: Photodynamic Therapy. *Pharmaceutics*, 2023, vol. 15, no. 1, p. 101. https://doi.org/ 10.3390/pharmaceutics15010101.
57. Tseimakh A.E., Mitschenko A.N., Kurtukov V.A., Shoikhet I.N., Kuleshova I.V. Effektivnost' palliativnoi fotodinamicheskoi terapii pri nerezektabel'nom rake zhelchnykh putei. Sistematicheskii obzor i metaanaliz. *Biomedical Photonics*, 2024, vol. 13, no. 2, pp. 34–42. https://doi.org/ 10.24931/2413-9432-2024-13-2-34-42.
58. Celli J., Spring B., Rizvi I., Evans C., Samkoe K., Verma S., Pogue B., Hasan T. Imaging and photodynamic therapy: mechanisms, monitoring, and optimization. *Chemical Reviews*, 2010, vol. 110, pp. 2795–2838. https://doi.org/ 10.1021/cr900300p.
59. Jarvi M.T., Niedre M.J., Patterson M.S., Wilson B.C. Singlet Oxygen Luminescence Dosimetry (SOLD) for Photodynamic Therapy: Current Status, Challenges and Future Prospects. *Photochemistry and Photobiology*, 2006, vol. 82, pp. 1198–1210. https://doi.org/ 10.1562/2006-05-03-IR-891.
60. Ong Y.H., Sheng T., Busch T.M., Zhu T.C. Reactive oxygen species explicit dosimetry for the evaluations of treatment efficiency of single and fractionated ALA-mediated photodynamic therapy. *Proc. SPIE 11220, Optical Methods for Tumor Treatment and Detection: Mechanisms and Techniques in Photodynamic Therapy XXIX*, 2020, 112200R. https://doi.org/ 10.1117/12.2546425.
61. Penjweini R., Liu B., Kim M.M., Zhu T.C. Explicit dosimetry for 2-(1-hexyloxyethyl)-2-devinyl pyropheophorbide-a-mediated photodynamic therapy: macroscopic singlet oxygen modeling. *Journal of Biomedical Optics*, 2015, vol. 20, no. 12, p. 128003. https://doi.org/ 10.1117/1.JBO.20.12.128003.
62. Jarvi M.T., Patterson M.S., Wilson B.C. Insights into photodynamic therapy dosimetry: simultaneous singlet oxygen luminescence and photosensitizer photobleaching measurements. *Biophysical Journal*, 2012, vol. 102, no. 3, pp. 661–671. https://doi.org/ 10.1016/j.bpj.2011.12.043.
63. Georgakoudi I., Foster T.H. Singlet oxygen- versus nonsinglet oxygen-mediated mechanisms of sensitizer photobleaching and their effects on photodynamic dosimetry. *Photochemistry and Photobiology*, 1998, vol. 67, no. 6, pp. 612–625.
64. James N.S., Cheruku R.R., Missert J.R., Sunar U., Pandey R.K. Measurement of cyanine dye photobleaching in photosensitizer cyanine dye conjugates could help in optimizing light dosimetry for improved photodynamic therapy of cancer. *Molecules*, 2018, vol. 23, no. 8, p. 1842. https://doi.org/ 10.3390/molecules23081842.
65. Alekseeva P., Makarov V., Efendiev K., Shiryaev A., Reshetov I., Loschenov V. Devices and methods for dosimetry of personalized photodynamic therapy of tumors: a review on recent trends. *Cancers*, 2024, vol. 16, no. 13, p. 2484. https://doi.org/ 10.3390/cancers16132484.

49. Guo S., Kang J.U. Convolutional neural network-based common-path optical coherence tomography A-scan boundary-tracking training and validation using a parallel Monte Carlo synthetic dataset // Opt Express. – 2022. – Т. 30, № 14. – С. 25876–25890.
50. Cassidy J., Nouri A., Betz V., Lilge L. High-performance, robustly verified Monte Carlo simulation with FullMonte // J Biomed Opt. – 2018. – Т. 23, № 8. – С. 1–11.
51. Woodhams J.H., Macrobert A.J., Bown S.G. The role of oxygen monitoring during photodynamic therapy and its potential for treatment dosimetry // Photochem Photobiol Sci. – 2007. – Т. 6, № 12. – С. 1246–1256.
52. Efendiev K., Alekseeva P., Linkov K., Shiryaev A., Pisareva T., Gilyadova A., Reshetov I., Voitova A., Loschenov V. Tumor fluorescence and oxygenation monitoring during photodynamic therapy with chlorin e6 photosensitizer // Photodiagnosis and Photodynamic Therapy. – 2024. – Т. 45. – С. 103969.
53. Gkigkitzis I., Feng Y., Yang C., Lu J.Q., Hu X. Modeling of Oxygen Transport and Cell Killing in Type-II Photodynamic Therapy // Photochemistry and Photobiology. – 2012. – Т. 88.
54. Porter J.R., Andrews B.W., Iglesias P.A. A framework for designing and analyzing binary decision-making strategies in cellular systems // Integr Biol (Camb). – 2012. – Т. 4, № 3. – С. 310–317.
55. Странадко Е.Ф., Баранов А.В., Дуванский В.А., Лобаков А.И., Морохотов В.А., Рябов М.В. Фотодинамическая терапия рака большого дуоденального сосочка и внепеченочных желчных протоков // Biomedical Photonics. – 2020. – Т. 9, № 2. – С. 18–28. https://doi.org/10.24931/2413-9432-2020-9-2-18-28.
56. Wang H., Ewetse M.P., Ma C., Pu W., Xu B., He P., Wang Y., Zhu J., Chen H. The "Light Knife" for Gastric Cancer: Photodynamic Therapy // Pharmaceutics. – 2023. – Т. 15, № 1. – С. 101. https://doi.org/10.3390/pharmaceutics15010101.
57. Цеймах А.Е., Митшенко А.Н., Куртуков В.А., Шойхет И.Н., Кулешова И.В. Эффективность паллиативной фотодинамической терапии при нерезектабельном раке желчных путей. Систематический обзор и метаанализ // Biomedical Photonics. – 2024. – Т. 13, № 2. – С. 34–42. https://doi.org/10.24931/2413-9432-2024-13-2-34-42.
58. Celli J., Spring B., Rizvi I., Evans C., Samkoe K., Verma S., Pogue B., Hasan T. Imaging and photodynamic therapy: mechanisms, monitoring, and optimization // Chemical Reviews. – 2010. – Т. 110. – С. 2795–2838. https://doi.org/10.1021/cr900300p.
59. Jarvi M.T., Niedre M.J., Patterson M.S., Wilson B.C. Singlet Oxygen Luminescence Dosimetry (SOLD) for Photodynamic Therapy: Current Status, Challenges and Future Prospects // Photochemistry and Photobiology. – 2006. – Т. 82. – С. 1198–1210. https://doi.org/10.1562/2006-05-03-IR-891.
60. Ong Y.H., Sheng T., Busch T.M., Zhu T.C. Reactive oxygen species explicit dosimetry for the evaluations of treatment efficiency of single and fractionated ALA-mediated photodynamic therapy // Proc. SPIE 11220, Optical Methods for Tumor Treatment and Detection: Mechanisms and Techniques in Photodynamic Therapy XXIX. – 2020. – 112200R. https://doi.org/10.1117/12.2546425.
61. Penjweini R., Liu B., Kim M.M., Zhu T.C. Explicit dosimetry for 2-(1-hexyloxyethyl)-2-devinyl pyropheophorbide-a-mediated photodynamic therapy: macroscopic singlet oxygen modeling // Journal of Biomedical Optics. – 2015. – Т. 20, № 12. – С. 128003. https://doi.org/10.1117/1.JBO.20.12.128003.
62. Jarvi M.T., Patterson M.S., Wilson B.C. Insights into photodynamic therapy dosimetry: simultaneous singlet oxygen luminescence and photosensitizer photobleaching measurements // Biophysical Journal. – 2012. – Т. 102, № 3. – С. 661–671. https://doi.org/10.1016/j.bpj.2011.12.043.
63. Georgakoudi I., Foster T.H. Singlet oxygen- versus nonsinglet oxygen-mediated mechanisms of sensitizer photobleaching and their effects on photodynamic dosimetry // Photochemistry and Photobiology. – 1998. – Т. 67, № 6. – С. 612–625.
64. James N.S., Cheruku R.R., Missert J.R., Sunar U., Pandey R.K. Measurement of cyanine dye photobleaching in photosensitizer cyanine dye conjugates could help in optimizing light dosimetry for improved photodynamic therapy of cancer // Molecules. – 2018. – Т. 23, № 8. – С. 1842. https://doi.org/10.3390/molecules23081842.
65. Alekseeva P., Makarov V., Efendiev K., Shiryaev A., Reshetov I., Loschenov V. Devices and methods for dosimetry of personalized photodynamic therapy of tumors: a review on recent trends // Cancers. – 2024. – Т. 16, № 13. – С. 2484. https://doi.org/10.3390/cancers16132484

66. Sirotkina M.A., Matveev L.A., Shirmanova M.V. et al. Monitoring photodynamic therapy using optical coherence angiography. *Sci. Rep.*, 2017, vol. 7, p. 41506. https://doi.org/ 10.1038/srep41506.
67. Yang W., Rastogi V., Sun H., Sharma D., Wilson B.C., Hadfield R.H., Zhu T.C. Multispectral singlet oxygen luminescent dosimetry (MSOLD) for Porfimer sodium-mediated photodynamic therapy. *Proceedings of SPIE*, 2023, vol. 12359, p. 1235908. https://doi.org/ 10.1117/12.2652590.
68. Romanishkin I., Ospanov A., Savelyeva T., Shugay S., Goryainov S., Pavlova G., Pronin I., Loschenov V. Multimodal method of tissue differentiation in neurooncology using Raman spectroscopy, fluorescence and diffuse reflectance spectroscopy. *Zhurnal voprosy neirokhirurgii imeni N. N. Burdenko*, 2022, vol. 86, pp. 5–12. https://doi.org/ 10.17116/neiro202286055.
69. Fang S., Wu S., Chen Z., He C., Lin L.L., Ye J. Recent progress and applications of Raman spectrum denoising algorithms in chemical and biological analyses: A review. *TrAC Trends in Analytical Chemistry*, 2024, vol. 172. https://doi.org/ 10.1016/j.trac.2024.117578.
70. Hamdoon Z., Jerjes W., Rashed D., Kawas S., Sattar A.A., Samsudin R., Hopper C. In vivo optical coherence tomography-guided photodynamic therapy for skin pre-cancer and cancer. *Photodiagnosis and Photodynamic Therapy*, 2021, vol. 36, p. 102520. https://doi.org/ 10.1016/j.pdpdt.2021.102520.
71. Zhao Y., Moritz T., Hinds M.F., Gunn J.R., Shell J.R., Pogue B.W., Davis S.J. *J. Biophotonics*, 2021, vol. 14, no. 11, e202100088. https://doi.org/ 10.1002/jbio.202100088.
72. Karakullukcu B., Kanick S.C., Aans J.B., Sterenborg H.J., Tan I.B., Amelink A., Robinson D.J. Clinical feasibility of monitoring m-THPC mediated photodynamic therapy by means of fluorescence differential path-length spectroscopy. *Journal of Biophotonics*, 2011, vol. 4, no. 10, pp. 740–751. https://doi.org/ 10.1002/jbio.201100051.
73. Sun H., Ong Y., Yang W., Sourvanos D., Dimofte A., Busch T.M., Singhal S., Cengel K.A., Zhu T.C. Clinical PDT dose dosimetry for pleural Porfimer sodium-mediated photodynamic therapy. *J. Biomed. Opt.*, 2024, vol. 29, no. 1, p. 018001. https://doi.org/ 10.1117/1.JBO.29.1.018001.
74. Schaberle F.A. Assessment of the actual light dose in photodynamic therapy. *Photodiagnosis and Photodynamic Therapy*, 2018, vol. 23, pp. 75–77. https://doi.org/ 10.1016/j.pdpdt.2018.06.009.
75. Kamel B., El-Daher M., Bachir W., Aljalali S. Effect of tissue optical properties on the fluorescence of BODIPY derivative as a photosensitizer for photodynamic therapy. *Spectroscopy*, 2024. https://doi.org/ 10.56530/spectroscopy.ye4569u1.
76. Clancy N.T., Arya S., Stoyanov D., Singh M., Hanna G.B., Elson D.S. Intraoperative measurement of bowel oxygen saturation using a multispectral imaging laparoscope. *Biomed. Opt. Express*, 2015, vol. 6, pp. 4179–4190.
77. Jacques S.L. Optical properties of biological tissues: a review. *Physics in Medicine and Biology*, 2013, vol. 58, no. 11, pp. R37–R61. https://doi.org/ 10.1088/0031-9155/58/11/R37.
78. Pilon L., Bhowmik A., Heng R.-L., Yudovsky D. Simple and accurate expressions for diffuse reflectance of semi-infinite and two-layer absorbing and scattering media: erratum. *Appl. Opt.*, 2015, vol. 54, pp. 6116–6117.
79. Bahl A., Segaud S., Xie Y., Shapey J., Bergholt M.S., Vercauteren T. A comparative study of analytical models of diffuse reflectance in homogeneous biological tissues: Gelatin-based phantoms and Monte Carlo experiments. *J. Biophotonics*, 2024, vol. 17, no. 6, e202300536. https://doi.org/ 10.1002/jbio.202300536.
80. Nishimura T., Takai Y., Shimojo Y. et al. Determination of optical properties in double integrating sphere measurement by artificial neural network based method. *Opt. Rev.*, 2021, vol. 28, pp. 42–47. https://doi.org/ 10.1007/s10043-020-00632-6.
81. Simpson C.R., Kohl M., Essenpreis M., Cope M. Near-infrared optical properties of ex vivo human skin and subcutaneous tissues measured using the Monte Carlo inversion technique. *Phys. Med. Biol.*, 1998, vol. 43, pp. 2465–2478. https://doi.org/ 10.1088/0031-9155/43/9/003.
82. Palmer G.M., Ramanujam N. Monte Carlo based inverse model for calculating tissue optical properties. Part 1, theory and validation on synthetic phantoms. *Appl. Opt.*, 2006, vol. 45, no. 5, pp. 1062–1071. https://doi.org/ 10.1364/AO.45.001062.
83. Rajaram N., Nguyen T.H., Tunnell J.W. A lookup-table based inverse model for measuring optical properties of turbid media.

66. Сироткина М.А., Матвеев Л.А., Ширманова М.В. и др. Мониторинг фотодинамической терапии с помощью оптической когерентной ангиографии // Sci Rep. – 2017. – Т. 7. – С. 41506. https://doi.org/10.1038/srep41506.
67. Yang W., Rastogi V., Sun H., Sharma D., Wilson B.C., Hadfield R.H., Zhu T.C. Multispectral singlet oxygen luminescent dosimetry (MSOLD) for Porfimer sodium-mediated photodynamic therapy // Proceedings of SPIE. – 2023. – Т. 12359. – С. 1235908. https://doi.org/10.1117/12.2652590.
68. Романишкин И.Д., Оспанов А., Савельева Т.А., Шугай С.В., Горяйнов С.А., Павлова Г.В., Пронин И.Н., Лощенов В.Б. Мультимодальный метод дифференциации тканей в нейроонкологии с использованием спектроскопии комбинационного рассеяния, флуоресценции и диффузного отражения // Вопросы нейрохирургии имени Н.Н. Бурденко. – 2022. – Т. 86. – С. 5–12. https://doi.org/10.17116/neiro202286055.
69. Fang S., Wu S., Chen Z., He C., Lin L.L., Ye J. Recent progress and applications of Raman spectrum denoising algorithms in chemical and biological analyses: A review // TrAC Trends in Analytical Chemistry. – 2024. – Т. 172. https://doi.org/10.1016/j.trac.2024.117578.
70. Hamdoon Z., Jerjes W., Rashed D., Kawas S., Sattar A.A., Samsudin R., Hopper C. In vivo optical coherence tomography-guided photodynamic therapy for skin pre-cancer and cancer // Photodiagnosis and photodynamic therapy. – 2021. – Т. 36. – С. 102520. https://doi.org/10.1016/j.pdpdt.2021.102520.
71. Zhao Y., Moritz T., Hinds M.F., Gunn J.R., Shell J.R., Pogue B.W., Davis S.J. // J. Biophotonics. – 2021. – Т. 14, № 11. – С. e202100088. https://doi.org/10.1002/jbio.202100088.
72. Karakullukcu B., Kanick S.C., Aans J.B., Sterenborg H.J., Tan I.B., Amelink A., Robinson D.J. Clinical feasibility of monitoring m-THPC mediated photodynamic therapy by means of fluorescence differential path-length spectroscopy // Journal of biophotonics. – 2011. – Т. 4, № 10. – С. 740–751. https://doi.org/10.1002/jbio.201100051.
73. Sun H., Ong Y., Yang W., Sourvanos D., Dimofte A., Busch T.M., Singhal S., Cengel K.A., Zhu T.C. Clinical PDT dose dosimetry for pleural Porfimer sodium-mediated photodynamic therapy // J. Biomed. Opt. – 2024. – Т. 29, № 1. – С. 018001. https://doi.org/10.1117/1.JBO.29.1.018001.
74. Schaberle F.A. Assessment of the actual light dose in photodynamic therapy // Photodiagnosis and photodynamic therapy. – 2018. – Т. 23. – С. 75–77. https://doi.org/10.1016/j.pdpdt.2018.06.009.
75. Kamel B., El-Daher M., Bachir W., Aljalali S. Effect of tissue optical properties on the fluorescence of BODIPY derivative as a photosensitizer for photodynamic therapy // Spectroscopy. – 2024. https://doi.org/10.56530/spectroscopy.ye4569u1.
76. Clancy N.T., Arya S., Stoyanov D., Singh M., Hanna G.B., Elson D.S. Intraoperative measurement of bowel oxygen saturation using a multispectral imaging laparoscope // Biomed. Opt. Express. – 2015. – Т. 6. – С. 4179–4190.
77. Jacques S.L. Optical properties of biological tissues: a review // Physics in medicine and biology. – 2013. – Т. 58, № 11. – С. R37–R61. https://doi.org/10.1088/0031-9155/58/11/R37.
78. Pilon L., Bhowmik A., Heng R.-L., Yudovsky D. Simple and accurate expressions for diffuse reflectance of semi-infinite and two-layer absorbing and scattering media: erratum // Appl. Opt. – 2015. – Т. 54. – С. 6116–6117.
79. Bahl A., Segaud S., Xie Y., Shapey J., Bergholt M.S., Vercauteren T. A comparative study of analytical models of diffuse reflectance in homogeneous biological tissues: Gelatin-based phantoms and Monte Carlo experiments // J. Biophotonics. – 2024. – Т. 17, № 6. – С. e202300536. https://doi.org/10.1002/jbio.202300536.
80. Nishimura T., Takai Y., Shimojo Y. и др. Determination of optical properties in double integrating sphere measurement by artificial neural network based method // Opt Rev. – 2021. – Т. 28. – С. 42–47. https://doi.org/10.1007/s10043-020-00632-6.
81. Simpson C.R., Kohl M., Essenpreis M., Cope M. Near-infrared optical properties of ex vivo human skin and subcutaneous tissues measured using the Monte Carlo inversion technique // Phys. Med. Biol. – 1998. – Т. 43. – С. 2465–2478. https://doi.org/10.1088/0031-9155/43/9/003.
82. Palmer G.M., Ramanujam N. Monte Carlo based inverse model for calculating tissue optical properties. Part 1, theory and validation on synthetic phantoms // Appl. Opt. – 2006. – Т. 45, № 5. – С. 1062–1071. https://doi.org/10.1364/AO.45.001062.
83. Rajaram N., Nguyen T.H., Tunnell J.W. A lookup-table based inverse model for measuring optical properties of turbid media

J. Biomed. Opt., 2008, vol. 13, no. 5, p. 050501. https://doi.org/10.1117/1.2981797.
84. Tseng S.H., Grant A., Durkin A.J. In vivo determination of skin near-infrared optical properties using diffuse optical spectroscopy. *J. Biomed. Opt.*, 2008, vol. 13, p. 014016. https://doi.org/10.1117/1.2829772.
85. Wisotzky E.L., Arens P., Dommerich S., Hilsmann A., Eisert P., Uecker F.C. Determination of the optical properties of cholesteatoma in the spectral range of 250 to 800 nm. *Biomed. Opt. Express*, 2020, vol. 11, pp. 1489–1500.
86. Shapey J., Xie Y., Nabavi E., Ebner M., Saeed S.R., Kitchen N., Dorward N., Grieve J., McEvoy A.W., Miserocchi A., Grover P., Bradford R., Lim Y.-M., Ourselin S., Brandner S., Jaunmuktane Z., Vercauteren T. *J. Biophotonics*, 2022, vol. 15, no. 4, e202100072. https://doi.org/10.1002/jbio.202100072.
87. Sweer J.A., Chen M.T., Salimian K.J., Battafarano R.J., Durr N.J. Wide-field optical property mapping and structured light imaging of the esophagus with spatial frequency domain imaging. *Journal of Biophotonics*, 2019, vol. 12, no. 9, e201900005. https://doi.org/10.1002/jbio.201900005.
88. Bashkatov A., Genina E., Kochubey V., Gavrilova A., Kapralov S., Grishaev V., Tuchin V. Optical properties of human stomach mucosa in the spectral range from 400 to 2000 nm: Prognosis for gastroenterology. *Medical Laser Application*, 2007, vol. 22, pp. 95–104.
89. Krivetskaya A.A., Savelieva T.A., Kustov D.M. et al. Method for Assessing the Optical Properties of Multilayer Tissues of the Gastrointestinal Tract ex Vivo. *Phys. Atom. Nuclei*, 2024, vol. 87, pp. 1727–1729. https://doi.org/ 10.1134/S1063778824100247.
90. Bashkatov A., Genina E., Kochubey V., Rubtsov V., Kolesnikova E., Tuchin V. Optical properties of human colon tissues in the 350–2500 nm spectral range. *Quantum Electronics*, 2014, vol. 44, p. 77.
91. Ben LaRiviere N., Ferguson L., Garman K.S., Fisher D.A., Jokerst N.M. Methods of extraction of optical properties from diffuse reflectance measurements of ex-vivo human colon tissue using thin film silicon photodetector arrays. *Biomed. Opt. Express*, 2019, vol. 10, pp. 5703–5715.
92. Zhu T.C., Sun H., Ong Y.H. et al. Real-time PDT Dose Dosimetry for Pleural Photodynamic Therapy. *Proc. SPIE Int. Soc. Opt. Eng.*, 2022, vol. 11940, p. 1194002. https://doi.org/ 10.1117/12.2612188.
93. Ong Y.H., Kim M.M., Finlay J.C. et al. PDT dose dosimetry for Porfimer sodium-mediated pleural photodynamic therapy (pPDT). *Phys. Med. Biol.*, 2017, vol. 63, no. 1, p. 015031. https://doi.org/ 10.1088/1361-6560/aa9874.
94. Lilge L., Wu J., Xu Y., Manalac A., Molehuis D., Schwiegelshohn F., Vesselov L., Embree W., Nesbit M., Betz V., Mandel A., Jewett M., Kulkarni G. Minimal required PDT light dosimetry for nonmuscle invasive bladder cancer. *Journal of Biomedical Optics*, 2020, vol. 25, no. 6, p. 068001. https://doi.org/ 10.1117/1.JBO.25.6.068001.
95. Saager R.B., Cuccia D.J., Durkin A.J. Determination of optical properties of turbid media spanning visible and near-infrared regimes via spatially modulated quantitative spectroscopy. *Journal of Biomedical Optics*, 2010, vol. 15, no. 1, p. 017012. https://doi.org/10.1117/1.3299322.
96. Jones L.R., Preyer N.W. Jr., Davis M.A., Grimes C., Edling K., Holdgate N., Wallace M.B., Wolfsen H.C. Light dosimetry calculations for esophageal photodynamic therapy using porfimer sodium. *Proc. SPIE 6139, Optical Methods for Tumor Treatment and Detection: Mechanisms and Techniques in Photodynamic Therapy XV*, 2006, p. 61391D. https://doi.org/ 10.1117/12.660155.
97. Sun H., Yang W., Zhu T.C. Real-time photosensitizer dosimetry for photodynamic therapy. *Proc. SPIE 13299, Optical Methods for Tumor Treatment and Detection: Mechanisms and Techniques in Photodynamic Therapy XXXIII*, 2025, p. 1329909. https://doi.org/10.1117/12.3044770.
98. Mousavi M., Moriyama L.T., Grecco C., Saito Nogueira M., Svanberg K., Kurachi C., Andersson-Engels S. Photodynamic therapy dosimetry using multiexcitation multiemission wavelength: toward real-time prediction of treatment outcome. *Journal of Biomedical Optics*, 2020, vol. 25, no. 6, p. 063812. https://doi.org/ 10.1117/1.JBO.25.6.063812.
99. Yassine A.-A., Lilge L., Betz V. Machine learning for real-time optical property recovery in interstitial photodynamic therapy: a stimulation-based study. *Biomedical Optics Express*, 2021, vol. 12, pp. 5401–5422. https://doi.org/ 10.1364/BOE.431310.

// J. Biomed. Opt. – 2008. – T. 13, № 5. – C. 050501. https://doi.org/10.1117/1.2981797.
84. Tseng S.H., Grant A., Durkin A.J. In vivo determination of skin near-infrared optical properties using diffuse optical spectroscopy // J. Biomed. Opt. – 2008. – T. 13. – C. 014016. https://doi.org/10.1117/1.2829772.
85. Wisotzky E.L., Arens P., Dommerich S., Hilsmann A., Eisert P., Uecker F.C. Determination of the optical properties of cholesteatoma in the spectral range of 250 to 800 nm // Biomed. Opt. Express. – 2020. – T. 11. – C. 1489–1500.
86. Shapey J., Xie Y., Nabavi E., Ebner M., Saeed S.R., Kitchen N., Dorward N., Grieve J., McEvoy A.W., Miserocchi A., Grover P., Bradford R., Lim Y.-M., Ourselin S., Brandner S., Jaunmuktane Z., Vercauteren T. J. Biophotonics. – 2022. – T. 15, № 4. – C. e202100072. https://doi.org/10.1002/jbio.202100072.
87. Sweer J.A., Chen M.T., Salimian K.J., Battafarano R.J., Durr N.J. Wide-field optical property mapping and structured light imaging of the esophagus with spatial frequency domain imaging // Journal of biophotonics. – 2019. – T. 12, № 9. – C. e201900005. https://doi.org/10.1002/jbio.201900005.
88. Bashkatov A., Genina E., Kochubey V., Gavrilova A., Kapralov S., Grishaev V., Tuchin V. Optical properties of human stomach mucosa in the spectral range from 400 to 2000 nm: Prognosis for gastroenterology // Medical Laser Application. – 2007. – T. 22. – C. 95–104.
89. Krivetskaya A.A., Savelieva T.A., Kustov D.M. и др. Method for Assessing the Optical Properties of Multilayer Tissues of the Gastrointestinal Tract ex Vivo // Phys. Atom. Nuclei. – 2024. – T. 87. – C. 1727–1729. https://doi.org/10.1134/S1063778824100247.
90. Bashkatov A., Genina E., Kochubey V., Rubtsov V., Kolesnikova E., Tuchin V. Optical properties of human colon tissues in the 350–2500 nm spectral range // Quantum Electronics. – 2014. – T. 44. – C. 77.
91. Ben LaRiviere N., Ferguson L., Garman K.S., Fisher D.A., Jokerst N.M. Methods of extraction of optical properties from diffuse reflectance measurements of ex-vivo human colon tissue using thin film silicon photodetector arrays // Biomed. Opt. Express. – 2019. – T. 10. – C. 5703–5715.
92. Zhu T.C., Sun H., Ong Y.H. и др. Real-time PDT Dose Dosimetry for Pleural Photodynamic Therapy // Proc SPIE Int Soc Opt Eng. – 2022. – T. 11940. – C. 1194002. https://doi.org/10.1117/12.2612188.
93. Ong Y.H., Kim M.M., Finlay J.C. и др. PDT dose dosimetry for Porfimer sodium-mediated pleural photodynamic therapy (pPDT) // Phys Med Biol. – 2017. – T. 63, № 1. – C. 015031. https://doi.org/10.1088/1361-6560/aa9874.
94. Lilge L., Wu J., Xu Y., Manalac A., Molehuis D., Schwiegelshohn F., Vesselov L., Embree W., Nesbit M., Betz V., Mandel A., Jewett M., Kulkarni G. Minimal required PDT light dosimetry for nonmuscle invasive bladder cancer // Journal of Biomedical Optics. – 2020. – T. 25, № 6. – C. 068001. https://doi.org/10.1117/1.JBO.25.6.068001.
95. Saager R.B., Cuccia D.J., Durkin A.J. Determination of optical properties of turbid media spanning visible and near-infrared regimes via spatially modulated quantitative spectroscopy // Journal of biomedical optics. – 2010. – T. 15, № 1. – C. 017012. https://doi.org/10.1117/1.3299322.
96. Jones L.R., Preyer N.W. Jr., Davis M.A., Grimes C., Edling K., Holdgate N., Wallace M.B., Wolfsen H.C. Light dosimetry calculations for esophageal photodynamic therapy using porfimer sodium // Proc. SPIE 6139, Optical Methods for Tumor Treatment and Detection: Mechanisms and Techniques in Photodynamic Therapy XV. – 2006. – C. 61391D. https://doi.org/10.1117/12.660155.
97. Sun H., Yang W., Zhu T.C. Real-time photosensitizer dosimetry for photodynamic therapy // Proc. SPIE 13299, Optical Methods for Tumor Treatment and Detection: Mechanisms and Techniques in Photodynamic Therapy XXXIII. – 2025. – C. 1329909. https://doi.org/10.1117/12.3044770.
98. Mousavi M., Moriyama L.T., Grecco C., Saito Nogueira M., Svanberg K., Kurachi C., Andersson-Engels S. Photodynamic therapy dosimetry using multiexcitation multiemission wavelength: toward real-time prediction of treatment outcome // Journal of biomedical optics. – 2020. – T. 25, № 6. – C. 063812. https://doi.org/10.1117/1.JBO.25.6.063812.
99. Yassine A.-A., Lilge L., Betz V. Machine learning for real-time optical property recovery in interstitial photodynamic therapy: a stimulation-based study // Biomedical Optics Express. – 2021. – T. 12. – C. 5401–5422. https://doi.org/10.1364/BOE.431310.

ФОТОСЕНСИБИЛИЗАТОРЫ НОВОГО ПОКОЛЕНИЯ ДЛЯ ФОТОДИНАМИЧЕСКОЙ ТЕРАПИИ

«ФОТОДИТАЗИН®» концентрат для приготовления раствора для инфузий — лекарственное средство (РУ № ЛС 001246 от 18.05.2012 г.)
«ФОТОДИТАЗИН®» гель — изделие медицинского назначения (РУ № ФСР 2012/13043 от 03.02.2012 г.)
«ФОТОДИТАГЕЛЬ®» — косметическое средство (ДС ЕАЭС № RU Д-RU.НВ42.В.06108/20 от 24.09.2020 г.)

Препараты применяются для флюоресцентной диагностики и фотодинамической терапии злокачественных новообразований, а также патологий неонкологического характера в следующих областях медицины:

- гинекология
- урология
- нейрохирургия
- торакальная хирургия
- офтальмология
- травматология
- ортопедия
- комбустиология
- гнойная хирургия
- дерматология
- косметология
- стоматология

www.fotoditazin.com
www.фотодитазин.рф

@FOTODITAZIN

@FOTODITAGEL_FDT

ООО «ВЕТА-ГРАНД»
123056, г. Москва, ул. Красина, д. 27, стр. 2
Тел.: +7 (499) 250-40-00, +7 (929) 971-44-46
E-mail: veta-grand@mail.ru